The efficacy of mycolic acid-enhanced PLGA nanoparticles for rifampicin delivery in tuberculosis treatment

by

Kruger Goosen

27366571

Supervisor:

Prof Yolandy Lemmer

Co-Supervisor:

Prof Jan Verschoor

Submitted in fulfilment of the degree *Magister Scientiae Biochemistry*

In the Faculty of Natural and Agricultural Sciences
University of Pretoria
Pretoria
2024

Submission declaration:

I, Kruger Goosen, declare that this dissertation, which I hereby submit for the degree Magister Scientiae Biochemistry in the Department of Biochemistry, Genetics and Microbiology at the University of Pretoria, is my own work and has not previously been submitted by me for a degree at this or any other tertiary institution.

SIGNATURE:……

DATE: 2025/01/28

DECLARATION OF ORIGINALITY

UNIVERSITY OF PRETORIA

Declaration

1. I understand what plagiarism is and am aware of the University's policy in this regard.

2. I declare that this dissertation is my own original work. Where other people's work has been used (either from a printed source, Internet or any other source), this has been properly acknowledged and referenced in accordance with departmental requirements.

3. I have not used work previously produced by another student or any other person to hand in as my own.

4. I have not allowed, and will not allow, anyone to copy my work with the intention of passing it off as his or her own work.

SIGNATURE ..... **DATE** 2025/01/28.....

Ethics statement

The author, whose name appears on the title page of this dissertation, has obtained the required research ethics approval/exemption for the research described in this work. The author declares that they have observed the ethical standards required in terms of the University of Pretoria's Code of ethics for scholarly activities.

SUMMARY

The efficacy of nanoparticle-encapsulated rifampicin formulations in treating high *Mycobacterium tuberculosis (M. tb)* bacillary loads was investigated using a guinea pig model. This study compared two formulations: rifampicin encapsulated in poly(lactic-co-glycolic acid) (PLGA/RIF) and PLGA/RIF with mycolic acid as a targeting ligand (PLGA/RIF/MA), against traditional rifampicin treatment and control groups. The guinea pig model was selected for its physiological and immunological similarities to human TB infection. Data obtained from this study will guide optimisation for future drug efficacy testing, particularly for targeted TB treatment.

Key findings indicated variations in survival rates, clinical signs of TB progression, and bacterial load reduction among the treatment groups. The PLGA/RIF group showed promising results in survival rates and bacterial load reduction, suggesting the benefits of nanoparticle-encapsulated drug formulations. The addition of MA resulted in reduced rifampicin loading capacity within PLGA particles, necessitating higher particle dosing, which may lead to possible side effects. This outcome highlights the complexity of optimising nanoparticle formulations for TB treatment.

The study also addressed challenges in achieving statistical significance in animal model research, particularly in pilot studies with limited sample sizes and high variability. Recommendations include refining methods to reduce variability and increase repeatability and exploring serological testing for TB biomarkers for early detection and treatment initiation. This approach could provide insights into infection dynamics and treatment responses.

This dissertation lays the groundwork for further exploration of nanoparticle-based drug delivery in TB treatment, emphasising the potential of PLGA as a drug carrier and the need for innovative approaches to improve TB therapy.

TABLE OF CONTENTS

Tables:

Figures:

Abbreviations:

TB - Tuberculosis
***M. tb* -** *Mycobacterium tuberculosis*
PLGA - Poly(lactic-co-glycolic acid)
RIF - Rifampicin
MA - Mycolic Acid
PVA - Polyvinyl Alcohol
DCM - Dichloromethane
W/O - Water-in-Oil
W/O/W - Water-in-Oil-in-Water
NPs - Nanoparticles
SEM - Scanning Electron Microscopy
DLS - Dynamic Light Scattering
LDE - Laser Doppler Electrophoresis
IFN-γ - Interferon-Gamma
TNF-α - Tumor Necrosis Factor-Alpha
IL-12 - Interleukin-12
LTBI - Latent TB Infection
MDR-TB - Multidrug-Resistant Tuberculosis
XDR-TB - Extensively Drug-Resistant Tuberculosis
TDR-TB - Totally Drug-Resistant Tuberculosis
HIV - Human Immunodeficiency Virus
WHO - World Health Organization
PCR - Polymerase Chain Reaction
CFU - Colony-Forming Unit
PrEP - Pre-Exposure Prophylaxis
IPT - Isoniazid Preventive Therapy
VH - Volume of the Homogenate
VP - Volume Plated
DFQ - Dilution Factor of the Sample
PBS - Phosphate-Buffered Saline
OECD - Organisation for Economic Co-operation and Development

1. INTRODUCTION AND LITERATURE REVIEW

1.1 Epidemiology of Tuberculosis

1.1.1 Prevalence and Incidence

Tuberculosis (TB) remains a significant global health challenge, with its incidence rates continuing to be a major concern worldwide. According to the World Health Organization (WHO), an estimated 10.6 million people developed TB in 2022, showing an upward trend from 10.3 million in 2021 and 10 million in 2020 (Global Tuberculosis Report 2023). The burden of TB is particularly high in low- and middle-income countries, where resource constraints and other socio-economic factors contribute to its persistence (Global Tuberculosis Report 2023).

The burden of TB disproportionately affects low- and middle-income countries, where systemic challenges such as resource constraints, access to quality healthcare, and socio-economic issues exacerbate the disease's impact. These factors, combined with the global health challenges posed by the COVID-19 pandemic, have further complicated efforts to control TB.

In 2022, the global TB mortality rate also reflected significant concerns, with 1.3 million deaths (including deceased with HIV co-infection/comorbidity), slightly reducing from the estimated 1.4 million deaths in both 2020 and 2021 (Global Tuberculosis Report 2023). This indicates a marginal improvement but underscores the ongoing need for intensified efforts to reduce TB mortality worldwide.

Tuberculosis continues to pose a significant public health challenge in regions such as sub-Saharan Africa, Southeast Asia, and the Western Pacific, where a combination of factors including high HIV co-infection rates, poverty, and limited healthcare resources exacerbate its impact. In sub-Saharan Africa, the TB epidemic is particularly severe, with the high prevalence of HIV/AIDS acting as a critical driver of the disease. HIV-related immune suppression greatly increases susceptibility to active TB, further complicating disease management and highlighting the interconnected nature of these health crises (Global Tuberculosis Report 2023).

Southeast Asia faces its own TB challenges, with countries like India, Indonesia, and Bangladesh accounting for a significant proportion of global TB cases. Factors such as dense populations, limited access to healthcare, and socio-economic disparities play

critical roles in the prevalence and management of TB in this region (Global Tuberculosis Report 2023).

The Western Pacific, including countries like China and the Philippines, also continues to grapple with TB. Urbanisation, migration, and lifestyle factors such as smoking contribute to the TB burden in these areas (Global Tuberculosis Report 2023).

1.1.2 Risk Factors

Several risk factors contribute to the acquisition and progression of TB. Human immunodeficiency virus infection is a major risk factor, as it significantly increases the susceptibility to TB due to the compromised immune system (World Health Organization., 2020). Tuberculosis is the leading cause of death among people living with HIV/AIDS, and the two diseases have a complex relationship, with each exacerbating the other's progression.

Close contact with active TB cases is another significant risk factor. Transmission of *Mycobacterium tuberculosis*, the bacterium causing TB, occurs through the inhalation of infectious droplets released into the air when an infected individual coughs or sneezes. Therefore, individuals living in overcrowded households or institutions with poor ventilation are at higher risk of contracting TB.

Socio-economic factors such as poverty, poor living conditions, and inadequate access to healthcare play a crucial role in the persistence of TB (Lönnroth *et al*., 2009). Malnutrition weakens the immune system and increases the risk of TB infection and progression. Tobacco smoking and substance abuse, particularly intravenous drug use, also contribute to the development of TB by impairing lung function and weakening the immune response (Wang *et al*., 2020).

Occupational settings can pose an increased risk of TB transmission. Healthcare workers, especially those in close contact with TB patients, are at higher risk due to their occupational exposure (Baussano *et al*., 2011). Similarly, correctional institutions and homeless shelters, where individuals live in crowded and confined spaces, can facilitate TB transmission (Centers for Disease Control and Prevention, 2006).

1.1.3 Vulnerable Populations

Certain populations are more vulnerable to TB infection and its adverse outcomes. Individuals living with HIV/AIDS are particularly susceptible to TB due to the weakened immune system caused by HIV infection (World Health Organization., 2020). The co-occurrence of TB and HIV/AIDS has a significant impact on global TB burden, as HIV-positive individuals are at a much higher risk of developing active TB and experiencing poorer treatment outcomes.

Children are also vulnerable to TB infection. Their immature immune systems make them more susceptible to TB, and they often experience more severe forms of the disease compared to adults. Additionally, children may have difficulties in accessing appropriate diagnostic and treatment services, leading to delayed diagnosis and poorer outcomes (Dodd *et al*., 2014).

The elderly population is at increased risk of TB due to age-related decline in immune function. Age-related comorbidities, such as diabetes mellitus and chronic kidney disease, further increase their susceptibility to TB and its complications (Negin *et al*., 2015). Moreover, elderly individuals may face challenges in accessing healthcare services, resulting in delayed diagnosis and treatment initiation.

Migrants and displaced populations are particularly vulnerable to TB due to a range of factors, including overcrowded living conditions, limited access to healthcare, and social determinants of health (Woldesemayat, 2021). Disruptions in healthcare services during migration and displacement can further impede TB prevention, diagnosis, and treatment.

Prisoners represent another vulnerable population with a higher risk of TB transmission and infection. Overcrowding, limited access to healthcare, and suboptimal living conditions in correctional facilities contribute to the higher incidence and prevalence of TB among incarcerated individuals (Centers for Disease Control and Prevention, 2006).

Efforts to control TB must consider the unique challenges faced by these vulnerable populations and address their specific needs. Tailored interventions, including improved access to healthcare services, targeted screening and diagnostic strategies, and comprehensive treatment and support programs, are essential to reduce the burden of TB in these populations.

1.2 Physiology and Biochemistry of *Mycobacterium tuberculosis* Infections: Causative Agent, Clinical Manifestation, and Pathogenesis

1.2.1 Causative Agent

Mycobacterium tuberculosis, the causative agent of tuberculosis (TB), is a slow-growing, aerobic, gram-positive bacillus belonging to the Mycobacteriaceae family. It is characterised by its acid-fast staining properties due to the high lipid content in its cell wall. The unique cell wall composition of *M. tb* plays a crucial role in its virulence and ability to withstand the host immune response.

The mycobacterial cell wall is rich in complex lipids, particularly mycolic acids, which contribute to its impermeability and resistance to antimicrobial agents (Daffé & Draper, 1997). These mycolic acids form a hydrophobic outer layer that acts as a barrier against the host immune system and antimicrobial drugs. The cell wall also contains other lipids, such as trehalose dimycolate (TDM), which plays a role in modulating the host immune response.

M. tuberculosis has a relatively small genome but exhibits genetic variability, giving rise to different strains with varying degrees of virulence and drug resistance. Genetic diversity in *M. tb* is mainly attributed to mutations and genomic rearrangements, which can impact the bacterium's pathogenicity, transmissibility, and response to treatment (Gagneux, 2018). Understanding the genetic diversity of *M. tb* is crucial for epidemiological surveillance and the development of effective control strategies.

1.2.2 Clinical Manifestations

Tuberculosis can manifest in various clinical forms, depending on the site of infection and the immune status of the individual. Pulmonary TB is the most common form, accounting for approximately 85% of all TB cases. It primarily affects the lungs and is characterised by symptoms such as chronic cough, chest pain, haemoptysis (coughing up blood), fever, night sweats, and weight loss (Menzies *et al*., 2018). Radiographic findings may include pulmonary infiltrates, cavities, and lymphadenopathy.

Extrapulmonary TB occurs when the infection spreads beyond the lungs to other organs or tissues. The most commonly affected sites include the lymph nodes, bones, joints, central nervous system, and genitourinary tract. Extrapulmonary TB can present with

diverse clinical manifestations depending on the affected site. For example, tuberculous lymphadenitis may manifest as painless swelling of the lymph nodes, while skeletal TB can cause bone pain and deformities.

In individuals with compromised immune systems, such as those living with HIV/AIDS or those receiving immunosuppressive therapy, TB can progress rapidly, and cause disseminated or miliary TB. Disseminated TB occurs when *M. tb* spreads throughout the body via the bloodstream, resulting in widespread organ involvement. Clinical manifestations of disseminated TB can include fever, weight loss, hepatosplenomegaly, and respiratory distress. Miliary TB refers to the dissemination of *M. tb* in a diffuse, millimetre-sized pattern, resembling millet seeds, throughout multiple organs. This form of TB is associated with high mortality rates if left untreated (Baykan *et al*., 2022).

1.2.3 Pathogenesis

The pathogenesis of TB involves a complex interplay between the host immune response and the strategies employed by *M. tb* to establish and maintain infection. Upon inhalation, aerosolised *M. tb* bacilli are deposited in the alveoli of the lungs and are phagocytosed by alveolar macrophages, which are key players in the innate immune response.

Mycobacterium tuberculosis has developed various mechanisms to evade the host immune response and survive within macrophages. The bacterium can inhibit phagosome-lysosome fusion, preventing the formation of phagolysosomes where intracellular pathogens are usually killed. Instead, *M. tb* resides within phagosomes, modifying the phagosome environment to create a favourable niche for its survival. Within the phagosome, *M. tb* is able to replicate and persist, leading to the formation of granulomas.

Granulomas are organised immune cell aggregates that serve as a host defence mechanism to contain the infection and prevent bacterial dissemination. Granulomas are composed of macrophages, lymphocytes, and other immune cells, and they encapsulate *M. tb*, forming a localised structure. The formation of granulomas involves a balance between pro-inflammatory and anti-inflammatory immune responses. Pro-inflammatory cytokines, such as tumour necrosis factor-alpha (TNF-α), play a crucial role in granuloma formation, while anti-inflammatory cytokines, such as interleukin-10 (IL-10), modulate the immune response to prevent tissue damage (Flynn & Chan, 2001).

TB manifests along a clinical spectrum, reflecting varying degrees of bacterial activity and immune response. The infection outcomes include clearance, latent TB infection (LTBI), incipient TB, subclinical TB, and active TB disease (Drain *et al*., 2018). LTBI represents a dormant state where bacteria remain viable but controlled by the immune system, carrying the risk of reactivation under immune compromise. Incipient TB describes a state where bacterial replication increases, but symptoms or signs are not yet clinically apparent. Subclinical TB progresses further, with bacterial burden detectable but minimal symptoms, bridging the gap to active disease.

Despite the containment within granulomas*, M. tb* can persist within the host for extended periods in a latent state, resulting in latent TB infection (LTBI). During LTBI, the bacteria remain dormant and do not cause active disease. However, latent infection carries the risk of reactivation, particularly in individuals with compromised immune systems, such as those with HIV infection or other immunosuppressive conditions. Reactivation of latent infection leads to the development of active TB disease, with the bacteria breaking out of the granulomas and causing tissue damage (Gideon & Flynn, 2011).

1.3 Predispositions and Measures of Prevention

1.3.1 Predispositions

Several factors contribute to the predisposition of individuals to TB infection and disease progression. Human immunodeficiency virus infection is a significant predisposing factor, as it leads to immune suppression and increases the risk of TB reactivation (World Health Organization., 2020). The interaction between HIV and TB is complex and synergistic, creating a dual epidemic that poses significant challenges for TB control efforts. HIV-infected individuals are estimated to have a 20 to 30 times higher risk of developing active TB compared to those without HIV. The immune system compromise caused by HIV infection allows *M. tb* to overcome host defences, leading to rapid disease progression.

Malnutrition is another important predisposing factor for TB. Inadequate intake of essential nutrients compromises the immune response, making individuals more susceptible to TB infection and increasing the risk of developing active disease (Löonnroth *et al*., 2010). Malnourished individuals have been found to have impaired cellular and humoral immune responses, reduced phagocytic activity, and altered cytokine production, all of which contribute to the increased susceptibility to TB. Additionally, malnutrition is often associated with poverty, overcrowding, and limited

access to healthcare, further exacerbating the risk of TB transmission and disease progression.

Diabetes mellitus has also been identified as a predisposing factor for TB. The association between diabetes and TB is bidirectional, with diabetes increasing the risk of TB infection and TB worsening glycaemic control and disease outcomes in individuals with diabetes (Sun *et al.*, 2022). Hyperglycaemia alters immune responses, impairs phagocytic function, and compromises the integrity of the lung epithelial barrier, facilitating the entry and establishment of *M. tb* in the lungs. The high prevalence of diabetes in many TB-endemic regions further contributes to the burden of TB.

Tobacco smoking is a well-established risk factor for various respiratory diseases, including TB. Smoking damages the respiratory tract, impairs mucociliary clearance, and weakens the immune system, making smokers more susceptible to TB infection and disease progression (Khan *et al.*, 2020). The toxic components of tobacco smoke, such as nicotine and reactive oxygen species, have been shown to impair immune responses, decrease antimycobacterial activity, and promote the growth and survival of *M. tb* within macrophages. Furthermore, smoking cessation has been found to reduce the risk of TB and improve treatment outcomes among TB patients.

Substance abuse, including alcohol and illicit drugs, is another predisposing factor for TB. Substance abuse can lead to impaired immune responses, increased susceptibility to infections, poor adherence to medication regimens, and high-risk behaviours such as needle sharing, which can contribute to TB transmission. Alcohol abuse has been associated with an increased risk of TB infection, disease progression, and poor treatment outcomes (Rehm *et al.*, 2009). Substance abuse treatment programs, integrated with TB control efforts, play a vital role in addressing this predisposing factor.

Certain medical conditions are also associated with an increased risk of TB. Chronic kidney disease, especially end-stage renal disease requiring dialysis, is a predisposing factor due to immune dysfunction and close contact with healthcare settings. Dialysis patients often have compromised immune systems, making them more susceptible to infections, including TB (Christopoulos *et al.*, 2009). Inadequate infection control practices and overcrowding in dialysis units can contribute to TB transmission among this vulnerable population. Similarly, occupational exposure to silica dust, as seen in industries such as mining and construction, can lead to the development of silicosis, a lung disease that increases the risk of TB infection and progression. Silica dust impairs

macrophage function, disrupts the immune response, and creates a favourable environment for the establishment and growth of *M. tb* within the lungs (Frieden *et al*., 2015).

Addressing these predispositions through targeted interventions and health promotion is crucial for effective TB prevention efforts. Strategies that focus on HIV prevention and treatment, nutritional support, diabetes management, tobacco cessation programs, and substance abuse treatment can significantly reduce the burden of TB in high-risk populations. Furthermore, comprehensive occupational health measures, including adequate ventilation, personal protective equipment, regular screening, and education for workers in high-risk industries, are essential to reduce occupational TB transmission.

1.3.2 Measures of Prevention

To combat tuberculosis (TB) effectively, a multifaceted approach that encompasses individual-level and population-level interventions is essential. The Bacillus Calmette-Guérin (BCG) vaccine has been a cornerstone of TB prevention efforts, especially in children. Although BCG provides partial protection against severe forms of TB, its efficacy in preventing pulmonary TB in adults has been variable (World Health Organization., 2020). As a result, researchers and public health authorities have focused on other preventive measures to further reduce the burden of TB.

One crucial aspect of TB prevention is the early diagnosis and prompt treatment of active TB cases. This approach helps limit the transmission of the bacteria to others and prevents the progression of the disease in affected individuals. Rapid diagnostic tests, such as GeneXpert, have revolutionised TB diagnosis by enabling the detection of TB and rifampicin resistance within a few hours (Zong *et al*., 2019). Additionally, efforts are ongoing to develop more sensitive and affordable point-of-care diagnostic tools to increase case detection rates, especially in resource-limited settings.

Infection control practices play a crucial role in preventing TB transmission, particularly in healthcare settings where the risk of nosocomial transmission is high. Implementing measures such as proper ventilation, the use of respiratory protective equipment, and adherence to standard precautions are vital to prevent healthcare-associated TB infections (Gerberding *et al*., 2005). Health facilities should develop and enforce infection control policies tailored to the local context to minimise the risk of transmission among patients and healthcare workers such as prompt identification and isolation of suspected

TB cases, regular TB screening for healthcare workers, and ensuring proper ventilation systems, including negative pressure rooms and HEPA filters. Additional measures include requiring N95 respirators for staff, providing masks to patients, conducting staff training on infection control, and establishing committees to monitor and update protocols.

Contact tracing and the management of close contacts of TB patients are pivotal in identifying individuals at risk of developing active TB. Identifying and screening these individuals for latent TB infection (LTBI) enables the timely initiation of preventive therapy, reducing the likelihood of TB reactivation. Isoniazid preventive therapy (IPT) is the most widely used regimen for LTBI treatment. Isoniazid preventive therapy involves the administration of isoniazid for a specified duration, typically six to nine months, to individuals with LTBI to prevent the development of active TB disease (World Health Organization., 2020). However, adherence to the full course of IPT remains a challenge, and alternative regimens, such as three months of weekly isoniazid and rifapentine, are being explored to enhance patient compliance.

In recent years, novel preventive strategies have emerged, targeting individuals at high risk of TB infection and progression to active disease. One such strategy is pre-exposure prophylaxis (PrEP), wherein individuals at substantial risk of TB, such as those living with HIV or household contacts of active TB cases, receive preventive treatment before exposure to the TB bacteria. Pre-exposure prophylaxis involves the administration of a combination of drugs, such as isoniazid and rifapentine, for a shorter duration than traditional IPT, usually three months (Sterling *et al*., 2011). This approach has shown promise in reducing the incidence of TB in high-risk populations.

Addressing social determinants of health is fundamental in tackling TB prevention, especially in vulnerable and marginalised populations. Poverty, overcrowded living conditions, and malnutrition are factors that fuel TB transmission. Strengthening social support systems, improving access to nutritious food, and providing adequate housing can contribute to reducing TB incidence. Furthermore, raising awareness about TB in communities and reducing stigma associated with the disease can encourage early healthcare seeking and promote treatment adherence.

Many measures have been developed to prevent , treat or curb infection and will be discussed in the following section (Global Tuberculosis Report 2023).

1.4 Current Treatments of Tuberculosis

1.4.1 Drug Regimens and Antibiotic Classes

The treatment of TB involves the administration of multiple antibiotics in combination to combat the disease and prevent the emergence of drug resistance (Mirzayev *et al*., 2021). The standard treatment for drug-susceptible TB consists of a four-drug regimen known as "first-line therapy." This regimen includes isoniazid, rifampicin, pyrazinamide, and ethambutol, which are typically administered for a period of six to nine months (Mirzayev *et al*., 2021).

Isoniazid and rifampicin are considered the cornerstone drugs in TB treatment due to their potent activity against *M. tb* (Zhang & Yew, 2015a). Isoniazid targets the synthesis of mycolic acids, which are essential components of the mycobacterial cell wall, while rifampicin inhibits RNA synthesis by binding to the bacterial RNA polymerase (Mitchison, 2000). Pyrazinamide acts on the bacterial metabolism, specifically disrupting the synthesis of fatty acids, and ethambutol inhibits the synthesis of arabinogalactan, an important component of the mycobacterial cell wall (Mitchison, 2000).

In cases of drug-resistant TB, alternative treatment regimens are necessary (Mirzayev *et al*., 2021). These regimens often involve the use of second-line drugs, such as fluoroquinolones (e.g., moxifloxacin, levofloxacin), injectable agents (e.g., amikacin, kanamycin), and other drugs (e.g., linezolid, bedaquiline) (Falzon *et al*., 2017). However, these regimens are more complex, longer in duration, and can be associated with increased toxicity (Falzon *et al*., 2017).

1.4.2 Treatment Regimens, Doses, and Toxicity

The duration of TB treatment depends on the type and extent of the disease. Standard drug-susceptible TB is typically treated with a six-month regimen, while cases with more extensive disease or drug resistance may require longer treatment durations (Nahid *et al*., 2016). The doses of TB medications are determined based on the patient's body weight, and adherence to the prescribed regimen is crucial to prevent treatment failure and the development of drug resistance (Blumberg *et al*., 2003).

Tuberculosis medications can cause various side effects, and close monitoring of patients is necessary throughout the treatment course (Blumberg *et al*., 2003). Hepatotoxicity, particularly associated with isoniazid and rifampicin, is a common side effect and requires regular monitoring of liver function (Tiberi *et al*., 2018). Gastrointestinal disturbances,

peripheral neuropathy, and ocular toxicity (associated with ethambutol) are also observed in some individuals (Tiberi *et al*., 2018). Regular monitoring of renal function, complete blood count, and other relevant parameters is essential to detect and manage adverse effects promptly (Tiberi *et al*., 2018).

1.4.3 Treatment Monitoring Strategies

Monitoring the response to TB treatment is crucial to evaluate treatment efficacy and detect treatment failure or relapse (Tiemersma *et al*., 2011). Various strategies are employed for monitoring patients undergoing TB treatment. Clinical evaluation, including monitoring symptoms, physical examination, and assessment of treatment response, is an integral part of monitoring (Steingart *et al*., 2006).

Microscopic examination of sputum smears is a widely used method to assess treatment response, but it has limitations in terms of sensitivity and specificity (Steingart *et al*., 2006). Culture-based methods, such as solid and liquid media cultures, provide a definitive diagnosis of TB and allow for drug susceptibility testing (Sotgiu *et al*., 2015). These methods help identify drug-resistant strains and guide adjustments to the treatment regimen accordingly (Sotgiu *et al*., 2015). Molecular diagnostic tests, such as the Xpert assay, have revolutionised TB diagnosis and treatment monitoring (Boehme *et al*., 2010). This assay enables rapid and accurate detection of *M. tb* and simultaneous testing for rifampicin resistance, facilitating early diagnosis of TB and appropriate adjustment of the treatment regimen (Boehme *et al*., 2010).

1.5 Drug Resistance in Tuberculosis

1.5.1 Types of Drug Resistance

Drug resistance in (TB) can be categorized based on resistance levels to anti-TB drugs, including multidrug-resistant TB (MDR-TB), extensively drug-resistant TB (XDR-TB), and totally drug-resistant TB (TDR-TB) (Dheda *et al*., 2014).

Multidrug-resistant TB (MDR-TB) is defined by resistance to isoniazid and rifampicin, the two most potent first-line drugs essential for TB treatment. MDR-TB significantly limits treatment options, necessitating the use of second-line drugs, which are less effective, more toxic, and require longer, costlier treatment regimens (Falzon *et al*., 2017). Extensively drug-resistant TB (XDR-TB) builds upon MDR-TB by including resistance to

fluoroquinolones and at least one injectable second-line drug, such as amikacin, kanamycin, or capreomycin. Often arising from improper MDR-TB treatment or direct transmission, XDR-TB results in worse treatment outcomes and poses a severe public health challenge due to the complexity of its management (Udwadia *et al*., 2012).

Totally drug-resistant TB (TDR-TB), while rare, represents the most severe resistance category, with strains resistant to all available first- and second-line drugs. This leaves healthcare providers without effective treatment options, often resulting in treatment failure and high mortality rates (Velayati *et al*., 2009).

The emergence of drug-resistant TB is driven by factors such as improper drug use, non-adherence to treatment, transmission of resistant strains, and inadequate healthcare systems. Limited access to quality diagnosis and treatment exacerbates the issue, contributing to its global spread (World Health Organization, 2020). Treatment requires specialized regimens involving combinations of second-line drugs, which often have reduced efficacy and higher toxicity compared to first-line options. The World Health Organization (WHO) has developed guidelines to support countries in managing MDR-TB and XDR-TB effectively, aiming to improve treatment outcomes (WHO Consolidated Guidelines on Tuberculosis Module 4: Treatment Drug-Resistant Tuberculosis Treatment 2022 Update).

1.5.2 Mechanisms of Drug Resistance

Drug resistance in *M. tb* arises primarily through spontaneous mutations in genes involved in drug targets or the metabolic pathways of anti-TB drugs (Zhang & Yew, 2015b). These genetic changes can alter the structure or function of the target proteins, resulting in reduced drug binding or efficacy. Key mutations include those in thekatG, inhA, and rpoB, which confer resistance to first-line drugs such as isoniazid and rifampicin (Seifert *et al*., 2015). In addition to mutations, the acquisition of resistance can occur through horizontal gene transfer, which involves the transfer of resistance-conferring genetic elements between different bacteria (Munita & Arias, 2016). This process contributes to the dissemination of drug-resistant strains within populations.

Recent studies have identified additional mutations and adaptations employed by M. tb to resist antimicrobials. For example, Dookie *et al*., 2018 highlight the diversity of target site mutations and describe physical and metabolic adaptations that enable M. tb to detoxify or desensitize itself against drugs. These adaptations include enzymatic

degradation of drugs, modification of target sites, and metabolic flux changes that reroute essential pathways to evade inhibition. Similarly, Sachan *et al*., 2023 and Datta *et al*., 2024 discuss mechanisms such as the upregulation of efflux pumps, which actively expel drugs from bacterial cells, and alterations in cell wall composition that hinder drug penetration.

Resistance to second-line drugs has also been linked to specific mutations. For instance, mutations in the *embB* gene, encoding the arabinosyltransferase enzyme involved in cell wall synthesis, are associated with ethambutol resistance (Telenti *et al*., 1997). Similarly, mutations in the *gyrA* and *gyrB* genes, encoding subunits of DNA gyrase, confer resistance to fluoroquinolones, while mutations in *rrs* and *eis* genes are linked to aminoglycoside resistance (Farhat *et al*., 2016).

The identification of resistance mechanisms has been facilitated by molecular and genetic-based assays. Whole-genome sequencing (WGS) and polymerase chain reaction (PCR)-based assays have significantly advanced the rapid detection of drug-resistant strains (Farhat *et al*., 2016). However, Rabaan *et al*., 2022,) emphasize that the repertoire of available assays has expanded to include high-throughput methods like next-generation sequencing (NGS) and CRISPR-based diagnostics. Despite these advances, the global distribution of mutations conferring resistance remains incomplete, particularly in regions like Africa and Asia. The Lancet Microbe (2024) highlights the need for broader data on clinical isolates to improve the sensitivity and specificity of existing assays.

In addition to genetic factors, environmental and physiological factors contribute to drug resistance. Alterations in bacterial metabolism, such as shifts in lipid metabolism, can enhance survival under drug pressure. The interplay of these factors with mutations underscores the complexity of resistance and the necessity of a multifaceted approach to combat it.

Addressing drug resistance requires integrating molecular diagnostics with global surveillance and expanding research into the epidemiology of resistance mutations. Efforts should also focus on improving diagnostic access in resource-limited settings, promoting adherence to treatment regimens, and strengthening healthcare systems to mitigate the spread of drug-resistant TB (Munita & Arias, 2016).

1.5.3 Implications for TB Treatment

The presence of drug-resistant TB poses significant challenges for treatment, requiring modified regimens that often involve the use of second-line drugs with potentially higher toxicity and reduced efficacy. These regimens are more complex and longer in duration compared to standard first-line therapy for drug-susceptible TB. In the case of MDR-TB, treatment typically includes a combination of second-line drugs, such as fluoroquinolones (e.g., moxifloxacin, levofloxacin), injectable agents (e.g., amikacin, kanamycin), and other drugs (e.g., linezolid, bedaquiline) (Dheda *et al*., 2014).

The treatment of drug-resistant TB requires close monitoring of treatment response, potential drug interactions, and the management of adverse effects. The prolonged duration of treatment increases the risk of poor adherence, which can lead to treatment failure and the development of additional drug resistance. Therefore, comprehensive support systems, including counselling, education, and social support, are essential to promote treatment adherence and minimise the risk of treatment failure (Tiberi *et al*., 2018).

In recent years, the development of new anti-TB drugs has provided additional treatment options for drug-resistant TB. Bedaquiline and delamanid, two novel drugs approved for the treatment of MDR-TB, have shown improved efficacy and safety profiles compared to some of the older second-line agents (Diacon *et al*., 2009). Bedaquiline, a diarylquinoline, targets the mycobacterial ATP synthase, disrupting the energy production of the bacterium. Delamanid, a nitroimidazole, inhibits the synthesis of mycolic acids, essential components of the mycobacterial cell wall. These drugs have demonstrated promising results in clinical trials, showing increased cure rates and improved treatment outcomes for patients with drug-resistant TB (Lienhardt *et al*., 2010).

However, despite the availability of these new drugs, their utilisation remains limited in many resource-limited settings due to factors such as high cost, limited availability, and challenges in implementing treatment programs. Access to these medications, particularly in low- and middle-income countries heavily burdened by drug-resistant TB, is crucial for improving treatment outcomes and reducing the global burden of drug-resistant TB (Mitnick *et al*., 2016). Efforts are underway to increase access and affordability of these drugs through partnerships, regulatory mechanisms, and funding initiatives.

In addition to the development of new drugs, research efforts are focused on identifying novel drug targets and exploring innovative treatment approaches. Advances in genomics and proteomics have facilitated the discovery of potential drug targets and the development of new compounds that can overcome drug resistance mechanisms (Dheda *et al*., 2017). Combination therapies, involving the use of multiple drugs with distinct mechanisms of action, are being investigated to enhance treatment efficacy and prevent the emergence of resistance.

Moreover, there is growing interest in exploring new drug delivery technologies to improve TB treatment outcomes. Targeted drug delivery systems aim to deliver drugs directly to the site of infection, increasing drug concentrations at the target site while minimising systemic exposure and reducing potential side effects. Slow-release drug delivery systems provide controlled release of drugs over an extended period, reducing the frequency of drug administration and improving patient adherence to treatment regimens. These technologies have the potential to enhance the effectiveness and convenience of TB treatment, particularly in the context of drug-resistant TB (Kumar *et al*., 2023).

The presence of drug-resistant TB necessitates modified treatment regimens with complex drug combinations and extended durations. The development of new anti-TB drugs provides hope for improved treatment outcomes, but challenges in accessibility and affordability persist (Patil *et al*., 2018). Addressing drug-resistant TB requires a multi-faceted approach involving research, diagnostics, treatment optimisation, and global collaboration to ensure effective management and control of this global health threat. Exploring new drug delivery technologies can further contribute to enhanced treatment outcomes and patient adherence in the fight against TB.

1.6 Nanoencapsulation of Drugs

1.6.1 Types of Nanoencapsulation

Nanoencapsulation, a modern approach in drug delivery, involves the encapsulation of therapeutic agents within nanoscale carriers. These carriers, such as liposomes, polymeric nanoparticles, and solid lipid nanoparticles, offer numerous benefits in terms of drug stability, controlled release, and targeted delivery (Kumar *et al*., 2023).

Liposomes, one of the most extensively studied nanoencapsulation systems, are lipid-based vesicles composed of phospholipids and cholesterol (Esim & Hascicek, 2020). These structures can accommodate both hydrophilic drugs within their aqueous core and

lipophilic drugs within the lipid bilayer. The amphiphilic nature of liposomes allows for the entrapment of a wide range of drugs, including small molecules, peptides, and nucleic acids. The composition and surface properties of liposomes can be tailored to optimise drug encapsulation efficiency, stability, and biocompatibility. Additionally, surface modifications of liposomes, such as the attachment of targeting ligands, enable active targeting to specific cells or tissues, enhancing therapeutic efficacy and reducing off-target effects.

Polymeric nanoparticles represent another versatile class of nanocarriers for drug delivery. These nanoparticles are composed of biocompatible polymers, such as poly(lactic-co-glycolic acid) (PLGA) or chitosan, which offer controlled release properties and biodegradability (Jain, 2000). Polymeric nanoparticles can encapsulate both hydrophilic and hydrophobic drugs, providing a platform for the delivery of a diverse range of therapeutics, including anticancer drugs, antibiotics, and anti-inflammatory agents. The physicochemical properties of the polymer, such as molecular weight and ratio of co-monomers, can be adjusted to control the release kinetics of the encapsulated drug and optimise its therapeutic efficacy. Furthermore, the surface of polymeric nanoparticles can be modified to enhance stability, prolong circulation time in the bloodstream, and enable targeted delivery to specific cell types or tissues.

Solid lipid nanoparticles (SLNs) have emerged as a promising nanoencapsulation system due to their unique properties (Jamous *et al*., 2023). These nanoparticles consist of lipids in a solid state at room temperature, forming a colloidal matrix that can encapsulate lipophilic drugs. The lipid composition and particle size of SLNs can be precisely engineered to achieve desired drug release profiles, including sustained release and controlled release kinetics. Solid lipid nanoparticles provide enhanced drug stability, protecting drugs from degradation and promoting their accumulation at the target site. The biocompatible nature of the lipid matrix allows for reduced toxicity and improved biocompatibility compared to other carrier systems. Additionally, SLNs can be functionalised with surface modifiers, such as polymers or ligands, to optimise their physicochemical properties and target specific tissues or cells.

The development of nanoencapsulation systems has revolutionised drug delivery, offering significant advantages in terms of improving drug stability, enhancing therapeutic efficacy, and enabling targeted delivery (Farokhzad & Langer, 2009). These nanocarriers can protect drugs from enzymatic degradation, prevent premature release, and increase drug accumulation at the desired site of action. Furthermore, the controlled release

capabilities of nanoencapsulation systems allow for sustained drug release, reducing the frequency of administration and improving patient compliance. The ability to target specific tissues or cells through surface modifications opens new possibilities for personalised medicine and precision therapeutics, minimising off-target effects and maximising therapeutic outcomes.

1.6.2 Advantages of Nanoencapsulation of Rifampicin and Other TB Drugs

The nanoencapsulation of rifampicin and other TB drugs offers significant advantages in TB treatment, addressing challenges such as poor bioavailability, limited drug targeting, and inadequate drug release kinetics. These advantages are particularly relevant for the effective management of TB (Ahmad *et al*., 2015).

Nanoencapsulation enhances the bioavailability and pharmacokinetics of TB drugs, including that for rifampicin. The encapsulation of these drugs within nanocarriers protects them from degradation and enzymatic metabolism, preventing their premature elimination from the body. As a result, the drugs can circulate in the bloodstream for longer periods, increasing their availability for interaction with the target cells or tissues. The improved bioavailability achieved through nanoencapsulation can lead to enhanced therapeutic outcomes and reduced dosage requirements (Pinto Reis *et al*., 2006).

In the case of TB, targeted drug delivery is crucial for optimising treatment efficacy while minimising off-target effects. Nanoencapsulation allows for the functionalisation of nanocarriers with ligands that have a specific affinity for *M. tb*-infected or infectable cells or tissues. These ligands can facilitate the targeted delivery of the encapsulated drugs to the site of infection, such as the lungs in pulmonary TB. By enhancing the interaction and uptake of the nanocarriers by the target cells, targeted drug delivery can maximise the drug concentration at the site of action, potentially reducing the dosage required and minimising systemic toxicity (Pinto Reis *et al*., 2006).

Another significant advantage of nanoencapsulation is the ability to achieve controlled drug release kinetics. This feature is particularly valuable in TB treatment, which often requires long-duration therapy. The sustained release of TB drugs from nanocarriers ensures that therapeutic levels are maintained over an extended period, allowing for continuous drug action and reducing the frequency of drug administration. This can address the challenge of poor patient adherence, as patients may find it difficult to comply with complex and frequent dosing regimens. Controlled release formulations can improve

patient convenience, simplify treatment protocols, and ultimately enhance treatment outcomes (Prabhu *et al*., 2015).

Moreover, nanoencapsulation can enable the co-delivery of multiple drugs within a single nanocarrier, providing a platform for combination therapy. This approach is especially relevant in the context of MDR-TB and XDR-TB, where the use of multiple drugs is necessary for effective treatment. Co-encapsulation of different drugs within nanocarriers allows for synergistic effects, improved drug ratios, and reduced drug resistance development. This approach has the potential to enhance the effectiveness of TB treatment, especially in cases where drug resistance poses a significant challenge (Pérez-Herrero & Fernández-Medarde, 2015).

Nanoencapsulation of rifampicin and other TB drugs offers several advantages in TB treatment. These include enhanced bioavailability, targeted drug delivery, controlled release kinetics, and the potential for combination therapy. By overcoming limitations associated with conventional drug formulations, nanoencapsulation holds great promise for improving the effectiveness and patient outcomes in the management of TB.

1.7 Ligand Targeting Nanoencapsulation Drugs

Ligand targeting nanoencapsulation takes the nanoencapsulation technology further by attaching specific ligands to the surface of nanoparticles, which can bind to corresponding receptors on target cells, thereby enhancing the specificity and efficacy of drug delivery (Peer *et al*., 2007).

The design of ligand-targeted nanoparticles involves the conjugation of a ligand known to have affinity for certain cell surface receptors that are overexpressed on diseased cells, such as cancer cells or infected host cells. These ligands can be antibodies, peptides, small molecules, or aptamers that provide the homing functionality to the nanoparticles (Allen & Cullis, 2013). Once the ligand-receptor interaction occurs, the nanoparticles can be internalised via receptor-mediated endocytosis, ensuring that the drug payload is delivered directly into the target cells (Bertrand *et al*., 2014).

In the context of cancer therapy, ligand targeting nanoencapsulation is particularly valuable due to the aberrant expression of certain receptors on tumour cells. For example, folic acid-modified nanoparticles have been used to target tumour cells overexpressing

the folate receptor, resulting in enhanced uptake of chemotherapeutic agents by the cancerous cells and minimised adverse effects on healthy tissue (Xu *et al*., 2015).

The success of ligand targeting nanoencapsulation hinges on several factors, including the choice of ligand, the stability of the ligand-nanoparticle conjugate, the size and charge of nanoparticles, and the drug release kinetics. The encapsulation efficiency and the release profile of the drug must be carefully optimised to ensure that the therapeutic concentration of the drug is maintained at the site of action for a sufficient duration to exert the desired biological effect (Patra *et al*., 2018).

Ligand targeting nanoencapsulation not only allows for increased concentration of the drug at the target site but also can improve the pharmacokinetic profile of the drug, reducing the frequency of dosing and potentially enhancing patient compliance. Moreover, by protecting the drug from premature degradation, this technology can also address challenges related to the solubility and stability of therapeutic agents (Carita *et al*., 2018).

Overall, ligand targeting nanoencapsulation represents a promising strategy in precision medicine, enabling the development of highly selective drug delivery systems that could revolutionise the treatment of various diseases. Continuous advancements in nanotechnology, ligand chemistry, and drug formulation are expected to further expand the capabilities and applications of this approach (Mura *et al*., 2013).

1.7.1 Mycolate Coated Nanoparticles

Ligand targeting strategies utilising mycolate-coated nanoparticles have emerged as a promising approach to enhance the delivery of anti-TB drugs. Mycolates, unique lipid components of the mycobacterial cell wall, have been harnessed for their potential in specific binding to *M. tb*-infected cells, thus facilitating targeted drug delivery. In addition to their targeting properties, mycolic acids, the major constituents of mycolates, possess intrinsic immunomodulating characteristics that further contribute to the efficacy of mycolate-coated nanoparticles in TB treatment (Lemmer *et al*., 2015).

Mycolic acids have been found to interact with the immune system, modulating the host response during *M. tb* infection. These lipids can act as pathogen-associated molecular patterns (PAMPs) that engage with pattern recognition receptors (PRRs) on immune cells, including macrophages and dendritic cells (Korf *et al*., 2005). This interaction

triggers downstream signalling cascades and immune responses, influencing the outcome of the infection. The immunomodulating effects of mycolic acids include the regulation of cytokine production, modulation of antigen presentation, and activation of immune cells.

By incorporating mycolic acids into the coating of nanoparticles, the immunomodulating characteristics of these lipids can be harnessed to enhance the therapeutic effect of anti-TB drugs. The interaction of mycolate-coated nanoparticles with immune cells can potentially promote immune activation and the generation of an effective immune response against *M. tb*. This immune response may involve the production of pro-inflammatory cytokines, such as tumour necrosis factor-alpha (TNF-α) and interleukin-12 (IL-12), which play crucial roles in controlling mycobacterial growth and stimulating adaptive immunity (Korf *et al*., 2005).

Furthermore, mycolate-coated nanoparticles can influence antigen presentation by immune cells, particularly dendritic cells. These nanoparticles can be taken up by dendritic cells, which serve as key antigen-presenting cells in the immune system. Through the presentation of mycolate-coated nanoparticles to T cells, dendritic cells can initiate specific immune responses and contribute to the generation of protective immunity against TB. This interaction between mycolate-coated nanoparticles and dendritic cells can promote the activation of T cells, leading to the production of T-helper 1 (Th1) cytokines, such as interferon-gamma (IFN-γ), that are essential for controlling *M. tb* infection (Jia *et al*., 2018).

The incorporation of mycolate-coated nanoparticles into the delivery of anti-TB drugs not only provides targeted drug delivery but also harnesses the immunomodulatory properties of mycolic acids. By combining the benefits of targeted drug delivery and immunomodulation, mycolate-coated nanoparticles offer a multifaceted approach to TB treatment. These nanoparticles can enhance the localisation of drugs to the site of infection while simultaneously activating the immune system, thereby promoting a more effective and comprehensive response against *M. tb* (Nabi *et al*., 2020).

In conclusion, mycolate-coated nanoparticles hold great potential as a ligand targeting strategy for the delivery of anti-TB drugs. The use of mycolates, unique lipid components of the mycobacterial cell wall, allows for specific binding to *M. tb*-infected cells, enabling the selective delivery of drugs to the site of infection. Moreover, the immunomodulating characteristics of mycolic acids can further enhance the efficacy of mycolate-coated

nanoparticles by promoting immune activation and antigen presentation. Continued research in this field will contribute to optimising the immunotherapeutic potential of mycolate-coated nanoparticles in the context of TB treatment.

1.8 Conclusion

Tuberculosis remains a significant global health challenge, necessitating continuous efforts to improve diagnosis and treatment strategies. The standard TB drug regimens, although effective, face limitations such as long treatment durations, poor patient adherence, and the emergence of drug resistance.

Nanoencapsulation of TB drugs offer a promising approach to overcome these challenges. Through the use of nanoscale carriers, such as liposomes, polymeric nanoparticles, and solid lipid nanoparticles, the bioavailability and pharmacokinetics of drugs like rifampicin can be enhanced. Targeted delivery to the site of infection, facilitated by ligand targeting strategies, allows for improved treatment efficacy while minimising off-target effects.

The development of mycolate-coated nanoparticles and other ligand-targeted nanosystems holds great potential in the field of TB drug delivery. These systems enable specific binding to *M. tb*-infected cells and efficient drug delivery, enhancing treatment outcomes and reducing systemic toxicity.

However, further research is needed to optimise these nanoencapsulation strategies, evaluate their long-term safety and efficacy, and overcome challenges related to scalability and cost-effectiveness. By harnessing the potential of nanotechnology, we can strive towards more effective and patient-friendly treatment options for TB.

1.9 Research Overview

Given the above, it is clear TB remains a global health challenge, causing significant morbidity and mortality worldwide. The emergence of drug-resistant strains of *M. tb*, has further complicated treatment efforts. Conventional anti-TB therapies face limitations in terms of efficacy, drug resistance, and delivery to the target site. However, recent advancements in nanotechnology have provided new opportunities for tackling these challenges. One promising approach is ligand targeting through mycolate, a key component of the *M. tb* cell wall.

Ligand targeting involves attaching specific ligands to the surface of nanocarriers, such as nanoparticles or liposomes, to enhance their affinity for *M. tb* cells. Mycolate, a unique lipid found in the *M. tb* cell wall, can serve as a valuable ligand for targeting drug-loaded nanocarriers to *M. tb*-infected cells. By functionalising nanocarriers with mycolate ligands, it is possible to improve their specificity and binding affinity to *M. tb*, thereby increasing drug accumulation at the infection site and reducing off-target effects.

In this work, the choice of nanoparticle for nanoencapsulation was poly(lactic-co-glycolic acid) (PLGA). Poly(lactic-co-glycolic acid) is a biodegradable and biocompatible polymer that has been extensively investigated for drug delivery applications. Its tuneable properties, such as particle size, surface charge, and degradation rate, make it an attractive candidate for encapsulating drugs and targeting *M. tb* cells. When combined with mycolate ligands, PLGA nanoparticles can facilitate the selective delivery of rifampicin, a first-line anti-TB drug, to *M. tb*-infected cells.

Rifampicin, encapsulated within PLGA nanoparticles functionalised with mycolate ligands, offers several advantages. Firstly, PLGA nanoparticles provide a stable and protective environment for the drug, preventing its degradation and promoting sustained release. Secondly, the mycolate ligands on the nanoparticle surface enhance the interaction with *M. tb* cells, promoting targeted uptake and intracellular drug delivery. This combination of PLGA nanoparticles and mycolate ligands offers a synergistic effect in improving the therapeutic efficacy of rifampicin against TB.

This dissertation aimed to investigate the potential of Rifampicin nanoencapsulation, particularly through mycolate ligand targeting using PLGA nanoparticles, as a novel approach for improving TB therapy in an infected guinea pig model. By exploring the benefits of targeted drug delivery and the utilisation of mycolate ligands, this research seeks to contribute to the development of more effective and efficient treatments for TB.

1.10 Research Objectives

The main objectives of this dissertation were as follows:

1. To develop and characterise nanoencapsulated particles containing anti-TB drugs through *in vitro* production and testing.

2. To establish a pilot guinea pig model of experimental *M. tb* infection for preliminary evaluation of nanoencapsulated drug efficacy, focusing on generating foundational data for model validation rather than statistical significance.
3. To provide a detailed analysis of pilot study results, emphasising the establishment of a drug research testing platform and the exploration of trends in treatment efficacy, safety, and delivery mechanisms.
4. To propose a framework for future research based on pilot findings, including recommendations for scaling the model, optimising drug formulations, and addressing the challenges identified in preliminary testing.

1.11 Study Aim and Hypothesis

This study aims to establish a guinea pig model for evaluating nanoparticle-encapsulated rifampicin, incorporating mycolic acids as targeting ligands, as a foundation for future investigations. It seeks to generate preliminary data on the distribution, safety, and potential efficacy of this approach, providing a basis for subsequent hypothesis-driven research. The study hypothesizes that nanoparticle-based formulations of rifampicin may enhance antibacterial efficacy and targeted delivery relative to standard treatments. While no definitive hypothesis on treatment efficacy or reduced off-target effects will be tested directly due to the pilot nature of the study, it will conduct statistical analyses to determine the achieved statistical power based on standard deviations observed, as well as calculate the sample size needed for future studies to test hypotheses such as the enhanced delivery and efficacy of nanoparticle-encapsulated rifampicin in guinea pigs infected with high *M. tb* bacillary loads.

2. DEVELOPMENT OF A NANO-FORMULATION ENCAPSULATING RIFAMPICIN IN A POLY DL, LACTIC-CO-GLYCOLIC ACID (PLGA) POLYMER INCORPORTING MYCOLIC ACIDS AS TARGETING LIGAND

2.1 Introduction

Among various nanocarriers, polymeric nanoparticles composed of poly(dl, lactic-co-glycolic acid) (PLGA) have emerged as promising platforms in drug delivery applications. PLGA nanoparticles offer several advantages, including excellent biocompatibility, controlled release properties, and the ability to protect drugs from degradation and premature elimination (Makadia & Siegel, 2011). These characteristics make them well-suited for the encapsulation of rifampicin, a first-line anti-TB drug, within PLGA nanoparticles.

Encapsulation of rifampicin within PLGA nanoparticles provides several benefits for TB treatment. Firstly, the encapsulation enhances the stability of rifampicin, protecting it from degradation and preserving its therapeutic activity. Rifampicin is susceptible to degradation due to acidic pH, oxidative stress, and exposure to heat and light, which can significantly reduce its efficacy (Bala *et al*., 2004). This is particularly important for rifampicin, which is known for its poor solubility and susceptibility to degradation. The PLGA matrix acts as a barrier, preventing drug degradation and maintaining the drug's integrity during storage and administration.

Moreover, the encapsulation of rifampicin within PLGA nanoparticles improves its bioavailability. PLGA nanoparticles have been shown to enhance drug absorption by increasing the surface area available for drug release and improving drug solubility (Pandey *et al*., 2005). These nanoparticles can effectively deliver the drug to the target site of infection, such as *M. tb*-infected cells, thereby increasing the concentration of rifampicin at the desired site.

Additionally, PLGA nanoparticles enable controlled release of rifampicin, ensuring sustained therapeutic levels over an extended period (Danhier *et al*., 2012a). The controlled release mechanism of PLGA nanoparticles allows for a prolonged and steady release of the encapsulated drug, reducing the frequency of drug administration and improving patient compliance. This sustained release profile is particularly advantageous in TB treatment, where long-duration therapy is required.

To further enhance the targeting efficiency of rifampicin to *M. tb*-infected cells, mycolic acids, unique lipid components of the *M. tb* cell wall, can be incorporated as targeting ligands within the PLGA nanoparticles. Mycolic acid incorporation into PLGA particles has demonstrated the ability to guide the particles into *M. tb*-infected cells, thereby potentially promoting drug accumulation at the site of infection, efficient drug delivery and minimising off-target effects (Lemmer *et al.,* 2015).

The development of a targeted nano-formulation encapsulating rifampicin within PLGA nanoparticles incorporating mycolic acids as targeting ligands holds significant potential in revolutionising TB therapy. This targeted nano-formulation aims to enhance the delivery of rifampicin to *M. tb*-infected cells, thereby improving treatment efficacy and reducing off-target effects. The specific recognition and binding of PLGA nanoparticles to infected cells mediated by mycolic acids can potentially improve the selectivity of drug delivery and minimise the systemic toxicity associated with non-targeted therapies.

In this study, the "semi-continuous" double emulsion solvent evaporation freeze-drying technique was employed to develop the nano-formulation for encapsulating rifampicin within PLGA nanoparticles and incorporating mycolic acids as targeting ligands. This technique allows for the controlled and efficient encapsulation of rifampicin within the PLGA nanoparticles, preserving its stability and enabling targeted drug delivery to *M. tb*-infectable cells.

Several techniques can be employed for the production of poly(dl, lactic-co-glycolic acid) (PLGA) nanoparticles, including nanoprecipitation, solvent evaporation, and emulsion solvent diffusion methods. These techniques offer distinct advantages in terms of particle size control, drug loading efficiency, and scalability.

The nanoprecipitation method involves the rapid mixing of a polymer solution with a non-solvent, resulting in the precipitation of nanoparticles. This technique allows for precise control over particle size by adjusting the mixing parameters and the concentration of polymer and non-solvent. It offers high drug loading efficiency due to the quick formation of nanoparticles, which can encapsulate a large amount of the drug. However, this method may have limitations in terms of scalability, as the production of nanoparticles on a large scale can be challenging (Lamprecht *et al*., 1999).

The solvent evaporation method entails the dissolution of the polymer and the drug in an organic solvent, followed by the evaporation of the solvent to form nanoparticles. Particle size control can be achieved by varying factors such as the polymer concentration, the

choice of organic solvent, and the method of solvent evaporation (e.g., rotary evaporation, freeze-drying). This technique offers excellent drug loading efficiency as the drug is dissolved within the polymer matrix. It is also relatively scalable, making it suitable for large-scale production. However, there may be challenges in obtaining uniform particle sizes and preventing aggregation during the evaporation process (Mai Hoa *et al*., 2009).

The emulsion solvent diffusion method involves the formation of a water-in-oil (W/O) emulsion, where the polymer and drug are dissolved in an organic solvent and then emulsified in an aqueous phase. The diffusion of the organic solvent into the aqueous phase leads to the formation of nanoparticles. This technique enables precise control over particle size by adjusting the emulsion parameters, such as the stirring speed, emulsifier concentration, and solvent evaporation rate. It offers good drug loading efficiency and scalability. However, there can be limitations in terms of particle size distribution and stability, as well as potential emulsification issues (Mai Hoa *et al*., 2009).

Among these techniques, the "semi-continuous" double emulsion solvent evaporation freeze-drying technique is often preferred for the encapsulation of rifampicin within PLGA nanoparticles. This technique involves the preparation of a water-in-oil-in-water (W/O/W) double emulsion, where the drug is first dissolved in an aqueous phase, which is then emulsified in an organic phase containing the polymer. Subsequently, the resulting W/O/W emulsion is freeze-dried to remove the solvents and obtain nanoparticles. This technique offers several advantages. It allows for precise control over particle size and drug loading efficiency by adjusting the emulsion parameters. The freeze-drying step enhances the stability of the nanoparticles and facilitates the formation of porous structures, which can improve the release kinetics of the drug. Moreover, the "semi-continuous" approach allows for efficient production and scalability, making it suitable for large-scale manufacturing. In this study the “semi-continuous" approach was used as the solvent evaporation technique (Hoa *et al*., 2012).

To characterise the developed formulation, various techniques were employed. Size and size distribution (polydispersity index) measurements were performed using dynamic light scattering (DLS) with a Zetasizer NanoZS instrument (Malvern Instruments Ltd., UK). The surface potential of the nanoparticles was determined by laser Doppler electrophoresis using the same instrument. Additionally, the surface morphology of the nanoparticles was examined using scanning electron microscopy (SEM). NPs were deposited onto aluminium stubs, coated with carbon in a glow-discharge apparatus, and visualised under SEM.

Quantification of rifampicin within the nanoparticles was achieved using a direct method. This method involved the extraction of rifampicin from the nanoparticles, followed by UV-VIS Spectrometry analysis to determine the drug content.

In conclusion, the development of a nano-formulation encapsulating rifampicin within PLGA nanoparticles incorporating mycolic acids as targeting ligands offers a promising approach for TB therapy. This targeted delivery system enhances the stability, bioavailability, and controlled release of rifampicin while facilitating specific recognition and binding to *M. tb*-infectable cells. The successful development of this formulation has the potential to significantly improve TB treatment outcomes by providing a more efficient and personalised therapeutic strategy.

2.2 Materials and Methods

2.2.1 Preparation of Nanoparticles for guinea pig experiments

The "semi-continuous" double emulsion solvent evaporation freeze-drying technique was employed in this study, with modifications based on the method described by Lemmer *et al.* in 2015. Initially, 1000 mg of poly(dl, lactic-co-glycolic acid) (PLGA) with a molecular weight range of 45000-75000 and a 50:50 lactide-to-glycolide ratio was dissolved in 60 ml of dichloromethane (DCM) at a concentration of 1.25% weight/volume (w/w).

For the formulation of particles containing mycolic acids (MA), isolated mycolic acids from *Mycobacterium tuberculosis* (*M. tb*) (M4537, Sigma-Aldrich, USA) were incorporated. Specifically, 20 mg of mycolic acids (equivalent to 1.7 µmol) was dissolved in 20 ml of DCM and added to the PLGA solution while stirring.

To create the first water-in-oil (w/o) emulsion, 20 ml of a 2% (w/v) polyvinyl alcohol (PVA) solution was added to the PLGA and mycolic acid mixture. The emulsion was homogenised at 10,000 rpm for 5 minutes using a bench-top homogenizer (IKA T25 Digital Ultra Turrax, United Scientific, South Africa) maintained at 4°C.

For the nanoparticles containing rifampicin (RIF), RIF (600 mg, equivalent to 729 µmol) was dissolved in the pre-dissolved PLGA solution. This ensured the encapsulation of rifampicin within the PLGA nanoparticles.

Subsequently, the second water-in-oil-in-water (w/o/w) emulsion was formed by adding 100 ml of a 1% (w/v) PVA solution dropwise to the w/o emulsion while homogenizing the mixture at 10,000 rpm. Following this, the first emulsion was added to an additional 150

ml of a 1% (w/v) PVA solution, and the emulsion was homogenized for an additional 3 minutes.

The resultant emulsion was then stirred using a magnetic bench top stirrer at 500 rpm overnight at room temperature and atmospheric pressure to facilitate the evaporation of the organic solvent (DCM). This step allowed for the formation of PLGA nanoparticles with the incorporated drug (rifampicin) and mycolic acids.

To recover the PLGA nanoparticles, centrifugation was performed at 33,000 rcf for 15 minutes. The supernatant obtained after the first centrifugation was further subjected to centrifugation to ensure maximum recovery of the nanoparticles.

The resulting PLGA nanoparticles were then dispersed in a 0.1% (w/v) trehalose solution to protect the particles during the freeze-drying process. The dispersion was subsequently lyophilised using a Virtis® Benchtop ™ 2K (SP Industries, USA) freeze dryer, resulting in the production of dry nanoparticles. Freeze drying was done under the following conditions: freezing at -40°C, primary drying at -20°C with 100–300 millitorr vacuum pressure, and secondary drying at 25°C, processing approximately 100 ml per batch over 48–72 hours. Alternatively, the particles were dispersed in Eudragit® L100 (Evonik Operations GmbH, Germany), a biocompatible polymer, and subjected to a second round of lyophilisation.

This methodology allows for the controlled and efficient encapsulation of rifampicin within PLGA nanoparticles, incorporating mycolic acids as targeting ligands. The freeze-drying process further preserves the stability of the nanoparticles, facilitating their long-term storage and reconstitution when needed.

A total of five batches of poly(dl, lactic-co-glycolic acid) (PLGA) nanoparticles containing rifampicin (RIF) only were prepared and labelled as 85.1 to 85.5. Additionally, three batches of PLGA nanoparticles loaded with mycolic acids (MA) and rifampicin were synthesised and labelled as 85.6 to 85.8. To assess the total yield, the lyophilised nanoparticles from each batch were carefully weighed using an analytical balance (Sartorius TE64 Analytical Balance, Germany) with a high degree of accuracy. The analytical balance provided the necessary sensitivity to detect even small changes in mass, ensuring reliable measurements of the freeze-dried products.

2.2.2 Nanoparticle characterisation

The collected nanoparticles (NPs) obtained after the lyophilisation process underwent rigorous characterisation to determine their size distribution, polydispersity index (PDI), surface potential, and surface morphology.

Size and size distribution analysis of the nanoparticles were performed using dynamic light scattering (DLS) on a Zetasizer NanoZS instrument (Malvern Instruments Ltd., UK). The NPs were suspended in PBS, pH 7.4, and the intensity fluctuations of the scattered light were measured. The data obtained from the DLS analysis provided information about the average size and the distribution of particle sizes within the sample.

The surface potential of the nanoparticles was assessed using laser Doppler electrophoresis (LDE) with the Zetasizer NanoZS instrument. This technique measures the velocity of charged particles under the influence of an electric field, allowing for the determination of the surface charge of the nanoparticles. The measurements were conducted to gain insights into the surface properties and stability of the NPs.

To examine the surface morphology of the nanoparticles, scanning electron microscopy (SEM) was employed (Zeiss Ariga Scanning Electron Microscope (Zeiss Ariga SEM). Prior to imaging, the NPs were deposited onto aluminium stubs and coated with a thin layer of carbon using a glow-discharge apparatus. This carbon coating enhances the conductivity of the samples and provides improved imaging during SEM analysis. The coated NPs were then imaged using a scanning electron microscope, which allowed for high-resolution visualisation of the surface structure and morphology of the nanoparticles.

The combination of dynamic light scattering, laser Doppler electrophoresis, and scanning electron microscopy provided a comprehensive understanding of the size distribution, surface potential, and surface morphology of the developed PLGA nanoparticles encapsulating rifampicin and incorporating mycolic acids as targeting ligands.

2.2.3 Quantification of Rifampicin within Nanoparticles

The quantification of rifampicin (RIF) encapsulated within the nanoparticles (NPs) was performed using the direct method, which involved the dissolution of the lyophilised NPs and subsequent measurement of RIF concentration in the resulting solution.

To initiate the quantification process, the lyophilised NPs were suspended in analytical grade chloroform (Sigma-Aldrich, USA) at a concentration of 1 mg/ml. The suspension

was kept at room temperature (RT) with continuous agitation overnight to ensure complete dissolution of the NPs and release of the encapsulated RIF into the solvent.

After the dissolution step, the suspension was subjected to centrifugation to separate the white precipitate, mainly consisting of the polymeric matrix of the NPs, from the supernatant. The supernatant, which contained the released RIF, was carefully collected for further analysis.

A standard curve was prepared fresh every day using known concentrations of pure RIF. The standard solutions covered a suitable concentration range to establish a linear relationship between the absorbance and the concentration of RIF. This standard curve served as a reference for quantifying the concentration of RIF in the NP samples.

The supernatant from the NP suspension was appropriately diluted if necessary to ensure that the RIF concentration fell within the linear range of the standard curve. Spectrophotometry (UV/VIS) was employed to measure the absorbance of the samples at 347 nm and 475 nm, corresponding to the characteristic absorption peaks of RIF.

The absorbance measurements were performed at 347 nm and 475 nm, corresponding to the characteristic absorption peaks of RIF. The absorbance values obtained from the samples were compared to the standard curve to determine the concentration of RIF encapsulated within the NPs.

UV/VIS spectrophotometry is a widely used technique for quantification due to its high sensitivity and accuracy. The specific wavelengths were selected based on the absorption characteristics of RIF, ensuring optimal detection and measurement of the drug.

The direct quantification method used in this study provided a reliable and straightforward approach for determining the amount of RIF released from the NPs. By utilising UV/VIS spectrophotometry, precise measurements of RIF concentration could be obtained, enabling the evaluation of drug loading efficiency and the optimisation of the NP formulation.

2.3 Results

2.3.1 Nanoparticle production yields

Two formulations were prepared following the procedure outlined in Section 2.2.1 (Figure 1). The first formulation consisted of PLGA encapsulating rifampicin (RIF), denoted as

RIF/PLGA. The second formulation included PLGA encapsulating rifampicin with mycolic acid as a targeting ligand (MA), referred to as PLGA/RIF/MA.

For the RIF/PLGA samples, a total of five batches were synthesised and denoted as 85.1 to 85.5. The production of these batches resulted in a combined yield of 12.928 g of PLGA/RIF, which was specifically intended for use in the Guinea pig experiment, as indicated in Table 1 and described in Chapter 3.

In parallel, the PLGA/RIF/MA samples were prepared in three separate batches labelled as 85.6 to 85.8. These batches yielded a total of 9.319 g of PLGA/RIF/MA, as summarised in Table 2. This formulation was also intended for use in the Guinea pig experiment. Yield for the particles with or without the inclusion of MA were similar. The production yield of the encapsulation process was ~ 60 % of particles over the initial solid mass of the reactants.

Figure 1: Representative Images of Nanoparticle Emulsions. This figure showcases representative images of the nanoparticle emulsions produced during the formulation process. The left image displays the emulsion after homogenization, while the right image shows the emulsion after overnight stirring to evaporate the solvent. These images provide a visual representation of the nanoparticles in their emulsified state.

Table 1: Production Yield of PLGA/RIF Samples. This table presents the yield of PLGA encapsulating rifampicin (RIF) for each batch produced. The five batches, labelled as 85.1 to 85.5, were synthesised following the outlined procedure. The table includes the batch labels and the corresponding total mass produced in grams.

Batch	Total Mass Produced (g)
85.1	1,1250
85.2	1,1107
85.3	3,7362
85.4	3,5059
85.5	3,4506
Total PLGA/RIF	12,928

Table 2: Production Yield of PLGA/RIF/MA Samples. This table presents the yield of PLGA encapsulating rifampicin with mycolic acid as a targeting ligand (PLGA/RIF/MA). The formulation was prepared in three separate batches, labelled as 85.6 to 85.8. The table includes the batch labels and the corresponding total mass produced in grams.

Batch	Total Mass Produced (g)
85.6	3,0138
85.7	3,0569
85.8	3,2481
Total PLGA/RIF	9,319

The amounts of PLGA/RIF and PLGA/RIF/MA produced are sufficient to provide the necessary quantities needed in the subsequent Guinea pig experimentation.

2.3.2 Nanoparticle characterisation

Following the production of NPs, they were subjected to characterisation as described in Section 2.2.2. The results of this characterisation are summarised in Table 3, which includes the average particle size and PDI as determined by DLS, as well as the zeta potential obtained through LDE.

Table 3: Physical Characteristics of Nanoparticles. This table presents the physical characteristics of the nanoparticles (NPs) prepared using the solvent evaporation freeze drying method. The table includes average particle size, polydispersity index (PDI), zeta potential, and rifampicin (RIF) loading for two different formulations: PLGA/RIF and PLGA/RIF/MA. The values are reported with standard deviations (±) based on three replicates. The representative batches 85.4 and 85.6 were used for this analysis.

Preparation	Average particle size (nm)	Poly dispersity index	Zeta potential (mV)	RIF loading (w/w)
PLGA/RIF	306 (± 10)	0.33 (± 0.1)	-17.3 (±6.5)	RIF: 16%
PLGA/RIF/MA	314 (± 16)	0.3 (± 0.1)	-28 (±2.3)	RIF: 5%

The different NPs were next observed under a SEM. Irrespective of size, the particles were mostly spherical, and their surface was generally smooth and uniform (Figure 2).

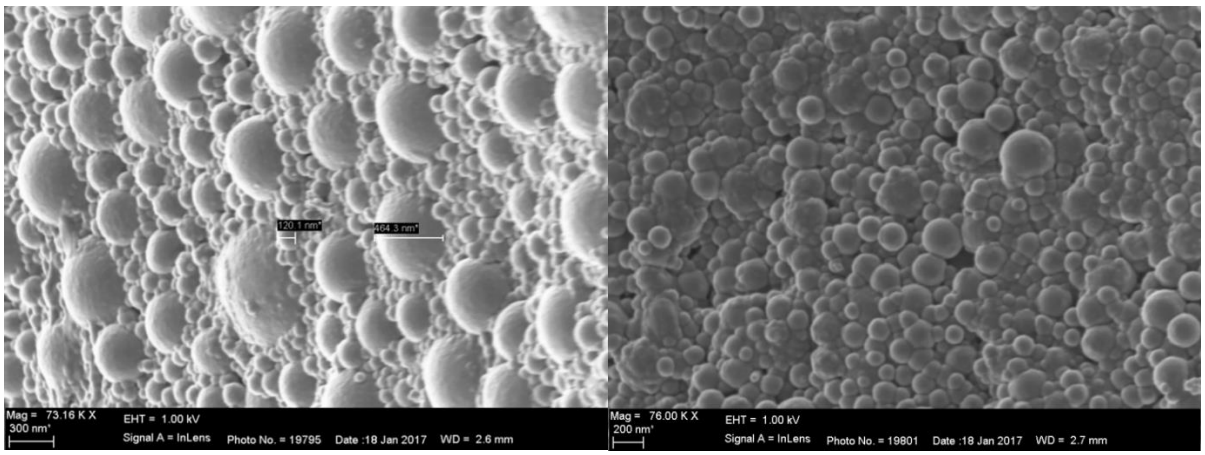

Figure 2: Morphological appearance of Nanoparticles. This figure illustrates the morphological appearance of the nanoparticles (NPs) observed under scanning electron microscopy (SEM). Freeze dried particles, recovered after encapsulation were processed for SEM. The left panel displays the RIF/PLGA particles, while the right panel shows the PLGA/RIF/MA particles. The majority of the particles exhibit a spherical shape and possess a smooth surface. The scale bars in the panels correspond to 0.3 µm and 0.2 µm, respectively.

2.3.3 Quantification of Rifampicin within Nanoparticles

The amount of rifampicin (RIF) present in both the PLGA/RIF and PLGA/RIF/MA nanoparticles was quantified following the method described in Section 2.2.3. To establish a calibration curve for RIF quantification, known concentrations of pure RIF were used. Absorbance measurements were taken at two wavelengths, 347 nm and 475 nm, which correspond to the characteristic absorption peaks of RIF. Table 4 summarises the absorbance values obtained from dilutions of RIF at both wavelengths, while Figure 3, illustrates the standard curve generated during the RIF quantification of Batch 85.1. as illustrated in Figure 3. By plotting the absorbance values against the corresponding RIF concentrations, a linear regression equation was derived: $y = 16.899x$, where y represents the absorbance and x represents the RIF concentration. This equation allowed for the quantification of RIF in the particles based on the absorbance values obtained from the samples. A new standard curve was prepared with known standards for each batch to ensure accuracy and consistency in the quantification process.

The absorbance measurements at 475 nm yielded a superior correlation coefficient ($R^2 = 0.9955$) compared to the measurements at 347 nm. Consequently, all subsequent RIF quantifications were performed using the readings at 475 nm.

Table 4: Absorbance Values and Concentrations of Rifampicin at Different Wavelengths. This table presents the absorbance values and concentrations of rifampicin (RIF) at two different wavelengths, 347 nm and 475 nm. The table includes a standard curve with various known concentrations of RIF and the corresponding absorbance readings at both wavelengths. The blank sample serves as a reference point with zero concentration and absorbance. The absorbance values obtained from the standard curve were used to determine the concentrations of RIF in the samples. The data presented in Table 4 played a crucial role in establishing the calibration curve and enabled the quantification of RIF in the nanoparticles.

Standard	Concentration (g/ml)	Wavelength 1 (nm)	Absorbance 1	Wavelength 2 (nm)	Absorbance 2
Blank	0	0	0	0	0
S8	0,0078125	347,5	0,3	475,86	0,17
S7	0,015625	347,1	0,57364	475,23	0,31
S6	0,03125	347,7	1,0949	475,92	0,58
S5	0,0625	347,1	2,055	475,98	1,12
S4	0,125	347,05	2,8082	475,26	2,0594
S3	0,25	347,58	2,9734	475,48	2,6927
S2	0,5	347,45	2,9754	475,33	2,701
S1	1	347,93	2,9456	475,48	2,7047

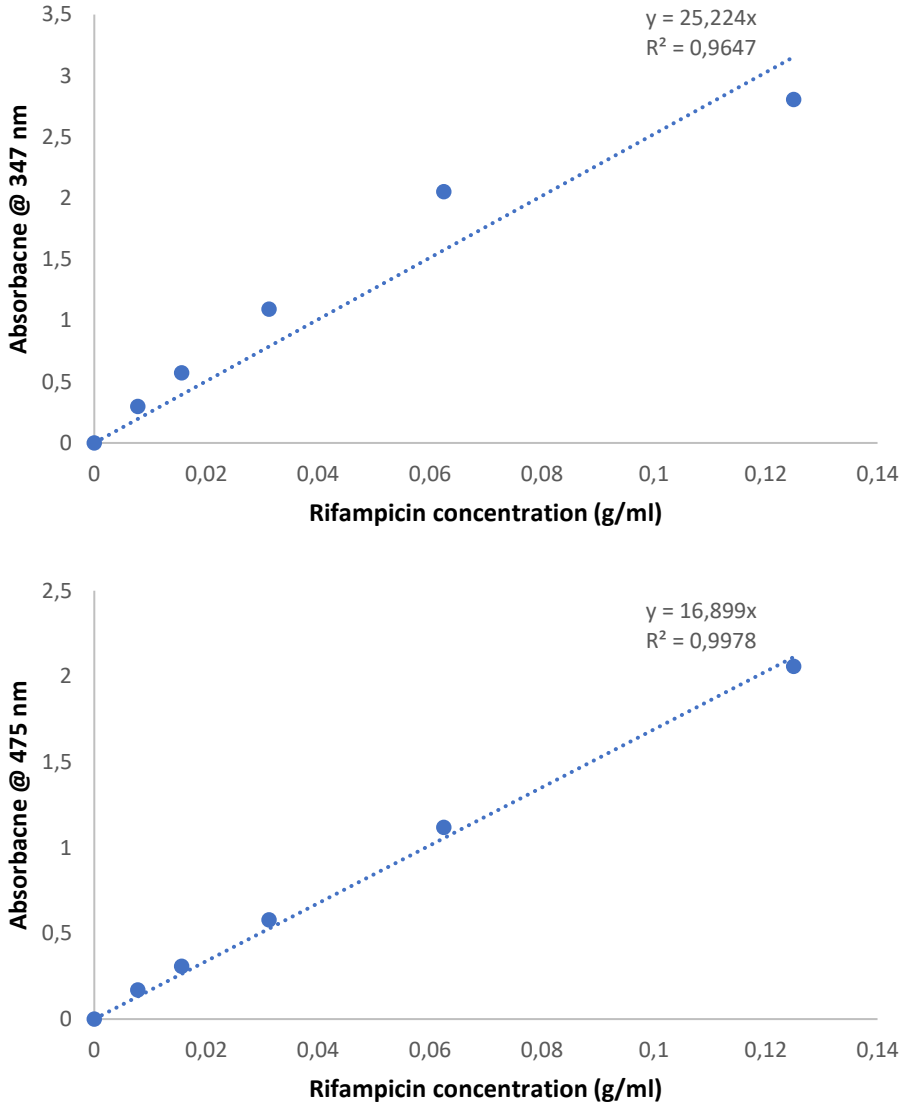

Figure 3: Standard Curve for Rifampicin Quantification in Batch 85.1. This figure illustrates the standard curve generated during the quantification of rifampicin (RIF) in Batch 85.1. The absorbance values obtained from the samples at 347 (top) and 475 nm (bottom) were plotted against the corresponding RIF concentrations. The resulting graph demonstrates a linear relationship between the absorbance and concentration of RIF. At 475, the linear regression equation, y = 16.899x, where y represents the absorbance and x represents the RIF concentration, was derived from the standard curve. This equation allowed for the accurate quantification of RIF in the nanoparticles based on the absorbance values obtained from subsequent samples. The high correlation coefficient (R^2 = 0.9955) indicates the reliability and accuracy of the standard curve in determining RIF concentrations.

To demonstrate the process of determining the amount of RIF in the particles, the data generated for Batch 85.3 is shown in Table 5. For each batch, multiple individual repeats of nanoparticle production were carried out (1a – 3c), and each repeat was quantified individually. This approach was adopted to ensure reproducibility and obtain accurate measurements of the nanoparticle characteristics. Additionally, by quantifying each individual repeat, it was possible to preserve the majority of the batch for future use and only resuspend a specific fraction of the nanoparticles for weekly chemotherapy in guinea

pigs. This strategy aimed to maintain the integrity and quality of the nanoparticles while minimising waste and ensuring sufficient quantities for the duration of the guinea pig trial.

Table 5: Individual Quantification Results for Multiple Repeats of Nanoparticle Production during batch 85.3. This table displays the individual quantification results obtained for multiple repeats of nanoparticle production. Each sample was labelled with a unique identifier, consisting of a combination of a letter (a, b, c) representing the repeat and a number (1, 2, 3) representing the batch. The mass of each sample, the absorbance measured at 475 nm, the calculated concentration, and the total amount of rifampicin (RIF) in each sample are provided. The table also includes the total values for the entire batch, such as the total mass of nanoparticles and the average RIF loading percentage. The individual quantification results highlight the reproducibility of the production process and provide valuable insights into the RIF content of each sample.

Sample	Mass of Sample (g)	Absorbance @ 475 nm	Concentration (g/ml)	Total RIF in sample (g)
1a	0,6922	2,1965	0,117127926	0,081075951
1b	0,1661	0,3645	0,01943689	0,003228467
2a	1,5468	2,5943	0,138340532	0,213985135
2b	0,0915	2,3447	0,125030662	0,011440306
3a	1,1131	1,8867	0,100607903	0,111986657
3b	0,0751	1,9113	0,101919693	0,007654169
3c	0,0514	1,4184	0,075635898	0,003887685
Total	3.7362			0.4333
Average RIF Loading %				**11.60%**

Table 6 demonstrates variations in RIF loading across the 5 PLGA/RIF batches, with RIF loading percentages ranging from 2.984% to 15.779%. The total RIF loading for all batches combined is 11.12%, based on a total mass of 12.928 g of nanoparticles.

Table 7 shows variations in RIF loading among the 3 PLGA/RIF/MA batches, with RIF loading percentages ranging from 4.770% to 5.312%. The total RIF loading for all batches combined is 5.01%, based on a total mass of 9.319 g of nanoparticles.

Table 6: RIF Loading in PLGA/RIF Nanoparticles. This table presents the results of the RIF loading in PLGA/RIF nanoparticles for batches 85.1 to 85.5. The total mass of the nanoparticles produced in each batch is listed, along with the corresponding total amount of RIF present in the particles. The RIF loading percentage, which indicates the proportion of RIF relative to the total mass of the nanoparticles, is also provided.

Batch	Total Mass of NPs (g)	Total RIF in particles (g)	RIF loading %
85.1	1,1250	0,0336	2,984
85.2	1,1107	0,1214	10.931
85.3	3,7362	0,4333	11,596
85.4	3,5059	0,5532	15,779
85.5	3,4506	0,2961	8,582
Total	**12,928**	**1,4376**	**11.12%**

Table 7: RIF Loading in PLGA/RIF/MA Nanoparticles. This table displays the RIF loading in PLGA/RIF/MA nanoparticles for batches 85.6 to 85.8. The total mass of the nanoparticles produced in each batch is presented, along with the corresponding total amount of RIF present in the particles. The RIF loading percentage, indicating the proportion of RIF relative to the total mass of the nanoparticles, is also provided.

Batch	Total Mass of NPs (g)	Total RIF in particles (g)	RIF loading %
85.6	3,0138	0,1437	4,770
85.7	3,0569	0,1624	5,312
85.8	3,2481	0,1606	4,944
Total	**9,319**	**0,4667**	**5.01%**

2.4 Discussion

The production yields of the two nanoparticle formulations, RIF/PLGA and PLGA/RIF/MA, were determined by synthesising multiple batches of each formulation. For the RIF/PLGA samples, a total of five batches (85.1 to 85.5) were produced, resulting in a combined yield of 12.928 g of PLGA/RIF. Similarly, three batches (85.6 to 85.8) were prepared for the PLGA/RIF/MA samples, yielding a total of 9.319 g of PLGA/RIF/MA. The amounts of nanoparticles obtained were deemed sufficient for the subsequent Guinea pig experiment.

The production yields of the nanoparticles were similar between the two formulations, with the encapsulation process yielding approximately 60% of particles over the initial solid mass of the reactants. These yields provide valuable information for scaling up the production process and ensuring an adequate supply of nanoparticles for further studies.

The physical characteristics of the nanoparticles were evaluated to assess their suitability for biomedical applications. The average particle size, polydispersity index (PDI), and zeta potential were determined using dynamic light scattering (DLS) and laser Doppler electrophoresis (LDE). The average particle sizes of the RIF/PLGA and PLGA/RIF/MA formulations were approximately 306 nm and 314 nm, respectively. These sizes, although slightly above the ideal range for systemic drug delivery (100-200 nm), remain within acceptable limits for nanoparticles designed for certain applications such as localised delivery or prolonged circulation (Danhier *et al*., 2012b). . The low PDI values (0.33 for RIF/PLGA and 0.3 for PLGA/RIF/MA) indicate a relatively narrow size distribution, suggesting reasonably good uniformity among the particles (acceptable PDI < 0.3) (Danaei *et al*., 2018). The zeta potential measurements revealed that the surface charge of the nanoparticles was negative for both formulations, with values of -17.3 mV for RIF/PLGA and -28 mV for PLGA/RIF/MA. These negative zeta potentials indicate a sufficient repulsion between the particles, reducing the likelihood of aggregation and improving their stability in suspension and which fall within the acceptable range for stability in suspension (±20 to ±30 mV) (Honary & Zahir, 2013). Scanning electron microscopy (SEM) images of the nanoparticles further confirmed their satisfactory size and morphology, with most particles appearing spherical and displaying smooth and uniform surfaces.

The quantification of rifampicin (RIF) content within the nanoparticles was performed to determine the drug loading efficiency. A standard curve was generated using known concentrations of pure RIF, and absorbance measurements were obtained at wavelengths of 347 nm and 475 nm, corresponding to the characteristic absorption peaks of RIF.

The quantification results revealed significant differences in the rifampicin (RIF) loading between the two nanoparticle formulations. The average RIF loading in PLGA/RIF nanoparticles was found to be 11.12%, indicating a relatively higher amount of RIF present in these particles compared to PLGA/RIF/MA nanoparticles. However, there was considerable variation observed within the PLGA/RIF formulation, with RIF loading percentages ranging from 2.984% to 15.779%. This wide range suggests that the encapsulation process for PLGA/RIF nanoparticles resulted in inconsistent loading of RIF among different batches. The observed inconsistency in rifampicin loading among different batches could be due to variability in the emulsification process, such as differences in mixing speed, solvent evaporation rates, or phase separation during the

double-emulsion technique. These factors can influence the uniformity of encapsulation and drug distribution within the nanoparticles.

Conversely, the PLGA/RIF/MA nanoparticles exhibited a lower average RIF loading of 5.01%. However, the RIF loading values for PLGA/RIF/MA nanoparticles were more consistent and reproducible, ranging narrowly from 4.770% to 5.312%. This indicates that the addition of mycolic acid as a targeting ligand in the PLGA/RIF/MA formulation led to a more controlled and uniform encapsulation of RIF. The narrower range of RIF loading percentages suggests a more reliable and predictable drug loading process for PLGA/RIF/MA nanoparticles.

MA has a long hydrophobic chain and bulky structure, which can affect the encapsulation efficiency and drug loading capacity of nanoparticles. When formulating drug-loaded nanoparticles, the encapsulation process involves the diffusion of the drug into the polymer matrix. The drug molecules need to penetrate the polymer matrix and reach the encapsulation sites within the nanoparticles. However, the presence of bulky molecules, such as MA, can create physical barriers or hinder the drug diffusion process. The bulky structure of MA may limit the available encapsulation sites within the polymer matrix, leading to lower drug loading efficiency. It can also affect the diffusion kinetics of rifampicin, making it more difficult for the drug to penetrate and be encapsulated within the nanoparticles. Consequently, the amount of RIF in the PLGA/RIF/MA nanoparticles may be reduced compared to the PLGA/RIF nanoparticles without the inclusion of MA. This reasoning aligns with the observation in the study where the RIF loading in the PLGA/RIF/MA nanoparticles was lower (5.01%) compared to the PLGA/RIF nanoparticles (11.12%). The decreased drug loading in the presence of MA suggests that the bulky structure of MA indeed influenced the encapsulation efficiency and drug loading capacity of the nanoparticles.

However, it is important to note that further experimental investigations, such as encapsulation studies with varying concentrations of MA and characterisation of the encapsulation process, would be necessary to provide more direct evidence and a comprehensive understanding of the influence of MA on drug loading in the nanoparticles.

Overall, the comprehensive characterisation of the nanoparticles demonstrated their satisfactory physical characteristics, including desirable particle size, uniformity, negative surface charge, and efficient drug loading. These findings suggest the suitability of the nanoparticles for use in the Guinea pig treatment study. .

3. ESTABLISHMENT OF A PILOT GUINEA PIG MODEL FOR PRELIMINARY EVALUATION OF PLGA-ENCAPSULATED RIFAMPICIN, WITH AND WITHOUT MYCOLIC ACID TARGETING LIGANDS, IN TUBERCULOSIS

3.1 Introduction

This chapter outlines the development and implementation of a pilot study using a guinea pig model to assess the preliminary effects of PLGA-encapsulated Rifampicin, both with and without mycolic acid (MA) as a targeting ligand. The aim is to establish a foundational experimental model that paves the way for future comprehensive studies focused on the efficacy and targeted delivery of nanoparticle-encapsulated anti-TB drugs. Recognising the exploratory nature of this study, the objective is to gather initial data and insights that will aid in refining experimental approaches and guide the design of more definitive efficacy studies in the context of TB treatment. This approach emphasises the pilot study's role in contributing to a larger framework for drug delivery research, specifically tailored towards enhancing the therapeutic outcomes of TB treatment through advanced drug delivery systems.

3.1.1 Guinea Pig Model of *M. tb* Infection

The selection of an appropriate animal model for studying *M. tb* infection is crucial for understanding the pathogenesis of TB and evaluating potential therapeutic interventions. These models range from the commonly used mice to guinea pigs, rabbits, non-human primates, and even zebrafish.

Mice are the predominantly used model of biomedical research in TB due to their conserved genetic pathways with humans, ease of handling, and well-characterised immune system. Their genetic manipulability further enhances their utility in studying human disease processes.. However, their utility in TB research is limited as they do not develop the granulomatous lesions characteristic of human TB and have a different immune response progression. Despite these limitations, mice have been invaluable in genetic and immunological studies of TB (Singh & Gupta, 2018).

Alternatively, the "humanised Kramnik mouse model" was considered which was engineered to mimic human-like immune responses, particularly in the context of TB research. This model was developed by Dr. Igor Kramnik and his team to study the host-pathogen interactions and the immune responses specific to TB infection (Calderon *et*

al., 2013). In these humanised mice, specific aspects of the mouse's immune system are modified to behave more like a human's. The humanised Kramnik mouse model is particularly valuable because it provides a more relevant animal model for studying TB, allowing researchers to observe how the disease progresses and responds to treatments in a system that closely mimics human physiology. However, this model is not suitable for research involving MA as targeting ligand as mice lack Type I CD1 receptors on its antigen presenting cells (Ulrichs *et al*., 2003).

Rabbits develop a granulomatous response to *M. tb* infection that includes caseous necrosis, closely mimicking human pathology. However, the limited genetic and immunological tools available for rabbits, alongside higher maintenance costs, restrict their widespread application in TB research (Singh & Gupta, 2018).

Non-human primates, especially macaques, mirror the human disease progression and immunological responses to TB, including the development of caseous granulomas. While their physiological similarity to humans makes them an excellent model for studying TB, ethical, financial, and care complexities limit their use (Singh & Gupta, 2018).

Zebrafish, using *Mycobacterium marinum*, offer a unique window into the infection process, benefiting from the transparent larvae to visualise the disease progression *in vivo*. This model has shed light on mycobacterial infections' genetic and immunological aspects but faces challenges in application to human TB due to environmental and biological differences (Singh & Gupta, 2018).

Guinea pigs have emerged as a valuable model for studying TB due to several key factors that closely resemble the human infection. Guinea pigs exhibit a high susceptibility to *M. tb* infection, which is similar to humans. Upon infection, guinea pigs develop caseating granulomas in their lungs, which is a characteristic feature of active TB in humans. These granulomas are formed by the aggregation of immune cells, such as macrophages and lymphocytes, around infected lung tissue. The formation of granulomas in guinea pigs closely mimics the pathological changes observed in human TB, providing a relevant and reliable model for studying the disease progression and evaluating treatment (Clark *et al*., 2015).

Moreover, guinea pigs mount a robust immune response against *M. tb*, which shares similarities with the immune response observed in humans. The immune cells in guinea pigs effectively control and contain the infection in granulomas. This immune response includes the recruitment and activation of various immune cells, production of pro-

inflammatory cytokines, and initiation of adaptive immune responses. Guinea pigs provide a unique opportunity to study the immunological aspects of TB, including the interplay between the host immune system and *M. tb*, the dynamics of immune cell recruitment, and the modulation of immune responses during infection and treatment (Singh & Gupta, 2018).

The similarities between guinea pigs and humans in terms of disease progression, pathological changes, and immune responses make guinea pigs an ideal animal model for investigating TB. Several studies showed that the guinea pig model represents the best model given the similarities to natural human infections in terms of the granuloma formation in the lungs as well as the subsequent necrosis and mineralisation of these lesions (Turner *et al*., 2014, Orme, 2005). In addition, bacterial persistence occurs in guinea pigs whereas it can't be modelled in wild type mice (Tsai *et al*., 2006).

When considering the inclusion of MA as targeting ligand, the additional argument against mice and for guinea pigs as animal model for TB resides in the immune response to lipid antigen. CD1-restricted T cells appear to respond to CD1 presented antigens that appear on the professional antigen presenting cells, i.e. dendritic cells. Certain lipid antigens, mainly those with long hydrophobic tails like MA, are presented by the so-called Type I CD1, comprising the human CD1a, CD1b and CD1c. The Type II CD1 presents preferably glycosylated lipids with shorter hydrophobic tails and comprises CD1d in humans. In mice, only Type II CD1 is found on antigen presenting cells. Type I CD1 presents lipid antigens to T cells, which respond by polyclonal activation, suggesting a relatively wide range of specificities for antigen binding ((Ulrichs *et al*., 2003),(Libero & Mori, 2014). Multiple members of the guinea pig CD1 family, including members that are homologous to the human CD1b and CD1c proteins, are expressed at the protein level on a large number of B cells in guinea pigs. Therefore, there are substantial similarities between the guinea pig and human CD1 systems, thus supporting the possibility that the guinea pig may offer significant advantages as an animal model (Hiromatsu *et al*., 2002).

3.1.2 Study Design and Treatment Groups

The experimental design of this study involves infecting guinea pigs with a defined inoculum of *M. tb* and subsequently assessing the efficacy of different treatment regimens. Guinea pigs were divided into six infected treatment groups:

1. **Baseline Group:** This infected group served as an infection control, with animals terminated on day 26 post-infection. The baseline data provides insights into the progression of the infection in the other groups and serve as a reference for evaluating the efficacy of the treatment interventions.
2. **Untreated Group:** Guinea pigs in this group did not receive any treatment, allowing for the observation of natural disease progression and assessing the effectiveness of the treatments in comparison.
3. **Free Rifampicin (RIF) Group:** Guinea pigs in this group received a daily dose of free rifampicin, administered orally, as the standard treatment. The dosage was based on the recommended dose for guinea pigs.
4. **Weekly Free Rifampicin Group:** Guinea pigs in this group received a weekly dose of free rifampicin, administered orally, at 2.5 times the daily dose. This regimen aims to explore the potential benefits of higher intermittent dosing in improving treatment efficacy.
5. **PLGA/RIF Weekly Group**: Guinea pigs in this group received a weekly dose of rifampicin encapsulated within PLGA nanoparticles. The nanoparticles were formulated to enhance drug delivery and prolong drug release, providing sustained therapeutic levels.
6. **PLGA/RIF/MA Weekly Group:** Guinea pigs in this group received a weekly dose of rifampicin encapsulated within PLGA nanoparticles with mycolic acid (MA) incorporated as a targeting ligand. Mycolic acid is expected to enhance nanoparticle targeting to *M. tb*-infected/-infectable cells and improve treatment efficacy.

3.1.3 Treatment Duration and Evaluation Parameters

Following the infection procedure, treatment was initiated on day 26 post-infection and continued for six weeks. Throughout the study, several parameters were evaluated to assess the efficacy of the treatments:

1. **Lung Bacterial Culturing:** Lung tissue samples were collected at specified time points and processed to determine the bacterial load. Quantitative culture techniques were employed to measure the number of viable *M. tb* bacilli present in the lungs.

2. **Spleen Culturing:** Spleen samples were also collected and cultured to assess the systemic dissemination of *M. tb* and evaluate the effectiveness of the treatments in controlling bacterial growth.
3. **Histopathology:** Lung, spleen, liver and hilar lymph node tissues underwent histopathological examination to examine the extent of granuloma formation, tissue damage, and inflammatory responses. This analysis provided insights into the pathological changes associated with the infection and the impact of the different treatment regimens.
4. **Survival Rate:** The survival rate of the guinea pigs in each treatment group was monitored throughout the study period. This parameter indicated the overall effectiveness of the treatment interventions in preventing mortality associated with *M. tb* infection.
5. **Weight Gain/Loss:** The change in body weight of the guinea pigs was monitored as an indicator of their general health and response to the treatments. Weight loss is a common clinical manifestation of TB infection and assessing weight gain/loss provided information on the effectiveness of the treatments in preventing disease-related wasting.

By assessing these parameters, we aim to comprehensively evaluate the *in vivo* efficacy of the different treatment regimens in the guinea pig model of TB. This approach helped elucidate the comparative effectiveness of nanoparticle-encapsulated drugs versus free drugs, as well as the potential advantages of incorporating the MA targeting ligand in the nanoparticle formulation.

3.1.4 Ethics Statement

All animal experiments were approved with written clearance from the Research ethics committee of the CSIR (approval number 108/2014) and the Animal Ethics Committee at the Faculty of Veterinary Science (NAS 254/2023). The ethics committee of La-Bio research verified that the animal facility operated within the standards and rules of the National Laboratory Animal Ethical Code of Conduct and the OECD guidelines for toxicity testing. All efforts were made to ensure that the animals were kept according to recognised international standards in animal husbandry practice.

3.2 Materials and Methods

3.2.1 Infectious Substance

Mycobacterium tuberculosis strain H37Rv (ATCC) was used in this study. The bacteria were cultured in Middlebrook 7H9 broth supplemented with 0.5% Tween 80, 0.2% glycerol, and 10% oleic acid-albumin-dextrose-catalase (OADC) enrichment. This nutrient-rich medium provided the necessary growth factors and nutrients to support the growth of *M. tb* (Brittle *et al*., 2009). The broth cultures were incubated at 37°C with shaking at 150 rpm until they reached mid-log phase, typically taking 5-7 days.

To preserve the bacterial stock, aliquots of the cultured *M. tb* were aseptically transferred into vials and frozen at -70 °C. The freezing process ensured the long-term viability and stability of the bacterial strain for subsequent guinea pig infections, allowing for consistent and standardised bacterial inoculation.

Prior to the experimental infection, the frozen vials were thawed and the *M. tb* strain H37Rv was revived by inoculating a small volume of the frozen stock into fresh Middlebrook 7H9 broth. The culture was incubated until it reached the mid-log phase, as determined by optical density measurements or colony-forming unit (CFU) counts.

The use of *M. tb* strain H37Rv, a well-characterised and commonly employed strain, ensured the reliability and reproducibility of the experimental results. The growth and preservation of the bacteria under controlled conditions, along with the use of standardised culture media and freezing techniques, contributed to the consistency and quality of the *M. tb* inoculum for subsequent infections.

3.2.2 Test Substances

In this study, three different formulations of rifampicin (RIF) were utilised: Free RIF, PLGA/RIF, and PLGA/RIF/MA. Each formulation offered distinct characteristics and advantages for the delivery of rifampicin.

1. **Free RIF (Free Rifampicin drug):** Free RIF refers to the unencapsulated form of rifampicin, which is the conventional formulation of the drug. It is a small molecule with excellent antibacterial activity against *M. tb*. Free RIF exhibits rapid release kinetics. However, it is prone to degradation and has limited bioavailability due to poor aqueous solubility and susceptibility to enzymatic degradation. The

administration of free RIF typically requires frequent dosing to maintain therapeutic levels in the body.

2. **PLGA/RIF (Rifampicin in a Poly DL, lactic-co-glycolic acid (PLGA) polymer):** PLGA/RIF refers to rifampicin encapsulated within a polymeric carrier made of poly DL, lactic-co-glycolic acid (PLGA). Poly DL, lactic-co-glycolic acid (PLGA) is a biocompatible and biodegradable polymer commonly used in drug delivery systems. The encapsulation of rifampicin within PLGA nanoparticles offers several advantages. First, it protects the drug from degradation and enhances its stability. Second, it allows for controlled and sustained release of the drug, extending its therapeutic effect. This sustained release profile reduces the frequency of dosing and improves patient compliance. Additionally, the nanoparticle size and surface properties can be tailored to enhance drug uptake and distribution within the body.
3. **PLGA/RIF/MA (Rifampicin in a nano-formulation of incorporated mycolic acids (MA) in a Poly DL, lactic-co-glycolic acid (PLGA) polymer):** PLGA/RIF/MA refers to a nano-formulation of rifampicin that incorporates mycolic acids (MA) into the PLGA polymer. Mycolic acids incorporation into the PLGA nanoparticles aims to enhance the targeting of rifampicin to the site of infection. The inclusion of MA in the formulation can facilitate the uptake of the nanoparticles by macrophages, which are the primary host cells for *M. tb*. This targeted delivery approach increases the concentration of rifampicin specifically at the site of infection, thereby improving its efficacy and reducing potential side effects associated with systemic drug exposure.

3.2.3 Safety Precautions

Required biosecurity and safety measures were strictly adhered to throughout the entire experimental process to ensure the protection of personnel, prevent contamination, and maintain a controlled environment. The following procedures and precautions were implemented in the La-Bio Research Animal Laboratory:

1. **Personal Protective Equipment (PPE):** All personnel involved in the experimental work wore appropriate PPE, including laboratory coats, filtered face masks, hairnets, gloves, and laboratory boots. These measures aimed to minimise the risk of contamination and ensure the safety of the personnel handling the experimental materials.

2. **Surface Cleaning and Sterilisation:** To maintain a clean and sterile working environment, all working surfaces, including any spills, were cleaned using F10, a broad-spectrum disinfectant. Following cleaning, the surfaces were sterilised using 3.6% formalin, a potent sterilising agent. Subsequently, 70% ethanol was applied to ensure additional disinfection. Finally, the surfaces were dried using paper towels to remove any remaining moisture.
3. **Animal Housing and Containment:** The animals were housed in individually ventilated cages that were equipped with High-Efficiency Particulate Air (HEPA) filters. These filters effectively removed airborne contaminants and provided a controlled environment for the animals. Entry into the animal lab was restricted to authorised personnel, including the veterinarian and study director. These individuals wore HEPA filtered personal protective hoods/helmets to prevent any potential contamination.
4. **Waste Management:** Proper waste management procedures were implemented to handle potentially infectious materials. All waste generated during the experimental procedures, including animal waste and contaminated materials, was chemically sterilised using 3.6% formalin. These waste materials were then disposed of in biohazard waste containers to prevent any potential spread of pathogens.
5. **Sterilisation and Disposal of PPE:** To ensure the safety of personnel and prevent any cross-contamination, all personal protective clothing, including laboratory coats, gloves, and other disposable items, were chemically sterilised before being discarded. This step helped to minimise the risk of transmitting any infectious agents outside the animal unit.
6. **Compliance with Standard Operating Procedures (SOPs):** All activities in the animal laboratory were carried out in strict adherence to the Standard Operating Procedures as directed by the facility's Biosafety Manual. This manual outlined the proper procedures for the disposal of biohazard materials, ensuring compliance with the established guidelines and regulations.

3.2.4 Test System

The Dunkin-Hartley strain of guinea pigs were the experimental animals used in the study, with an average weight of approximately 300 g. Guinea pigs were procured from National Health Laboratory Service (NHLS), South Africa. These guinea pigs were specifically

chosen for the study based on their established suitability as an animal model for various research purposes. The Dunkin-Hartley strain is commonly used in biomedical research due to its well-documented characteristics and genetic stability, which make it a reliable choice for experimental studies (Clark *et al.*, 2015). Young adult guinea pigs, aged between six to eight weeks, were selected for the experiment. Both male and female guinea pigs were included, with a total of 28 animals, consisting of 11 males and 17 females. Only nulliparous (never having given birth) and non-pregnant females were included. This ensured consistency in the reproductive status of the female guinea pigs throughout the experiment.

Before the start of the study, all animals underwent a period of acclimatisation in the animal unit of La–Bio Research. During this acclimatisation period, which lasted for five days, the guinea pigs were housed in a controlled environment. The room temperature was maintained between 18-24 °C, and the humidity levels ranged from 30% to 70%. A 12-hour light/dark cycle was maintained, providing a consistent day/night rhythm for the animals. The light intensity in the animal unit was regulated to be between 70-100 Lux. To ensure the animals' well-being and proper housing conditions, the guinea pigs were housed in HEPA filtered individually ventilated cages. These cages maintained negative pressure, creating a barrier unit that helped maintain disease-free conditions. The cages provided ample space for the guinea pigs to engage in their species-specific behaviours, promoting their overall welfare. The size of the cages complied with European standards for housing laboratory animals.

The guinea pigs' diet consisted of rat/mice feed obtained from Epol®, a reputable supplier of animal nutrition. The animals had ad libitum access to water, allowing them to consume water freely and meet their hydration needs. Water was supplemented with 500 mg/l vitamin C.

To track and identify each guinea pig individually throughout the study, a unique identification number was assigned to each animal. This facilitated accurate data collection and ensured the proper monitoring of individual animals throughout the experimental period.

By providing a suitable and controlled environment, proper nutrition, and individual identification, the study aimed to maintain the welfare and integrity of the guinea pigs throughout the experiment. These measures ensured standardised conditions and allowed for reliable and accurate data collection and analysis.

3.2.5 Guinea Pig Infection Model

The guinea pig infection model utilised in this study aimed to closely simulate the natural transmission of *M. tb* in a controlled laboratory setting. This involved the exposure of the animals to a dose-calculated aerosol of *M. tb* strain H37Rv. All guinea pigs from groups 1 to 6 were subjected to this infection procedure to establish a consistent and controlled model for studying the effects of different treatments on *M. tb* infection.

To establish the infection model, a measured aerosol containing of *M. tb* H37Rv was generated. This aerosol was delivered to the guinea pigs using a mesh nebuliser. The liquid used in the nebulisation chambers was prepared with a known concentration of $1x10^7$ colony-forming units (CFU) per millilitre, as determined by CFU counts. Prior calibrations were performed to determine the appropriate nebulisation time needed to deliver an average of 20-30 bacilli per animal. This meticulous calibration process ensured that the bacterial inoculum was consistently delivered to each guinea pig, minimising variations in the infection dose. The exposure duration was carefully controlled to last for the determined 15 seconds, ensuring uniformity across all animals.

To maintain strict biosecurity measures during the aerosol exposure procedure, the experiments were conducted within a class 2 biosafety cabinet located within an animal laboratory. This biosafety cabinet provided a contained environment that prevented the release of aerosolised *M. tb* into the laboratory and minimised the risk of cross-contamination. Furthermore, the animals were infected by the study veterinarian wearing a positive pressure suit connected to a HEPA filtered airline.

The incubation period of an infectious disease refers to the time interval between the initial exposure to the pathogen and the appearance of clinical symptoms. In the case of the guinea pig model of *M. tb* infection used in this study, the incubation period was determined to be 26 days.

After the guinea pigs were exposed to a calculated aerosol of *M. tb* H37Rv, they were closely monitored for any signs of infection during the incubation period of 26 days. Clinical symptoms such as coughing, weight loss, and respiratory distress were assessed regularly to determine the onset of disease progression.

The choice of a 26-day incubation period for this study was based on previous research and observations of *M. tb* infection in guinea pigs. It was found that this duration allowed

for the establishment of an infection and the subsequent development of pathological changes and immune responses associated with active TB. This period allowed sufficient time for the infection to progress, ensuring that the animals exhibited consistent and measurable responses to the treatments administered.

By utilising a 26-day incubation period, this study aimed to capture the critical stages of *M. tb* infection and evaluate the efficacy of different treatment interventions. It provided a suitable timeframe to assess parameters such as lung bacterial burden, spleen bacterial burden, histopathological changes, survival rates, and weight loss/gain.

3.2.6 Guinea Pig Treatment and Grouping

To assess the bacterial load at the start of infection, three guinea pigs from Group 1 were sacrificed after 26 days of *M. tb* infection, just before the initiation of treatment. This allowed for the determination of the baseline bacterial load in the animals.

For the animals in Groups 2 to 6, the oral treatment regimen commenced 26 days post-infection, as outlined in Table 8. The control group (Group 2) received the carrier vehicle only, without any active treatment. This group served as a control to assess the natural progression of the infection without any intervention. Group 3 received free rifampicin (RIF) drug administered orally as a daily dose of RIF, five times per week. The dose level of RIF was 12 mg/kg/day, resulting in a weekly dose of 60 mg/kg. Groups 4 and 5 received RIF encapsulated in different formulations. Group 4, labelled as PLGA/RIF, received a 2.5 times dose of RIF encapsulated in a Poly DL, lactic-co-glycolic acid (PLGA) polymer once per week. The weekly dose of RIF in this group was 30 mg/kg. Group 5, designated as PLGA/RIF/MA, received the same 2.5 times dose of RIF encapsulated in a nano-formulation that incorporated mycolic acids (MA) within the PLGA polymer. The treatment was administered once per week, with a weekly dose of 30 mg/kg. Group 6, like Group 3, received free RIF. The guinea pigs in this group were administered the 2.5 times dose of RIF once per week, resulting in a weekly dose of 30 mg/kg.

Each animal's dosage was calculated individually based on the animal's weight to ensure the exact required dosage of rifampicin was met. Calculations for dosing were based on the individual concentrations of rifampicin in each batch. Furthermore, to eliminate any variance in dosing among different animals, a single batch of each formulation—PLGA/RIF and PLGA/RIF/MA—was employed at each time point for all animals within the same group. It was calculated that guinea pigs in the PLGA/RIF/MA group received

approximately 2.37 times more PLGA carrier than those in the PLGA/RIF group. This significant difference is due to the different rifampicin loading percentages in the two formulations; 11.12% vs 5.01%. Consequently, to deliver the required 12 milligrams of rifampicin to a 400-gram guinea pig (calculated as 30 mg/kg), the total mass of nanoparticles needed was 107.91 milligrams for the PLGA/RIF formulation and 239.52 milligrams for the PLGA/RIF/MA formulation. After accounting for the rifampicin content, this resulted in 95.91 milligrams of PLGA carrier in the PLGA/RIF group and 227.52 milligrams in the PLGA/RIF/MA group

Table 8: Grouping of Animals and Treatment Regimens. The dose level of rifampicin administered to the animals per week is expressed in mg/kg body mass.

Group	No of animals	Treatment regimen	Dose level of RIF
1. Baseline control group	3 (2 females & 1 male)	none	-
2. Untreated	5 (3 female & 2 males)	Sucrose vehicle only	-
3. Free RIF drug	5 (3 female & 2 males)	Daily dose 5 times per week	12 mg/kg/day, i.e 60 mg/kg/week
4. PLGA/RIF	5 (3 female & 2 males)	2.5 times dose once per week	30 mg/kg/week
5. PLGA/RIF / MA	5 (3 female & 2 males)	2.5 times dose once per week	30 mg/kg/week
6. Free RIF High dose	5 (3 female & 2 males)	2.5 times dose once per week	30 mg/kg/week

To ensure palatability, the doses for all treatment groups were prepared using a sucrose vehicle. The sucrose vehicle consisted of 40% (w/v) sucrose and 20% (w/v) pumpkin puree (Butternut, Purity, Nestle), supplemented with vitamin C (50 mg/kg of mean body weight) and commercial Lactobacillus (0.1 g/kg/day) (BD Lactinex). The required dose volume of the treatment substance was calculated based on the weight of each individual guinea pig. The treatment substance was then prepared by combining the specified dose of RIF with the appropriate vehicle to a total volume of 2ml.

Individual guinea pigs were dosed by gently supporting the animal's neck and head while allowing the animal to support its own weight on the surface of the biosafety cabinet (Figure 4). The guinea pigs were fed with 4 ml of the treatment substance containing the vehicle, which was delivered using a plastic Pasteur pipette. This method ensured accurate dosing and allowed for precise administration of the treatment substance to each animal.

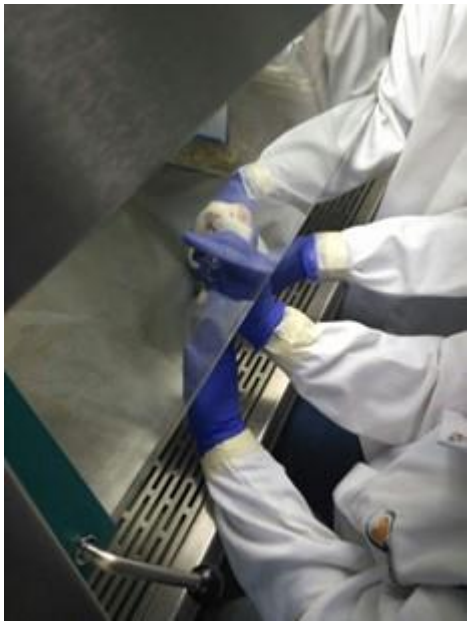

Figure 4: Administration of Treatment Substance to Guinea Pigs.

The treatment period continued for 6 weeks, during which the guinea pigs received their respective treatments according to the designated regimens. Five days after the completion of the last treatment, the guinea pigs were euthanised by Pentobarbital injection. The organs, including the lungs, spleen, and any other organs showing macropathology, were collected aseptically for subsequent analysis.

3.2.7 Clinical Observations of Guinea Pigs

In order to monitor the health and well-being of the guinea pigs throughout the study, both daily and weekly observations were conducted. The daily observations aimed to detect any general adverse effects that may have occurred. These observations were performed once a day, with additional inspections conducted at least twice daily to check for any signs of mortality or morbidity.

Weekly observations were conducted to gather more comprehensive data on the guinea pigs' condition and detect a wide range of symptoms associated with the disease. These observations included several aspects, starting with the regular weighing of the animals at weekly intervals. This allowed for monitoring changes in body weight over time, which can be indicative of their overall health status.

Furthermore, detailed clinical observations were performed once prior to infection and once every week thereafter for the duration of the study. A scoring system was employed to standardise the assessment of various signs and symptoms exhibited by the guinea pigs. The scoring chart provided a framework for evaluating specific signs, including respiratory issues, motor activity, convulsions, ocular symptoms, salivation, piloerection, oedema, erythema, righting reflex, and startle reflex. Each symptom was graded on a scale from 0 (none) to 3 (severe), allowing for a consistent assessment of severity across animals and observation periods.

In situations where an animal became moribund or experienced severe pain or distress during the study, ethical considerations were prioritised, and humane end point applied by administering euthanasia to prevent unnecessary suffering. At the end of the study, the remaining surviving animals were sacrificed according to the approved Standard Operating Procedure, ensuring proper and ethical handling of the animals' well-being.

3.2.8 Histopathology

After euthanasia, a specific protocol was followed to ensure proper fixation and preservation of the lung, hilar lymph node and spleen tissues for histopathological assessment. A small section of the left cranial lung lobe, the left hilar lymph node and a small section of the spleen were carefully removed and immediately placed in 10% buffered formalin. The formalin solution helped to fix and preserve the tissue samples, preventing any degradation or loss of cellular structures.

The fixated tissue samples were then kept in the formalin solution for a minimum of 48 hours to ensure adequate fixation. This duration allowed for the penetration of formalin into the tissues and ensured that the cellular structures were well-preserved. After fixation, specific tissue blocks were prepared by cutting small sections from the lung and spleen samples. These tissue blocks were then placed in tissue cassettes and labelled with the corresponding animal number for proper identification and tracking.

To prepare the tissue blocks for histological evaluation, an automated tissue processor was used. The tissue blocks were processed overnight. This automated process involved several steps, including dehydration, clearing, and impregnation of the tissues with paraffin wax. These steps ensured optimal tissue embedding in the wax, allowing for consistent and precise sectioning.

Once the tissue blocks were properly processed, wax blocks were created. From these wax blocks, thin sections measuring 5-6 µm in thickness were cut using a microtome. These sections were then transferred onto glass slides, and specific staining techniques, Hematoxylin and Eosin stain, were applied. Hematoxylin stained the nuclei of cells blue-purple, while Eosin stained the cytoplasm pink. This staining method provided contrast and enabled the visualisation of cellular structures and tissue morphology.

The histopathological slides were carefully examined under a microscope for detailed evaluation. The slides were assessed for any abnormal cellular or tissue changes, such as inflammation, necrosis, or granuloma formation. Photographic documentation of selected areas of interest was performed to capture and record significant findings.

3.2.9 Culturing and Enumeration of *Mycobacterium tuberculosis*

The lung and spleen tissues collected from the guinea pigs were utilised for determining the number of viable *M. tb* organisms present. Except for a small piece reserved for histological examination, the entire lung and spleen were used in the analysis.

To prepare the samples for analysis, manual tissue homogenizers were used to homogenise the lung and spleen tissues separately in phosphate-buffered saline (PBS). The lung tissues were placed in a 50 ml Falcon tube, to which 9 ml of PBS was added. The spleen tissues were placed in a separate 50 ml Falcon tube, with 4.5 ml of PBS added. Using a manual tissue homogenizer, the tissue was thoroughly homogenized with repeated up-and-down strokes for approximately 3-5 minutes until a uniform suspension of cells was achieved. To determine the number of viable *M. tb* organisms, serial dilutions of the tissue homogenates were prepared. A volume of 50 µl from each dilution was plated onto nutrient Middlebrook 7H10 agar plates in quadruplicate. These plates were specifically prepared according to the instructions provided by the manufacturer. The agar plates contained the necessary nutrients and conditions to support the growth of *M. tb* organisms.

After the plating process, the agar plates were sealed in bags to create a controlled incubation environment. They were then placed in an incubator set at a temperature of 37°C. The plates were left to incubate for a duration of 21 days, allowing sufficient time for *M. tb* colonies to grow.

At the end of the incubation period, the viable *M. tb* colonies on the agar plates were counted. The colony counts were recorded for each plate, and the average count was determined. To facilitate data analysis, the colony counts were converted to logarithmic values using the following equation (Orme & Roberts, 1999):

$$\text{CFU/ORGAN} = \frac{CC_Q \times V_H}{V_P \times DF_Q}$$

In the formula, CFU/organ represents the number of colony-forming units per organ, CC_Q is the colony count on a single plate, V_H is the total volume of the homogenate, V_P is the volume plated, and DF_Q is the dilution factor of the sample on the plate. By using this formula, the colony forming units per organ can be determined, providing valuable information about the bacterial load in the lung and spleen tissues of the guinea pigs.

3.2.10 Statistical Analysis

Statistical analyses were performed using Minitab software. A one-way Analysis of Variance (ANOVA) was conducted to determine whether statistically significant differences existed between the mean lung colony-forming unit (CFU) counts of the treatment groups. All statistical tests were conducted at a 95% confidence level ($\alpha = 0.05$). Post hoc analysis was performed to compare specific group means when significant differences were observed. Statistical power was assessed to evaluate the reliability of the findings, and the sample size requirements for achieving 80% power were calculated to guide future studies.

3.3 Results

3.3.1 Clinical Observations

At day 25, a notable shift in the clinical condition of the guinea pigs was observed, indicating the need for treatment initiation due to the progression of *M. tb* infection. It is

important to note that no symptoms were evident until day 24, and the guinea pigs exhibited good weight gain up to that point.

The guinea pigs exhibited mild cyanosis, characterised by a slight bluish discoloration of the mucous membranes and skin, particularly around the nose and mouth. Mild cyanosis is indicative of compromised oxygenation and is commonly associated with respiratory distress.

Respiratory abnormalities were also prominent among the clinical signs observed. The guinea pigs displayed increased respiratory rate, slightly laboured breathing, and occasional coughing. These respiratory symptoms reflected compromised pulmonary function and suggested the involvement of the respiratory system in the progression of *M. tb* infection. In addition to the respiratory symptoms, the guinea pigs showed a slight decrease in motor activity. They exhibited reduced mobility and slightly reduced energy levels, indicating a decline in physical activity.

Overall, the guinea pigs exhibited mild clinical signs of respiratory distress, including mild cyanosis, increased respiratory rate, and reduced motor activity. These manifestations collectively indicated the progression of *M. tb* infection and the need for treatment initiation to mitigate the disease's impact on the guinea pigs' health and well-being.

3.3.2 Survival rate & Weight Gain/Loss Profile

The survival rate and weight profile of the 28 experimental animals displayed a diverse pattern across different treatment groups, over the 73-day observation period (Table 9).

Table 10 represents fluctuations in weight, reflecting the response of each animal to its respective treatment regimen.

Table 9: Survival rates of guinea pigs across different treatment groups at the study endpoint. The numbers represent the count of surviving animals out of the total in each group. Group 1 had a scheduled termination point at day 26 while groups 2 to 6 had a scheduled termination point at day 73.

Treatment:	Survival to endpoint
1. Baseline control group	3/3
2. Untreated	1/5
3. Free RIF drug daily	3/5
4. PLGA/RIF	4/5
5. PLGA/RIF / MA	1/5
6. Free RIF weekly	0/5

Table 10: Weight (g) gain/loss profile of all 28 experimental animals. An uppercase symbol next to the last recorded weight for each animal indicates their status on the last day of survival: E = euthanised/died, and S = survived.

Treatment groups	Animal	Day 0	Day 7	Day 14	Day 21	Day 26	Day 33	Day 40	Day 47	Day 54	Day 61	Day 68	Day 73
1	4	404	424	436	450	421^{S}							
1	16	357	392	417	409	361^{S}							
1	23	290	314	335	328^{S}								
2	1	310	344	332	354	357	349	390	418	417	440	477	502^{S}
2	5	332	340	350	386	372	375	334^{E}					
2	6	363	395	422	439	444	453	419	394^{E}				
2	7	309	350	390	410	422	452	473	459	424	380^{E}		
2	8	325	350	374	383	416	410	360^{E}					
3	9	370	369	391	420	442	469	455	495	533	519	552	565^{S}
3	10	333	377	425	442	435	429	389	365	348	369^{E}		
3	11	329	347	361	372	381	415	357	356	370	356	327	292^{S}
3	12	301	318	337	335	325	340	344	365	374	414	428	436^{S}
3	13	361	404	447	438	453 ^{E}							
4	2	358	350	383	392	429	446	450	483	505	553	585	588^{S}
4	14	312	323	337	334	343	351	337	336^{E}				
4	15	379	351	373	386	383	400	406	446	459	491	524	541^{S}
4	17	364	383	418	414	422	420	455	488	538	597	626	666^{S}
4	18	328	363	393	401	436	468	480	490	511	569	655	685^{S}
5	3	366	387	433	475	509	536	595	620	704	734	778	790^{S}
5	19	319	354	367	379	375	337^{E}						
5	20	320	321	332	328	314	312^{E}						
5	21	306	333	348	361	360	355	336^{E}					
5	22	309	313	320	300	295	280^{E}						
6	24	379	404	440	441	445	456^{E}						

6	**25**	356	387	409	428	446	465	411[E]					
6	**26**	360	367	387	391	423	441	459	422	389	373[E]		
6	**27**	282	293	328	335	339	350	342	315[E]				
6	**28**	304	325	355	374	350	359	295	256[E]				

Notably, some animals show a consistent increase in weight, while others exhibit fluctuations or a decrease, particularly towards the later stages of the study. The cessation of weight data for certain animals indicates their premature exit from the study due to death or humane end points.

In evaluating the efficacy and safety of therapeutic interventions in infectious diseases like TB, measuring the average weight of surviving animals can sometimes provide an incomplete picture. When treatment-associated toxicity or the disease itself leads to mortality, average weights may appear stable or even increase as weaker, possibly lighter animals die, skewing the data. To address this, the total remaining body weight of the group is a more holistic measure, as it accounts for both the health of the surviving animals and the impact of mortality on the group (Figure 5). This approach ensures that the detrimental effects of both disease progression and potential drug toxicity are not masked. It serves as a crucial metric in studies where survival is variably affected across treatment groups, providing a more accurate reflection of a treatment's overall impact on the health and survival of the population under study.

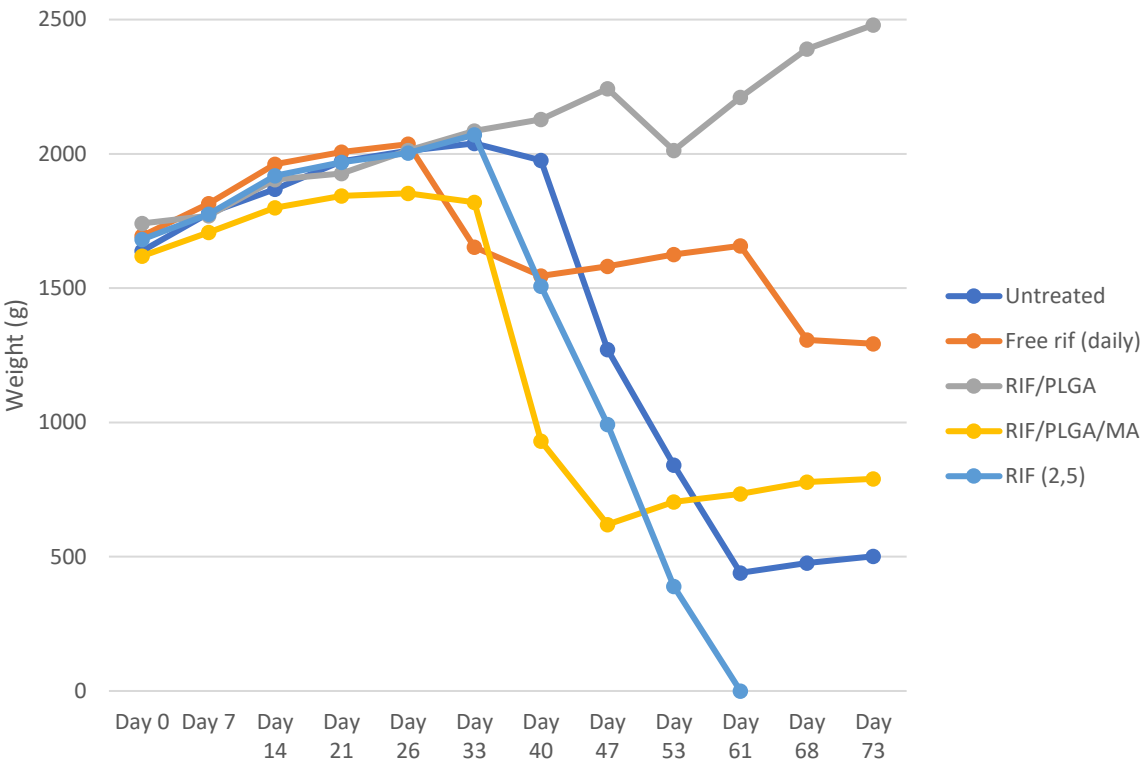

Figure 5: The remaining total combined body weight of guinea pigs within each treatment group throughout the study duration, from Day 0 to Day 73.

Weight loss serves as a critical indicator of disease severity in TB-infected guinea pigs. The data shows that untreated animals experienced a progressive decrease in body weight, signifying a high disease burden with a low survival rate. Conversely, daily RIF treatment stabilised body weight, suggesting mitigation of disease symptoms, which is corroborated by a 60% survival rate. Excess-dose RIF treatment once a week resulted in no beneficial impact on body weight and was coupled with poor survival, which may indicate a dual impact of disease severity and potential drug toxicity. Interestingly, the single survivor in the PLGA/RIF/MA group exhibited substantial weight gain, hinting at the effectiveness of the treatment for some individuals. An essential aspect to consider is the evaluation of the different PLGA dosages administered to the PLGA/RIF and PLGA/RIF/MA groups, as a result of the variable rifampicin (RIF) loading across these nanoparticle formulations as elucidated in Chapter 3.3.3. The PLGA/RIF nanoparticles exhibited a higher average rifampicin (RIF) loading of 11.12%, compared to the 5.01% in the PLGA/RIF/MA formulation. Consequently, to deliver a consistent therapeutic level of RIF, a significantly greater volume of nanoparticles was required in the PLGA/RIF/MA group. As indicated in Chapter 3.3.4, the PLGA/RIF/MA group received approximately 2.37 times more PLGA carrier than the PLGA/RIF group.

This increased dosage of PLGA, particularly when combined with MA, has significant implications for both treatment efficacy and potential toxicity. The high Dose of PLGA and consequently the high concentration of MA could enhance the targeting and efficacy of the drug delivery system; however, it also raises concerns about the additive effects of the carrier, especially given the increased PLGA content. Higher concentrations of PLGA and MA may lead to a higher incidence of adverse reactions, an aspect that needs to be carefully monitored in future studies.

The PLGA/RIF group stands out with better survival and consistent weight increase, suggesting this formulation offers therapeutic advantages, possibly due to enhanced drug stability and controlled release, which aligns with the expectations of nanoparticle-encapsulated drug delivery systems. This group presents a promising treatment profile, balancing efficacy and tolerability.

3.3.3 Macropathology

At necropsy, the following macropathological findings were made as illustrated by Figure 6. The untreated group's raised granulomas align with typical advanced TB pathology, suggesting a severe disease progression. In contrast, treated groups presenting with flat lesions may indicate a response to therapy, possibly limiting the disease's progression. The dark-coloured, necrotic lungs in the weekly RIF group could signal exacerbated pathology, potentially from treatment toxicity or advanced infection. Splenomegaly in the daily RIF, weekly RIF, and untreated groups further points to systemic infection and immune response. Notably, the absence of splenomegaly in the PLGA/RIF and PLGA/RIF/MA groups may suggest a protective effect of these treatments against the systemic spread of TB, aligning with the observed survival and body weight data that suggest these formulations were more effective and potentially less toxic.

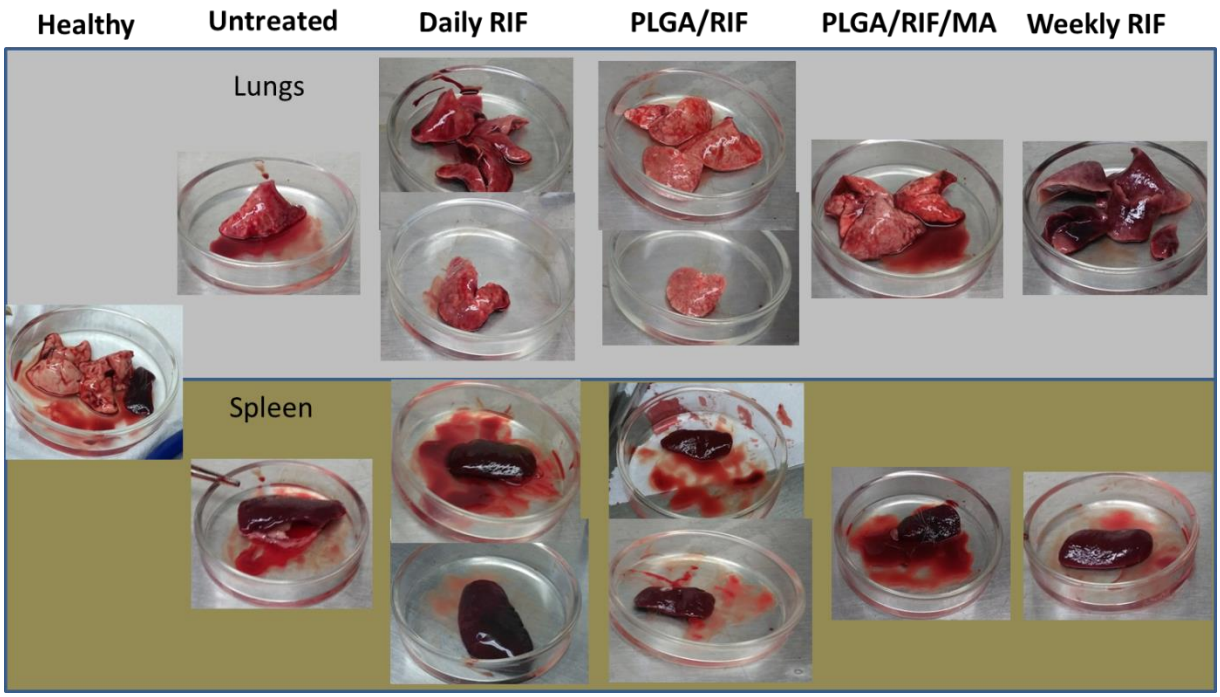

Figure 6: Comparative visual presentation of lung and spleen tissues from guinea pigs subjected to different TB treatment regimens. The images provide a qualitative assessment of pathological changes in size, coloration, and lesion development, indicative of the infection's progression or response to treatment across the study groups.

3.3.4 Histopathology

During the histopathological examination at the end of the study, the following observations were made across all specimens observed.

Lungs:

Interstitial granulomatous pneumonia (multifocal or diffuse):

The lung lesions revealed severe interstitial granulomatous pneumonia where hypertrophic alveolar macrophages appeared to predominate and filled numerous alveoli. These lesions were either multifocal or diffuse (more progressed form of disease) in the different lung sections. In the terminal bronchiole some vacuolated macrophages, polymorphonuclear cell debris as well as desquamated epithelial cells could be detected.

Peribronchial / perivascular lymphoplasmacytic cuffing:

Lymphocytic infiltrates could be detected along some of the bronchioli as well as around blood vessels in the lung tissue.

Vacuolar hypertrophic alveolar macrophages (foam cells):

These macrophages (also known as foam cells) were observed as part of the inflammatory macrophages in the lung alveoli as well as in terminal bronchioli originating from the alveolar macrophages. They were hypertrophic and revealed a vacuolated cytoplasm.

Lymph node:

Lymphoid hyperplasia:

The lymphoid hyperplasia found in some of the lymph node sections is indicative of an immune responsive reaction where the cortical as well as the paracortical lymphoid tissue appears hyperplastic and reactive.

Granulomatous lymphadenitis:

Granulomatous lymphadenitis refers to multifocal areas of hypertrophic epithelioid macrophages infiltrating parts of the lymph node. Small foci of coagulative necrosis were also present within these areas of granulomatous lymphadenitis.

Spleen:

Multinodular lymphoid hyperplasia:

The hyperplastic changes in lymphoid tissue appeared to be most prominent in the white pulp of the spleen. Lymphocytic cells as well as plasma cells and some extramedullary haemopoietic cells were observed in the splenic red pulp.

Granulomatous multifocal splenitis:

Within some of the spleen sections areas of granulomatous inflammation could be detected within the splenic pulp and again epithelioid macrophages appeared to predominate in these granulomatous multifocal areas of splenitis.

Liver:

Vacuolar centrilobular hepatopathy:

This vacuolar change appeared to be around the centrilobular areas where hydrophobic degeneration and a vacuolar cytoplasmic change within hepatocytes could be detected.

Granulomatous multifocal hepatitis:

Foci of necrosis and granulomatous inflammatory infiltrates by macrophages were observed within some of the liver sections.

Table 16 (appendix A) provides a summary of the histopathological findings in lung, lymph node, and spleen tissues from guinea pigs subjected to various TB treatment regimens. Lung tissue findings include multifocal and diffuse interstitial granulomatous pneumonia, peribronchial/perivascular lymphoplasmacytic cuffing, and vacuolar hypertrophic alveolar macrophages, with severity rated from 0 to 3+. The lymph nodes had instances of lymphoid hyperplasia and granulomatous lymphadenitis. In the spleen, multifocal lymphoid hyperplasia and granulomatous multifocal splenitis were observed. Severity gradings vary across individuals, and certain specimens were not sampled (NS) or showed severe freeze artifacts (SFA).

Figure 7 through Figure 17 provide microscopy images at various magnifications comparing healthy and diseased lung tissue, illustrating normal macrophage distribution versus granuloma formation and hypertrophic macrophages, as well as spleen tissue showing granulomatous inflammation.

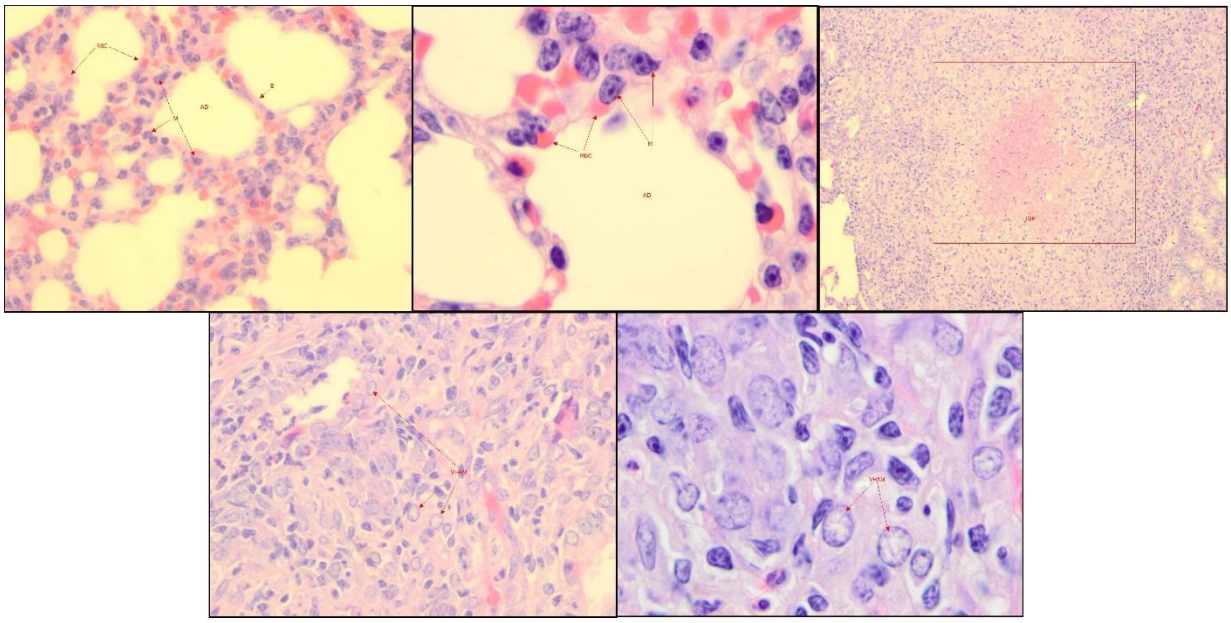

Figure 7: Light microscopy comparison of lung tissue (40X magnification). Top left: Shows normal lung tissue. Top Middle and Top Right: Shows multifocal interstitial granulomatous pneumonia as seen for animal no 3 (group 5) and 18 (group 4). Bottom Left and Bottom Right: shows diffuse interstitial granulomatous pneumonia as seen for animal no 20 and 21 (both group 5)

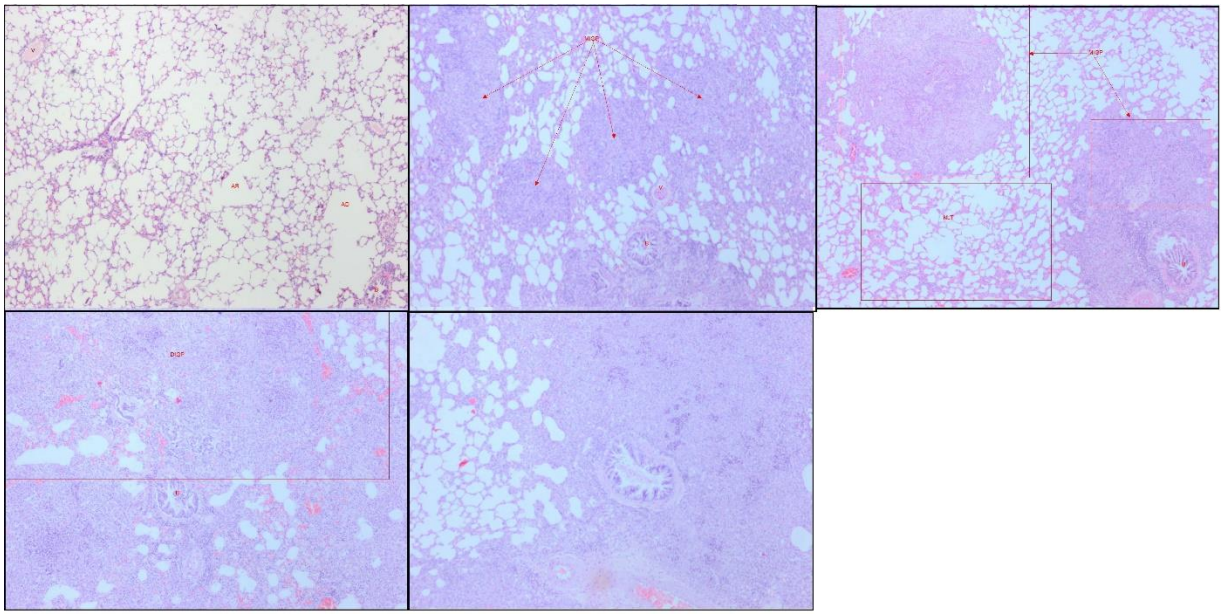

Figure 8: Resident alveolar macrophage comparison. Top Left (400X) and Top Middle (1000X) shows normal alveolar macrophage distribution and morphology. Top Right (40X) shows the formation of a

granuloma. Bottom Left (400X) and Bottom Right (1000X) shows vacuolar hypertrophic alveolar macrophages (foam cells) as seen in animal 1 (group 2)

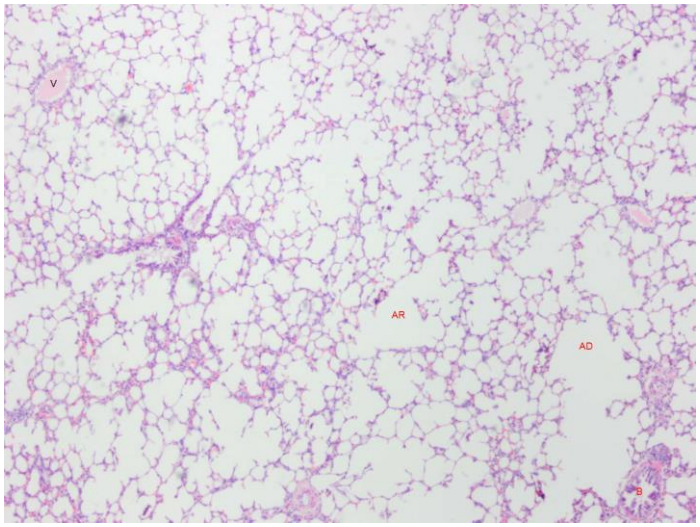

Figure 9: Normal lung tissue. A 40X magnification of lung tissue. Clearly visible are the thin endothelial walls around the alveolar sacks. AR - Alveolar Ring; AD – Alveolar Duct; V –Vein

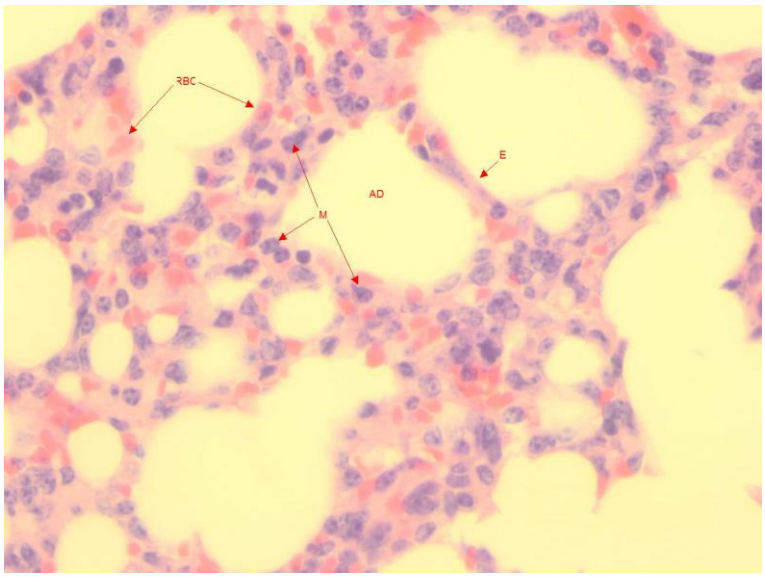

Figure 10: Normal alveolar macrophage distribution. A 400X magnification showing normal distribution and morphology of alveolar macrophages. E – Endothelium; RBC – Red Blood Cell; M –Alveolar Macrophage; AD – Alveolar duct

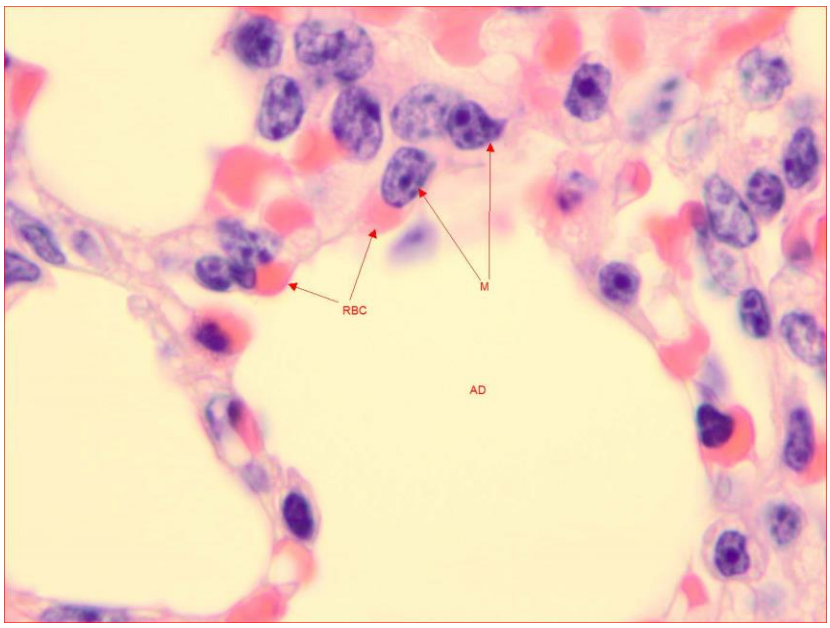

Figure 11: Normal alveolar macrophage distribution. A 1000X magnification showing normal distribution and morphology of alveolar macrophages. AD- Alveolar Duct.

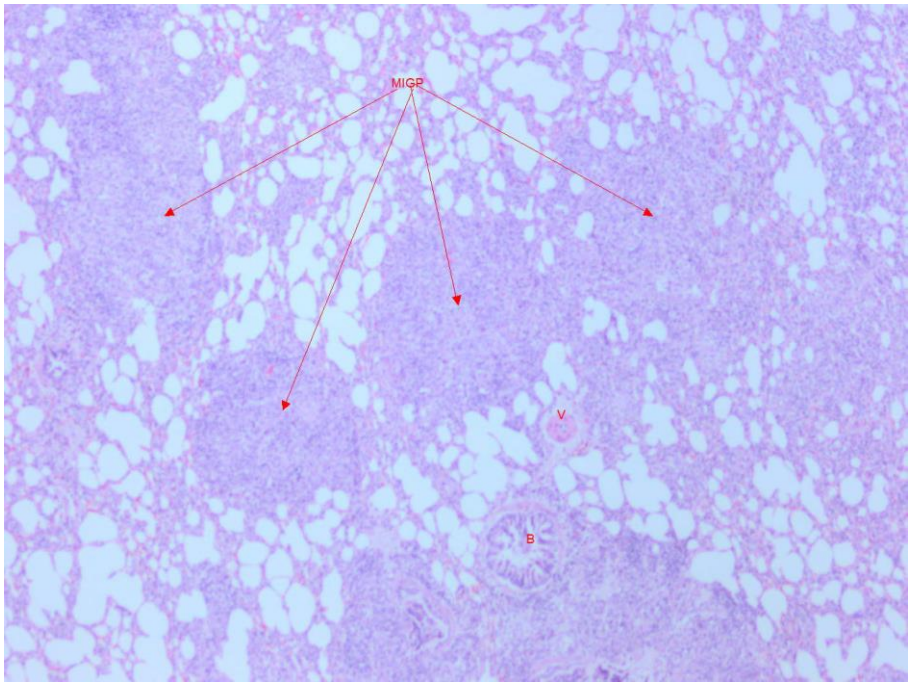

Figure 12: Multifocal interstitial granulomatous pneumonia. A 40X magnification showing distinct multifocal granuloma formation as seen for animal no 18 (group 4). B- Bronchiolus; MIGP - Multifocal Interstitial Granulomatous Pneumonia

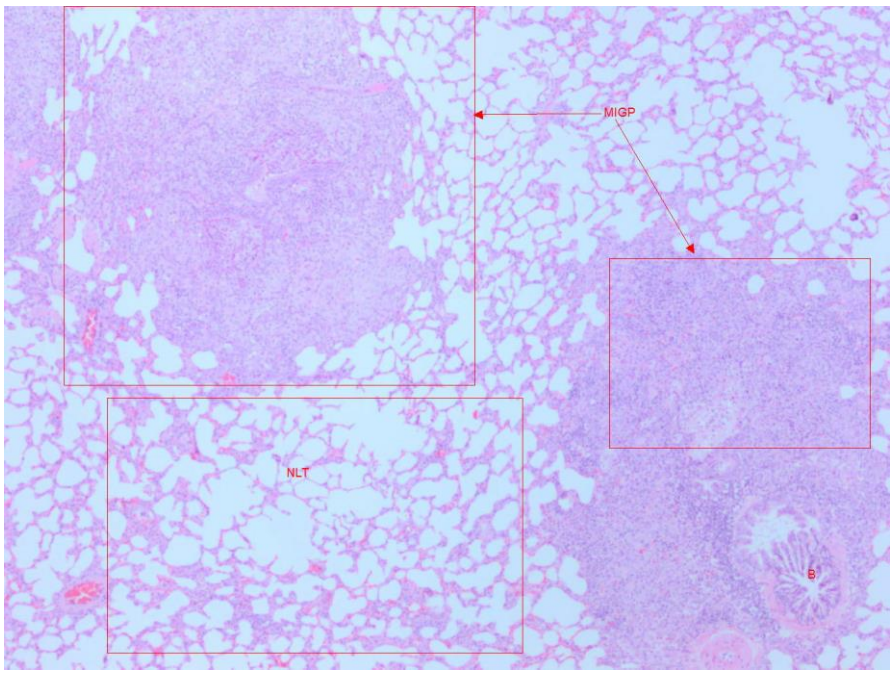

Figure 13: Multifocal interstitial granulomatous pneumonia. A 40X magnification showing distinct multifocal granuloma formation with surrounding normal tissue as seen for animal no 3 (group 5). NLT – Normal Lung Tissue

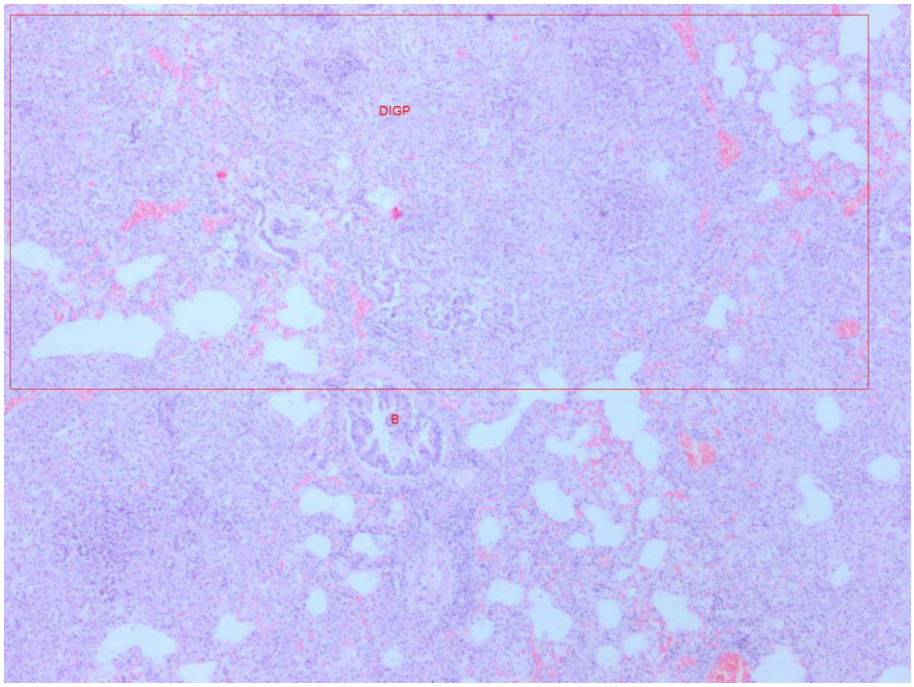

Figure 14: Diffuse interstitial granulomatous pneumonia. A 40X magnification showing diffuse granuloma formation as seen for animal no 20 (group 5). DIGP - Diffuse Interstitial Granulomatous Pneumonia, B- Blood vessel

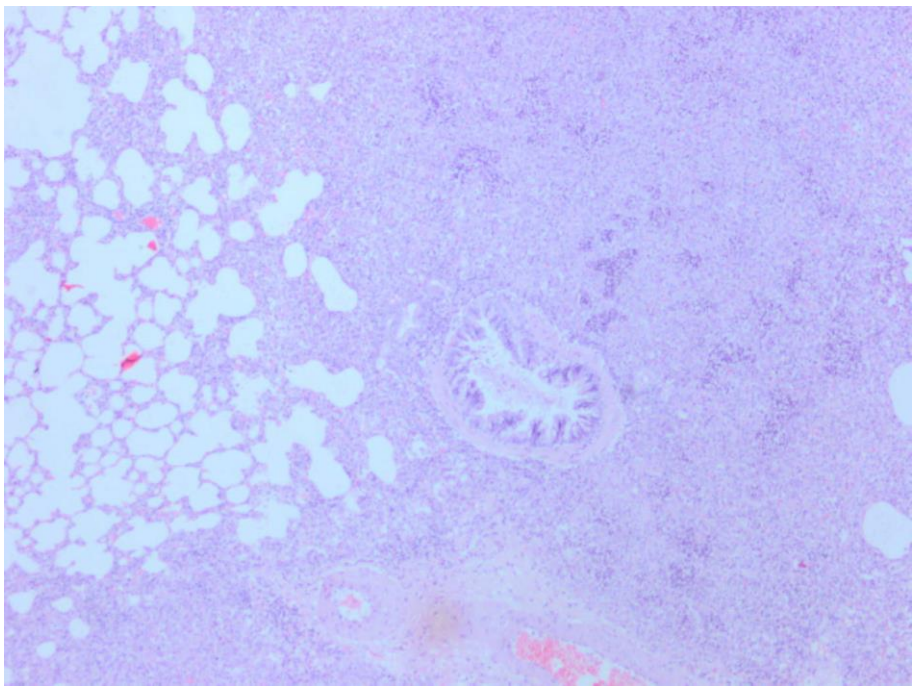

Figure 15: Diffuse interstitial granulomatous pneumonia. A 40X magnification showing diffuse granuloma formation as seen for animal no 21 (group 5).

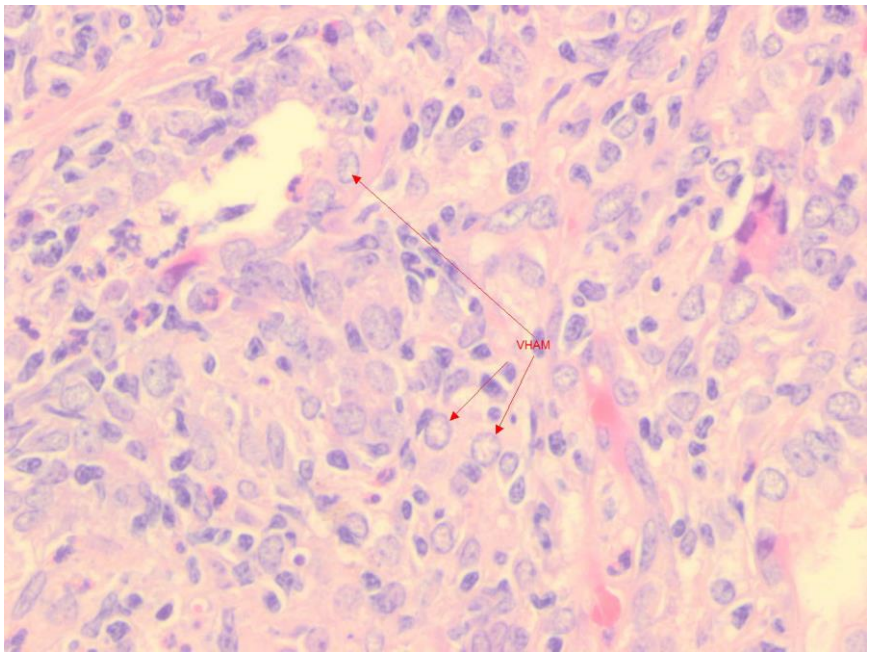

Figure 16: Vacuolar Hypertrophic Alveolar Macrophages (foam cells). A 400X magnification showing inflamed granulomatous vacuolated macrophages as seen for animal no 1 (group 2). VHAM - Vacuolar Hypertrophic Alveolar Macrophages

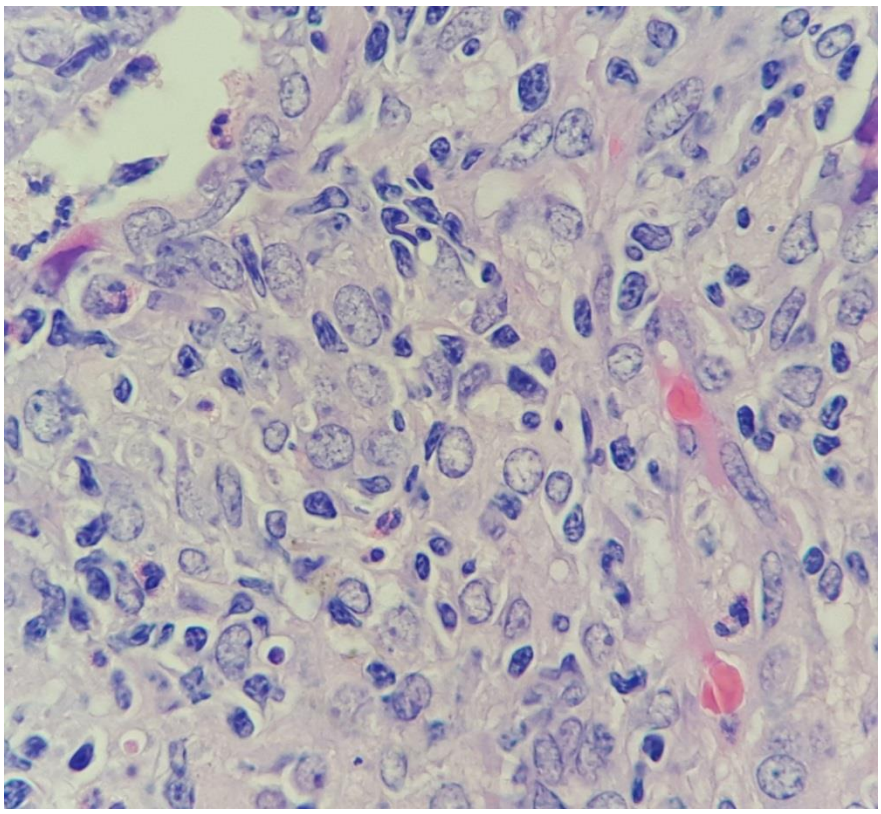

Figure 17: Vacuolar Hypertrophic Alveolar Macrophages (foam cells). A 1000X magnification showing inflamed granulomatous vacuolated macrophages as seen for animal no 1 (group 2)

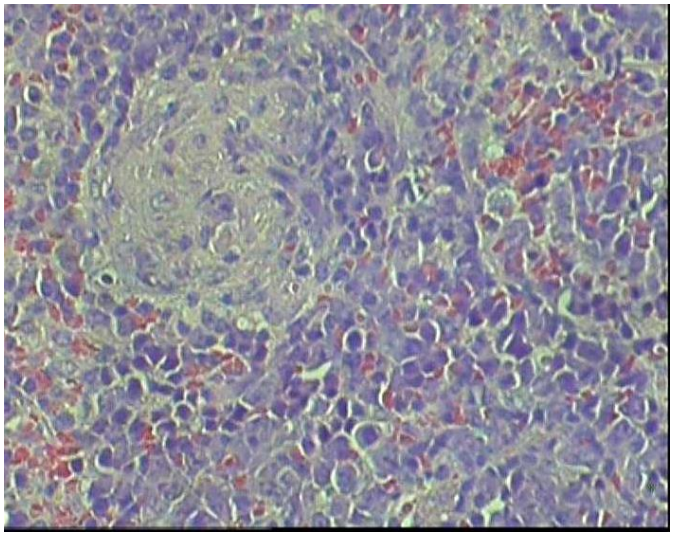

Figure 18: Granulomatous splenitis. A 200X magnification showing areas of granulomatous inflammation as seen for animal no 16 (group 1).

Table 11 and Table 12 present the frequency of histopathological findings in the different groups. Multifocal interstitial granulomatous pneumonia was observed more frequently in the PLGA/RIF group, whereas diffuse interstitial granulomatous pneumonia was most

common in untreated and weekly RIF groups. For granulomatous multifocal splenitis, the untreated and baseline groups showed the highest incidence.

Table 11: Distribution of multifocal versus diffuse interstitial granulomatous pneumonia in guinea pigs across different treatment groups including baseline, untreated, daily Rifampicin (RIF), PLGA encapsulated RIF (PLGA/RIF), PLGA encapsulated RIF with mycolic acid (PLGA/RIF/MA), and weekly RIF. The table quantifies the presence of each pneumonia type within each group, highlighting the impact of treatment modalities on disease pathology.

Group	Multifocal interstitial granulomatous pneumonia	Diffuse interstitial granulomatous pneumonia
Baseline	0/3	3/3
Untreated	1/4	3/4
Daily RIF	1/5	4/5
PLGA/RIF	4/5	1/5
PLGA/RIF/MA	1/5	4/5
Weekly RIF	0/5	5/5

Table 12: Incidence of granulomatous multifocal splenitis across different treatment groups. The table shows the number of guinea pigs displaying granulomatous multifocal splenitis out of the total examined in each group, highlighting the effect of various treatments on splenic pathology.

Group	Granulomatous multifocal splenitis
Baseline	3/3
Untreated	4/4
Daily RIF	3/5
PLGA/RIF	1/5
PLGA/RIF/MA	1/5
Weekly RIF	2/5

3.3.5 Culturing and Enumeration of *Mycobacterium tuberculosis*

Table 13, Figure 19 and Figure 20 compares bacterial loads in guinea pigs infected with *M. tb*, detailing lung and spleen CFU counts post-infection. Baseline animals, all euthanised at 26 days post-infection, showed high CFUs in both organs. Untreated guinea pigs had varying survival days and CFU counts, with one showing complete bacterial clearance (Notably animal 1 – indicating possible lack of successful infection). The daily RIF group generally had lower CFU counts, indicating some treatment efficacy. The PLGA/RIF and PLGA/RIF/MA groups showed low CFU counts, especially in the spleen, with one animal in the PLGA/RIF/MA group having no detectable lung CFUs. The weekly RIF group presented a range of CFU counts. The inclusion of the nebulised control serves as a baseline to estimate the initial exposure of the guinea pigs to *M. tb* H37Rv.

This control is crucial for interpreting the subsequent bacterial counts from lung and spleen samples.

Table 13: Detailed comparison of bacterial loads in the lungs and spleen of guinea pigs across various treatment groups infected with *Mycobacterium tuberculosis* H37Rv. It quantifies Colony-Forming Units (CFU) in both organs, reflecting the bacterial burden post-infection and the efficacy of each treatment regimen.

Groups	Animal	Days survived after infection	CFU	
			Lung	Spleen
Baseline	4	26	4.14E+07	2.25E+05
	16	26	4.86E+07	9.0E+05
	23	26	5.45E+07	2.25E+05
Untreated	1	73	0	0
	5	44	3.28E+08	1.35E+06
	6	46	8.1E+06	0
	7	58	1.84E+08	6.75E+05
	8	45	2.7E+08	3.38E+06
Daily RIF	9	73	1.62E+07	1.35E+04
	10	60	1.76E+06	0
	11	73	1.80E+06	0
	12	73	1.35E+06	0
	13	27	1.22E+07	2.84E+05
PLGA/RIF	2	73	2.160E+05	0
	14	53	9.41E+07	1.28E+05
	15	73	1.32E+06	2.25E+03
	17	73	1.35E+06	2.25E+03
	18	73	6.21E+05	0
PLGA/RIF/MA	3	73	0	4.500E+03
	19	38	2.33E+08	1.26E+05
	20	33	1.04E+09	1.80E+06
	21	40	3.24E+08	9.00E+05
	22	38	2.3E+08	8.10E+04
Weekly RIF	24	37	2.03E+07	0
	25	44	3.15E+06	1.10E+04
	26	54	2.97E+07	5.50E+05
	27	51	3.22E+08	6.05E+06
	28	56	1.98E+08	2.20E+06
Nebulised	NA	0	3.9000E+04	NA

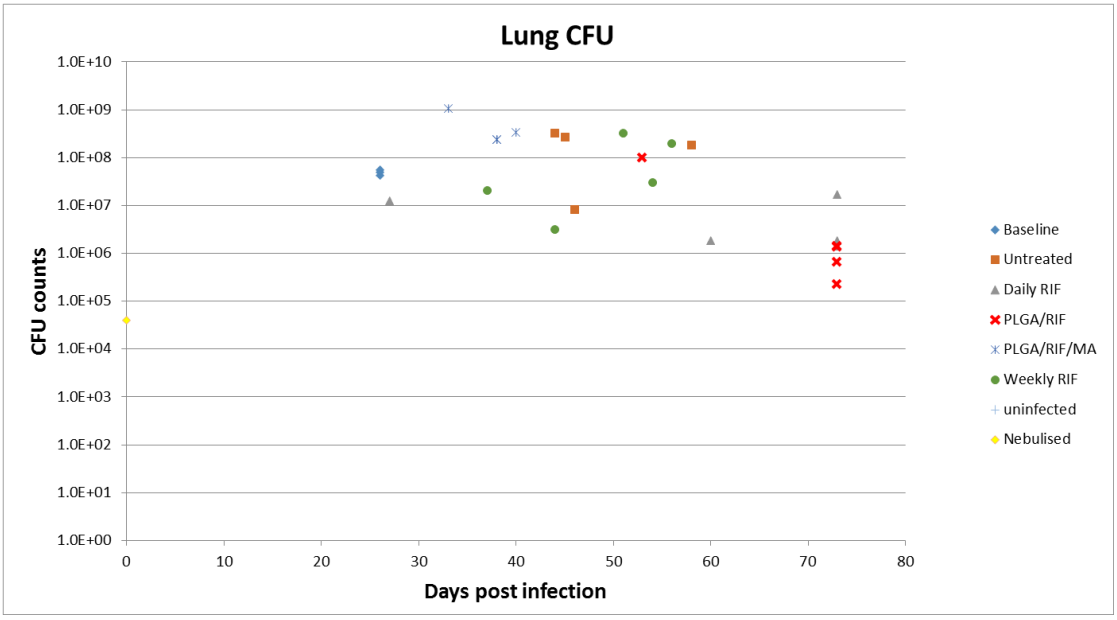

Figure 19: Scatter plot to illustrate the Colony-Forming Unit (CFU) counts in the lungs of guinea pigs at various days post-infection, across different treatment groups: baseline, untreated, daily Rifampicin (RIF), PLGA encapsulated RIF (PLGA/RIF), PLGA encapsulated RIF with mycolic acid (PLGA/RIF/MA), weekly RIF, uninfected, and nebulised *Mycobacterium tuberculosis* H37Rv. Each point represents the bacterial load in an individual animal's lungs, providing a visual comparison of the bacterial burden across the treatment regimens and over time.

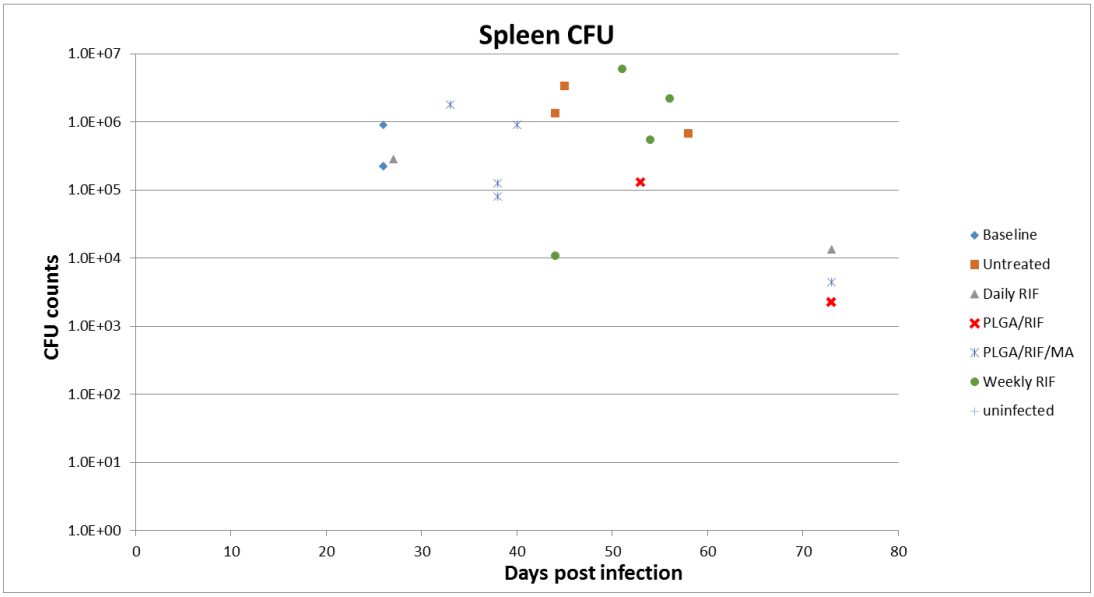

Figure 20: Scatter plot of the Colony-Forming Unit (CFU) counts in the spleen of guinea pigs after infection with *Mycobacterium tuberculosis* H37Rv, charting the bacterial burden at various days post-infection for different treatment groups: baseline, untreated, daily Rifampicin (RIF), PLGA encapsulated RIF (PLGA/RIF), PLGA encapsulated RIF with mycolic acid (PLGA/RIF/MA), and weekly RIF, including a comparison with uninfected animals. Each symbol corresponds to a particular treatment, illustrating the variation in spleen CFU counts over time.

Figure 21 and Figure 22 illustrate the interval plots for lung and spleen CFU culturing, respectively. Notably, the data is characterised by significantly large error bars, which denote considerable standard deviations across the measurements.

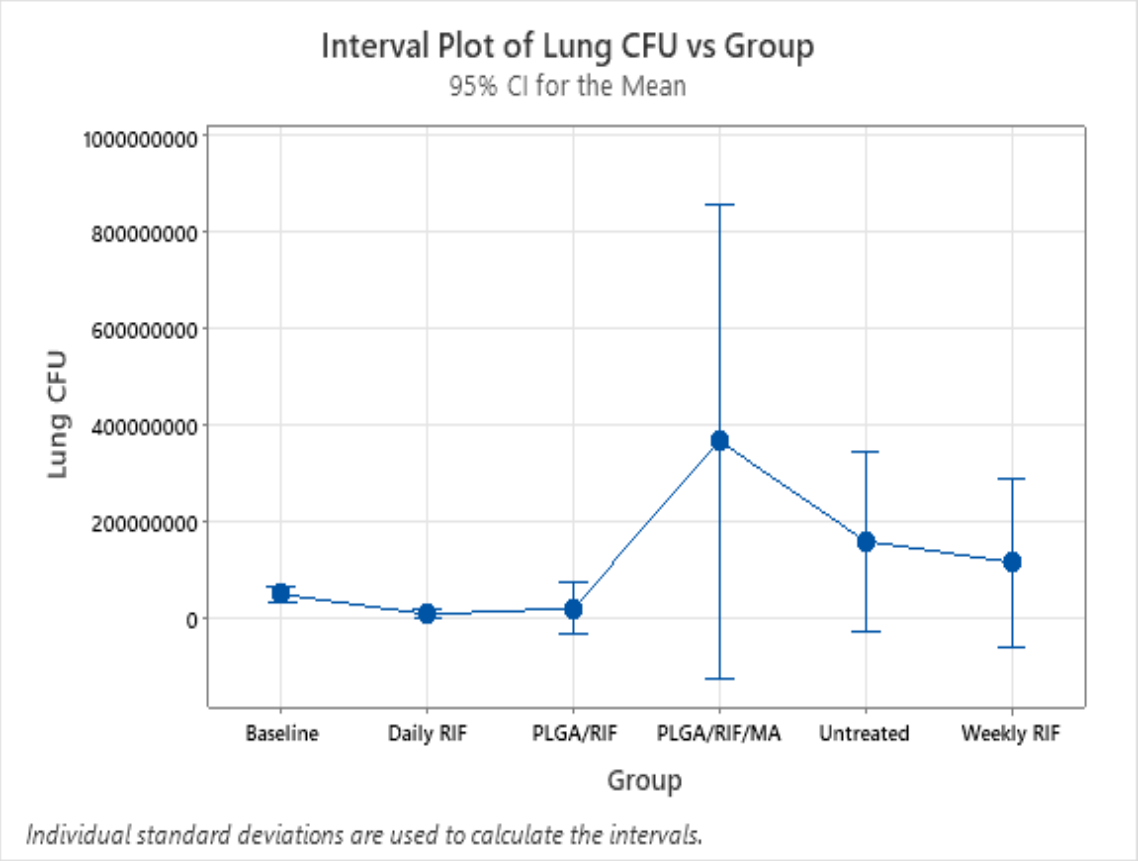

Figure 21: Interval Plot of Lung Colony-Forming Units (CFU) by Treatment Group. This plot displays the mean lung CFU counts and their corresponding 95% confidence intervals (CIs) for different treatment groups in a guinea pig model of tuberculosis. Groups compared include baseline, daily administered Rifampicin (RIF), Rifampicin encapsulated in poly(lactic-co-glycolic acid) (PLGA), Rifampicin in PLGA with mycolic acid targeting ligand (PLGA/RIF/MA), untreated control, and weekly administered RIF. The error bars represent the variability within each group, calculated using individual standard deviations.

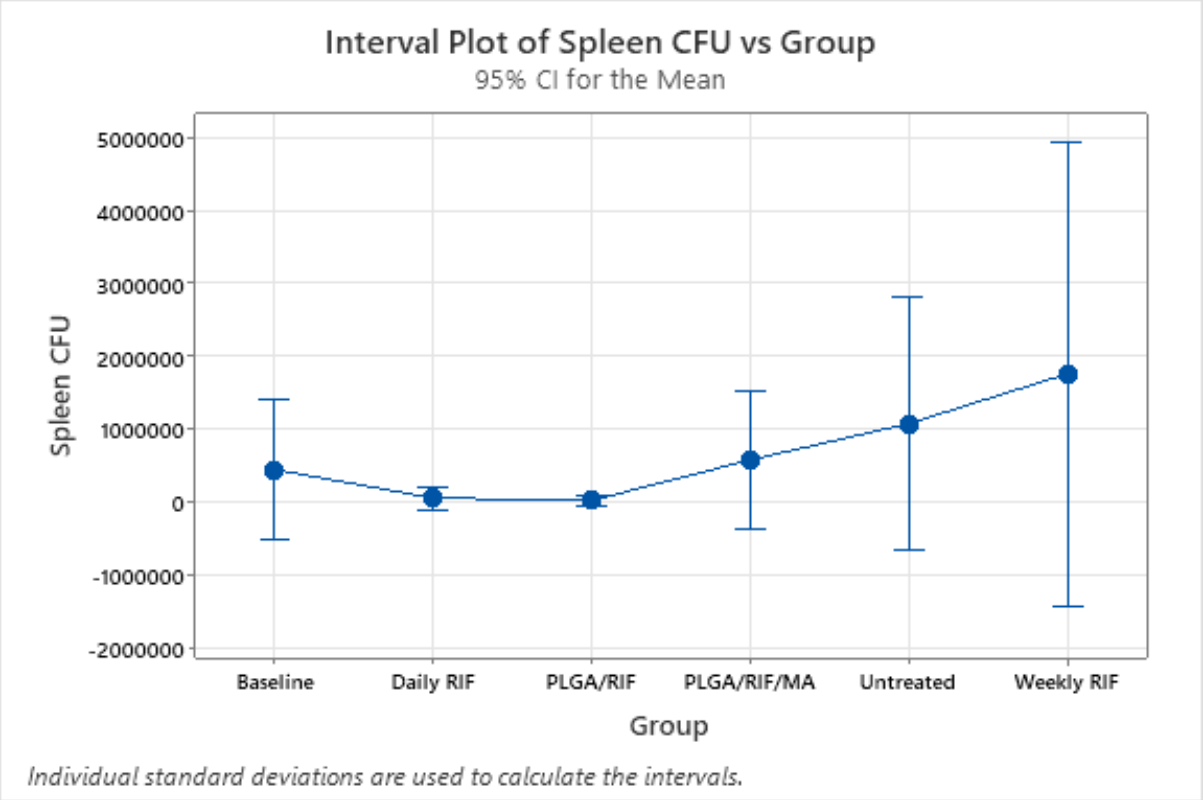

Figure 22: Interval Plot of Spleen Colony-Forming Units (CFU) by Treatment Group. This plot displays the mean spleen CFU counts and their corresponding 95% confidence intervals (CIs) for different treatment groups in a guinea pig model of tuberculosis. Groups compared include baseline, daily administered Rifampicin (RIF), Rifampicin encapsulated in poly(lactic-co-glycolic acid) (PLGA), Rifampicin in PLGA with mycolic acid targeting ligand (PLGA/RIF/MA), untreated control, and weekly administered RIF. The error bars represent the variability within each group, calculated using individual standard deviations.

A One-way ANOVA analysis was undertaken to ascertain if discernible statistical differences exist amongst the mean lung CFU counts for the various treatment cohorts, presented in Figure 23. All analysis were done at a 95% confidence level (α=0.05). Results indicated that the Daily Rif group exhibited CFU counts that were statistically lower than those of the baseline control group, with a 95% confidence interval affirming this outcome. Nonetheless, the analysis did not reveal any other statistically significant differences between groups. The lack of significant findings may be attributed to the notably low statistical power observed in this study, as depicted in Figure 24. Specifically, when assessing a CFU count difference of 1×10^7 as substantial, the experimental power fluctuated between only 1.88% and 15.82%. To achieve an 80% statistical power for discerning differences in lung CFU counts across the treatment groups, the data suggests that a considerably larger sample size, estimated at 23,001 animals per group, would be needed.

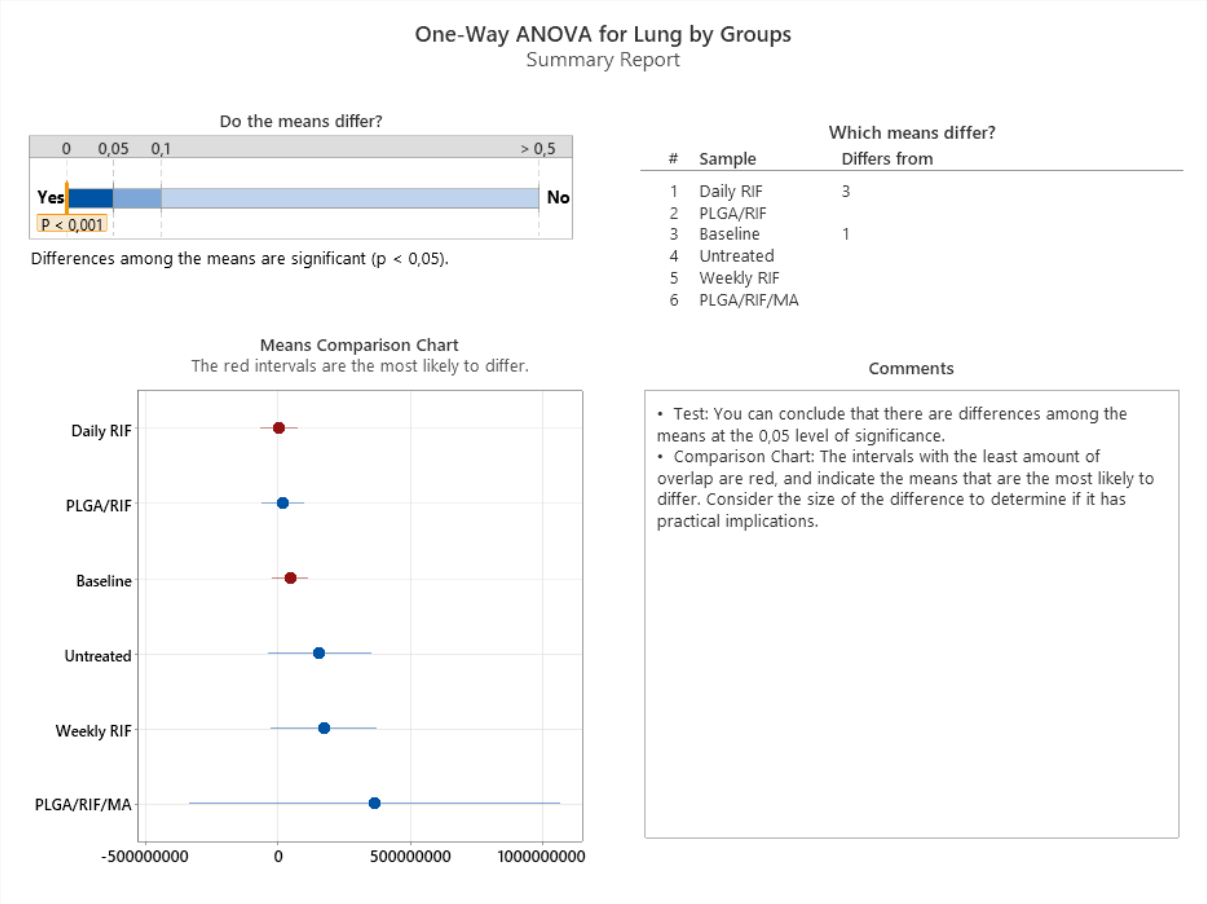

Figure 23: One-Way ANOVA Summary for Lung CFU Counts by Treatment Group. This figure summarises the statistical analysis of lung colony-forming units (CFU) among different treatment groups using one-way ANOVA. The analysis confirms significant differences in the mean lung CFUs ($p < 0.05$). Non-overlapping red intervals suggest groups with means most likely to differ. The table on the right outlines which specific group means are statistically different from each other.

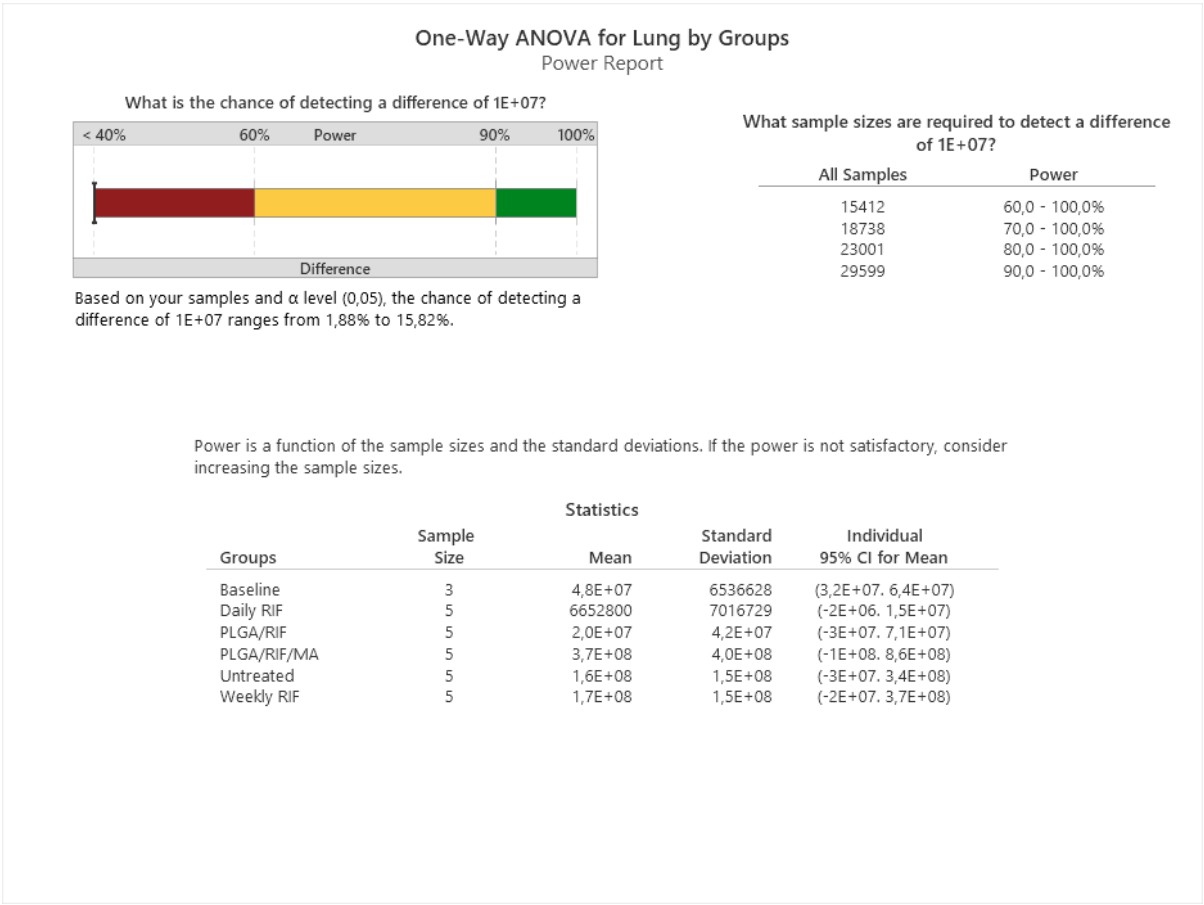

Figure 24: Power Analysis and Required Sample Size for Lung CFU Detection in a One-Way ANOVA. This figure illustrates the statistical power achieved in detecting a difference of 1E+07 in lung CFU counts between treatment groups, with current power ranging from 1.88% to 15.82%. It also indicates the substantial increase in sample size required to achieve higher statistical power

The principal factor contributing to the insufficient statistical power and the consequent requirement for a large sample size is attributed to the considerable pooled standard deviation, which was determined to be 192,749,593 (Table 14).

Table 14: Summary of the pooled standard deviations of lung colony-forming units (CFUs) across different experimental groups, providing a statistical basis for comparing the variability of *M. tb* infection burden within each treatment category in the study.

Groups	N	Mean	StDev	95% CI
Baseline	3	48150000	6536628	(-182638952. 278938952)
Daily RIF	5	6652800	7016729	(-172115553. 185421153)
PLGA/RIF	5	19512000	41670784	(-159256353. 198280353)
PLGA/RIF/MA	5	365400000	395657428	(186631647. 544168353)
Untreated	5	158020000	149627878	(-20748353. 336788353)
Weekly RIF	5	174970000	153616005	(-3798353. 353738353)

Pooled StDev = 192749593

If methodological refinements could reduce the standard deviation to approximately $1x10^7$, the sample size needed to detect significant differences between the treatment groups, previously indistinguishable in this preliminary study, would be substantially decreased to just 27 animals, according to calculations presented in (Table 15).

Table 15: Sample size calculation at α=0.05 assuming a standard deviation of 10 000, to detect a difference of 1 x 10^7.

Maximum Difference		Sample Size	Target Power	Actual Power
10000000		27	0,8	0,807185

The sample size is for each level. Assumed standard deviation = 10000000

Analysis of spleen CFU counts revealed no statistically significant differences among the treatment groups at a 95% confidence interval, as shown in Figure 25. Similar to the findings for lung CFU counts, the statistical power of the analysis was suboptimal, ranging from 1.36% to 6.61% (Figure 26). To attain adequate power, an exceedingly large sample size of 10,872 would be necessary, which is not feasible. Future research can attain manageable sample sizes with improved experimental precision, as demonstrated by the modelled reduction of standard deviations in lung CFU counts.

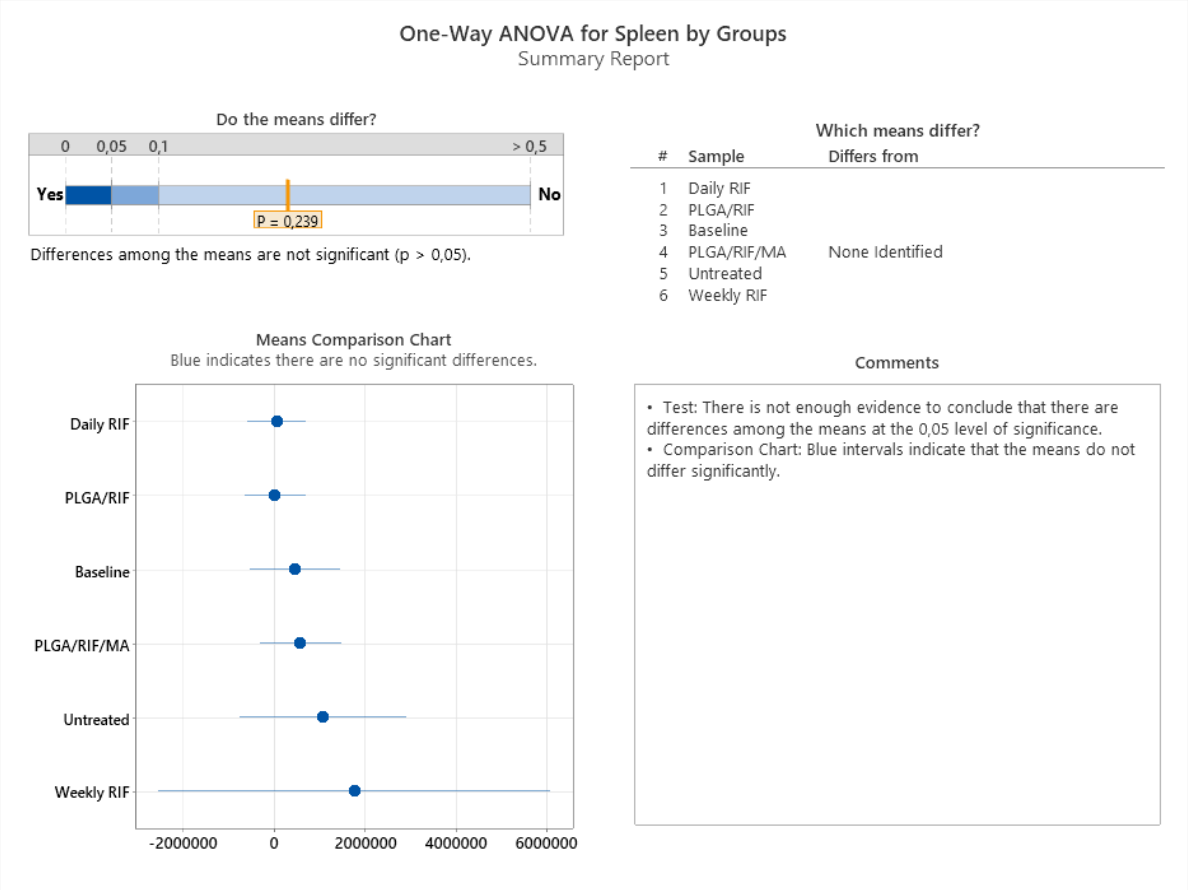

Figure 25: One-Way ANOVA Summary for Spleen CFU Counts by Treatment Group. This figure summarises the statistical analysis of spleen colony-forming units (CFU) among different treatment groups using one-way ANOVA. The analysis confirms no significant differences in the mean spleen CFUs ($p < 0.05$).

One-Way ANOVA for Spleen by Groups
Power Report

What is the chance of detecting a difference of 100000?

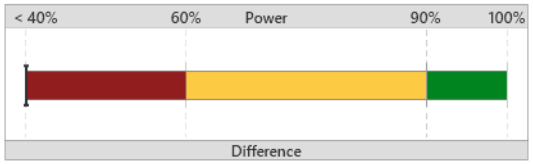

Based on your samples and α level (0,05), the chance of detecting a difference of 100000 ranges from 1,36% to 6,61%.

What sample sizes are required to detect a difference of 100000?

All Samples	Power
7286	60,0 - 100,0%
8857	70,0 - 100,0%
10872	80,0 - 100,0%
13991	90,0 - 100,0%

Power is a function of the sample sizes and the standard deviations. If the power is not satisfactory, consider increasing the sample sizes.

Statistics

Groups	Sample Size	Mean	Standard Deviation	Individual 95% CI for Mean
Baseline	3	450000	389711	(-518097. 1418097)
Daily RIF	5	59400	125412	(-96320. 215120)
PLGA/RIF	5	26550	56863	(-44055. 97155)
PLGA/RIF/MA	5	582300	770891	(-374887. 1539487)
Untreated	5	1080000	1399710	(-657969. 2817969)
Weekly RIF	5	1762200	2560194	(-1E+06. 4941101)

Figure 26: Power Analysis and Required Sample Size for Spleen CFU Detection in a One-Way ANOVA. This figure illustrates the statistical power achieved in detecting a difference of 1E+05 in spleen CFU counts between treatment groups, with current power ranging from 1.36% to 6.61%. It also indicates the substantial increase in sample size required to achieve higher statistical power.

3.4 Discussion

The investigation of nanoencapsulated anti-TB drug delivery represents an advancement for the enhancement of efficacy and tolerability of TB treatment. Prior investigations, primarily done in animal models, have set the foundation for understanding how nanoencapsulation can improve therapeutic outcomes (Nair *et al*., 2023). These studies have predominantly employed murine models, guinea pigs, and occasionally non-human primates to assess the pharmacodynamics, pharmacokinetics, and potential toxicity of nanoencapsulated anti-TB drugs. The appeal of nanoencapsulation lies in its ability to target drug delivery more precisely to the infected cells, thereby maximising drug efficacy while minimising systemic side effects (Nabi *et al*., 2020).

Despite the promising results in animal studies, the transition to clinical trials in humans encounters several challenges. Key among these challenges is the need for exhaustive toxicity profiling to ensure that nanoencapsulated formulations do not induce adverse effects over the long-term treatment courses typical for TB therapy. Moreover, the

complexity of human TB, particularly in the face of co-morbidities such as HIV, necessitates a deeper understanding of how nanoencapsulated drugs interact within the human physiological environment. Another significant barrier is the scalability of nanoencapsulation processes for mass production, ensuring that these innovative treatments can be manufactured at a cost and scale feasible for widespread clinical application (Kumar *et al*., 2023).

This pilot study was inspired by the state-of-the-art research in nanoencapsulated anti-TB drug delivery, aiming to contribute to the body of evidence needed to advance towards human clinical trials. By focusing on the guinea pig model of high *M. tb* bacillary load infection, which closely mirrors the human condition in terms of disease progression and immune response, this investigation sought to gather preliminary data on the efficacy of various nanoencapsulated treatments. Guinea pigs offer a more representative model for human TB, particularly in the formation of granulomatous lesions and the overall pathogenesis of the disease, compared to the conventional mouse models.

As a pilot study with a limited sample size, this research did not aim to establish statistical significance but rather to explore trends and gather preliminary data on the efficacy of various treatments for *M. tb* infection in guinea pigs. The observed clinical signs, such as mild cyanosis, increased respiratory rates, and decreased motor activity, emerged as indicators of disease progression by day 25, which is consistent with the known pathology of TB. The absence of symptoms until day 24 aligns with the insidious nature of TB, where clinical manifestations often appear only after significant disease progression (Achkar & Jenny-Avital, 2011).

These clinical presentations underscored the need for prompt treatment to address the respiratory distress and overall decline in health caused by the *M. tb* infection. The collected data points to the critical timing of treatment initiation in the disease course, where delayed intervention could lead to exacerbated symptoms and poorer health outcomes (Tedla *et al*., 2020).

The survival rate and weight gain/loss profile over a 73-day period offer initial insights into the treatment efficacy for TB in guinea pigs. The varying survival outcomes across groups, with the PLGA/RIF group showing the highest survival rate (4/5), point to the potential effectiveness of nanoparticle-encapsulated drugs. The weight data, demonstrating consistent increase in some and decrease or fluctuations in others, especially in later stages, underscores the importance of considering both morbidity and

mortality in evaluating treatment impact. The total remaining body weight metric provides a more comprehensive assessment by accounting for the combined health status of the surviving animals and the impact of any fatalities. This data, indicating a progressive decrease in weight among untreated animals and weight stabilisation with daily PLGA/RIF treatment, suggests that encapsulated drug forms like PLGA/RIF may offer a balance of efficacy and tolerability, a hypothesis that should be tested in larger, statistically powered studies.

The macropathological findings from this pilot study offer insights into the pathogenesis and treatment response of TB in guinea pigs. Raised granulomas in untreated guinea pigs were indicative of advanced disease progression. On the other hand, the presence of flat lesions in treated groups, especially in those receiving nanoparticle formulations, may reflect a therapeutic response, potentially to contain the disease's advancement.

Observations of darkened, necrotic lung tissue in the weekly RIF group could indicate severe infection or adverse drug reactions. Moreover, the detection of splenomegaly in both untreated and certain treated groups suggested systemic infection. Notably, its absence in the PLGA/RIF and PLGA/RIF/MA cohorts might reflect the protective efficacy of these treatments.

The histological assessment of lung tissues across all animals, including those that did not survive until the endpoint, revealed a clear distinction in disease presentation between treatment groups. The occurrence of diffuse interstitial granulomatous pneumonia was prevalent in untreated and free Rifampicin (RIF) treated animals, marked by a 3+ severity rating in the majority of these subjects. This pattern, indicative of an uncontrolled and widespread disease, contrasts with the multifocal interstitial granulomatous pneumonia observed in the PLGA/RIF group, which suggests a more localised and potentially controlled infection. The presence of peribronchial/perivascular lymphoplasmacytic cuffing and vacuolar hypertrophic alveolar macrophages in this group point to an active immune response, yet the severity was comparatively less than that observed in the untreated cohorts.

The comparative analysis of multifocal versus diffuse pathology in both the lung and spleen tissues is revealing. Multifocal lesions, as seen in the PLGA nanoparticle-treated groups, are typically associated with a more contained infection, where the immune response has potentially localised and isolated the disease. Conversely, diffuse

pathology often suggests an overwhelmed immune system and a more aggressive disease state, as observed in the untreated and free RIF groups.

The differential histopathological outcomes observed could be attributed to the sustained release and targeted delivery of the PLGA encapsulated treatments, which might afford a more effective concentration of the drug at the site of infection, thereby enhancing the therapeutic response. The encapsulation within PLGA could also mitigate systemic toxicity associated with RIF and reduce the occurrence of adverse reactions like splenomegaly. However, the higher dosage of PLGA and MA in the PLGA/RIF/MA formulation, due to lower RIF loading raised the prospect of increased PLGA-associated toxicity. The work of Lemmer *et al*. (2015) underscores the significance of recognising a threshold toxicity level for PLGA, especially relevant given the potent targeting capabilities endowed by MA. This targeting efficiency could lead to PLGA and MA accumulation within phagocytic cells, highlighting the need for a delicate balance between therapeutic advantage and the risk of adverse outcomes.

The presence of MA in higher concentrations, as necessitated by the lower rifampicin loading percentage in the PLGA/RIF/MA formulation, calls for a critical examination beyond the known dose-dependent toxicity of PLGA. While MA enhances the delivery system's specificity and efficiency—targeting the bacterial cell wall components of *M. tb*—its elevated levels in our formulation may introduce complex biological effects. Specifically, as our study found that the PLGA/RIF/MA group received approximately 2.37 times more PLGA carrier compared to the PLGA/RIF group, the implications extend to the MA component as well. At such elevated levels, MA could exert immunomodulatory effects that, while potentially beneficial in modulating the host's immune response to *M. tb*, might also trigger unintended immune reactions or interfere with normal cellular functions. This dual potential underscore the necessity of understanding the cumulative impact of increased concentrations of both PLGA and MA. Enhanced carrier volumes not only raise concerns about dose-dependent toxicity but also about how increased MA concentrations influence treatment efficacy and safety profiles, potentially exacerbating side effects or altering therapeutic outcomes (H. Wang *et al*., 2024). These findings highlight the importance of optimising nanoparticle formulations to balance efficacy with safety, ensuring that the benefits of targeting and delivery efficiency do not come at the cost of increased adverse reactions.

The literature on TB treatment highlights the importance of targeted drug delivery systems in enhancing the efficacy of therapeutics (Nair *et al*., 2023). The observed

histopathological patterns align with these findings, as encapsulated formulations have been shown to direct the drug to the macrophages, the primary host cells of *M. tb* (Nair *et al*., 2023). This targeted approach may result in reduced tissue damage and a more robust containment of the infection, as reflected in the histopathological findings of this study.

The study's findings on the culturing and enumeration of *M. tb* from guinea pigs' lungs and spleen reveal significant insights into treatment efficacy. Lower bacterial counts in the lungs and spleen, especially in the groups treated with daily Rifampicin, suggest these treatments were effective in controlling the bacterial load. The variability in CFU counts within the weekly Rifampicin group and the high bacterial loads in untreated animals underscore the challenge of TB treatment. The inclusion of a nebulised control provided a baseline for initial bacterial exposure, essential for contextualising the treatment outcomes. These results highlight the potential of nanoparticle-encapsulated drugs in reducing the bacterial burden of TB, warranting further investigation in larger, more definitive studies.

The pilot study aimed to simulate a clinical setting with a high challenge TB model but encountered limited statistical power due to the small sample size and significant standard deviations. Optimising methods, particularly the exposure protocol to *M. tb*, could enhance consistency and reduce variability. Future studies could be improved by standardising the infection model, using a fixed volume of bacterial culture for each guinea pig exposure, and initiating treatment earlier. Incorporating serological tests for the detection of anti-mycolate antibodies offers a promising strategy to enhance the early identification of TB in animal models (Ndlandla *et al*., 2016). By measuring the presence and levels of anti-mycolate antibodies, one can potentially identify TB infection before clinical symptoms or significant pathological changes occur. Adopting this serological approach could significantly improve the timing of therapeutic interventions in TB studies, allowing for treatment initiation at the earliest stages of infection. These adjustments should be aimed at standardising infection rates and survival outcomes, potentially allowing for more robust statistical comparisons across uniform post-infection analysis points.

This study suggests that nanoparticle encapsulation, particularly with PLGA, offers a promising avenue for improving TB treatment efficacy, reducing systemic toxicity, and enhancing the survival rate of affected subjects. Further studies are warranted to confirm

these benefits and to fully understand the mechanisms underlying the improved outcomes observed in nanoparticle-treated groups.

4. CONCLUDING DISCUSSION

This study explored the therapeutic potential of poly(lactic-co-glycolic acid) (PLGA)-encapsulated Rifampicin, both with and without mycolic acid (MA) as a targeting adjunct, in a guinea pig model of TB. It generated valuable insights, including clinical observations, survival metrics, weight dynamics, macroscopic and microscopic pathological analyses, along with bacterial load quantification. These aspects collectively reveal the potential benefits and challenges inherent in these innovative therapeutic strategies.

Key Findings:

Clinical Efficacy and Survival Rates: The PLGA/RIF group demonstrated enhanced survival and health outcomes compared to traditional Rifampicin treatments and untreated controls, suggesting improved treatment efficacy of the nanoparticle-encapsulated form.

Weight Gain/Loss Patterns: Stability in weight among treated groups highlights the tolerability of the nanoparticle formulations, with the PLGA/RIF group showing consistent weight increase, indicative of treatment efficacy.

Macropathological and Histopathological Insights: Pathological assessments revealed reduced disease progression and systemic infection in nanoparticle-treated groups, suggesting targeted delivery's role in enhancing drug efficacy and reducing off-target effects.

Bacterial Load Reduction: Suggested reductions *in M. tb* CFU counts in lung and spleen tissues in nanoparticle-treated groups point to a potential beneficial antimicrobial activity of these formulations, which justify further investigation.

Implications for Future Research:

These preliminary findings pave the way for continued development and optimisation of nanoparticle-based drug delivery systems for TB treatment.

The differential RIF loading leading to variations in PLGA and MA administration underscores critical considerations for future nanoparticle-based drug delivery research.

In this study, it was calculated that guinea pigs in the PLGA/RIF/MA group received approximately 2.37 times more PLGA carrier than those in the PLGA/RIF group, due to the differing RIF loading percentages of 11.12% and 5.01%, respectively. The relationship between increased dosages of PLGA, the incorporation of MA, and their collective impact on treatment outcomes will be crucial. Future research directions should include the evaluation of the pharmacodynamics, therapeutic efficacy, and potential toxicity associated with higher doses of both PLGA and MA. This includes exploring dose-response relationships, identifying maximum safe dosages, and elucidating the mechanistic pathways through which PLGA and MA exert their effects, particularly in the context of targeted nanoparticle delivery systems. Such investigations will ensure that the therapeutic benefits derived from the use of PLGA and MA are not outweighed by toxicity concerns, leading the way for optimised, safe, and effective TB treatment strategies. Future studies should thus prioritise the quantification of potential risks associated with higher doses of these components, ensuring that nanoparticle therapy remains a viable and safe option for TB treatment.

However, the incorporation of MA as a targeting ligand within PLGA nanoparticles, despite showing variability in efficacy, offers a promising direction for achieving more targeted and effective therapies. Further research, focusing on optimising the formulation, dosing regimens, and understanding the mechanisms underlying the observed therapeutic benefits, is recommended. Additionally, expanding the scope of studies to include larger sample sizes and diverse TB strains could provide more comprehensive insights into the potential of nanoparticle-encapsulated Rifampicin and similar strategies in TB management.

Conclusion:

The pilot study's outcomes highlight the promise of nanoparticle-encapsulated Rifampicin formulations in enhancing TB treatment efficacy. By offering sustained drug release, improved drug stability, and targeted delivery, these innovative approaches could significantly contribute to the global fight against TB.

Given the limitations of this pilot study, statistical significance was not achieved. The limitations include:

Small Sample Size: The study utilised a relatively small number of animals, limiting its statistical power to detect significant differences between treatment groups. Small sample sizes increase the likelihood of type II errors, where true effects are not detected.

High Variability: Substantial variability in outcomes, such as CFU counts and weight changes, was observed across individuals within treatment groups. This high variability, reflected in large standard deviations, complicates the interpretation of results and necessitates larger sample sizes to achieve statistical significance.

Limited Duration: The study's duration may not have fully captured the long-term effects of treatments on TB progression. Tuberculosis is a disease that evolves over time, and longer studies may provide more insight into the efficacy and safety of the treatments.

Dose Standardisation Issues: Variability in the drug loading of nanoparticles, particularly between PLGA/RIF and PLGA/RIF/MA formulations, introduces complexity in dose standardisation. This inconsistency could affect the comparative analysis of treatment efficacy.

Potential Toxicity of Higher Doses: The necessity to use higher doses of PLGA in the PLGA/RIF/MA group, due to lower RIF loading, raises concerns about the potential toxicity of PLGA, especially in conjunction with mycolic acid. The effects of high concentrations of both compounds on treatment safety and efficacy were not fully explored.

Single Animal Model: The study was conducted using only guinea pigs, which, while relevant, may not fully represent the complexity of TB in humans. Different animal models or human cell-based systems might provide additional insights.

Measurement and Exposure Consistency: Variability in the method of *M. tb* exposure and the quantification of bacterial load could contribute to the observed variability in outcomes. Standardising these aspects may improve the reliability of future studies.

Late disease detection: The rigid choice of Day 26 after infection to assume disease detection in all animals could be refined by rather applying a serological assay on a weekly basis to detect TB as treatment initiation parameter, rather than clinical signs and symptoms.

The lack of statistical significance is a common outcome in preliminary research where the primary goal is to explore trends and feasibility rather than definitive efficacy. The high variability observed, particularly in terms of bacterial counts and survival rates, likely contributed to the wide confidence intervals and the resultant inability to achieve statistical significance. This study, however, lays a foundational framework for a drug research testing platform. It highlights the importance of optimising dosage regimens, improving the consistency of infection models, and incorporating targeted drug delivery systems.

Future studies with larger sample sizes and refined methodologies are essential to validate these findings and potentially achieve statistical significance.

REFERENCES

Achkar, J. M., & Jenny-Avital, E. R. (2011). Incipient and subclinical tuberculosis: Defining early disease states in the context of host immune response. *Journal of Infectious Diseases*, *204*(SUPPL. 4). https://doi.org/10.1093/infdis/jir451

Ahmad, J., Akhter, S., Rizwanullah, M., Amin, S., Rahman, M., Ahmad, M. Z., Rizvi, M. A., Kamal, M. A., & Ahmad, F. J. (2015). Nanotechnology-based inhalation treatments for lung cancer: State of the art. In *Nanotechnology, Science and Applications* (Vol. 8, pp. 55–66). Dove Medical Press Ltd. https://doi.org/10.2147/NSA.S49052

Allen, T. M., & Cullis, P. R. (2013). Liposomal drug delivery systems: From concept to clinical applications. In *Advanced Drug Delivery Reviews* (Vol. 65, Issue 1, pp. 36–48). https://doi.org/10.1016/j.addr.2012.09.037

Bala, I., Hariharan, S., & Kumar, M. R. (2004). PLGA Nanoparticles in Drug Delivery: The State of the Art; *Critical Reviews in Therapeutic Drug Carrier Systems*, *21*(5), 387–422. https://doi.org/10.1615/CritRevTherDrugCarrierSyst.v21.i5.20

Baussano, I., Nunn, P., Williams, B., Pivetta, E., Bugiani, M., & Scano, F. (2011). Tuberculosis among health care workers. *Emerging Infectious Diseases*, *17*(3), 488–494. https://doi.org/10.3201/eid1703.100947

Baykan, A. H., Sayiner, H. S., Aydin, E., Koc, M., Inan, I., & Erturk, S. M. (2022). Extrapulmonary tuberculosıs: an old but resurgent problem. *Insights into Imaging*, *13*(1), 39. https://doi.org/10.1186/s13244-022-01172-0

Bertrand, N., Wu, J., Xu, X., Kamaly, N., & Farokhzad, O. C. (2014). Cancer nanotechnology: The impact of passive and active targeting in the era of modern cancer biology. In *Advanced Drug Delivery Reviews* (Vol. 66, pp. 2–25). Elsevier B.V. https://doi.org/10.1016/j.addr.2013.11.009

Blumberg, H. M., Burman, W. J., Chaisson, R. E., Daley, C. L., Etkind, S. C., Friedman, L. N., Fujiwara, P., Grzemska, M., Hopewell, P. C., Iseman, M. D., Jasmer, R. M., Koppaka, V., Menzies, R. I., O'Brien, R. J., Reves, R. R., Reichman, L. B., Simone, P. M., Starke, J. R., & Vernon, A. A. (2003). American Thoracic Society/Centers for Disease Control and Prevention/Infectious Diseases Society of America: treatment of tuberculosis. *American Journal of Respiratory and Critical Care Medicine*, *167*(4), 603–662. https://doi.org/10.1164/rccm.167.4.603

Boehme, C. C., Nabeta, P., Hillemann, D., Nicol, M. P., Shenai, S., Krapp, F., Allen, J., Tahirli, R., Blakemore, R., Rustomjee, R., Milovic, A., Jones, M., O'Brien, S. M., Persing, D. H., Ruesch-Gerdes, S., Gotuzzo, E., Rodrigues, C., Alland, D., & Perkins, M. D. (2010). Rapid Molecular Detection of Tuberculosis and Rifampin Resistance. *New England Journal of Medicine*, *363*(11), 1005–1015. https://doi.org/10.1056/nejmoa0907847

Brittle, W., Marais, B. J., Hesseling, A. C., Schaaf, H. S., Kidd, M., Wasserman, E., & Botha, T. (2009). Improvement in mycobacterial yield and reduced time to detection in pediatric samples by use of a nutrient broth growth supplement. *Journal of Clinical Microbiology*, *47*(5), 1287–1289. https://doi.org/10.1128/JCM.02320-08

Calderon, V. E., Valbuena, G., Goez, Y., Judy, B. M., Huante, M. B., Sutjita, P., Johnston, R. K., Estes, D. M., Hunter, R. L., Actor, J. K., Cirillo, J. D., & Endsley, J. J. (2013). A Humanized Mouse Model of Tuberculosis. *PLoS ONE*, *8*(5). https://doi.org/10.1371/journal.pone.0063331

Carita, A. C., Eloy, J. O., Chorilli, M., Lee, R. J., & Leonardi, G. R. (2018). Recent Advances and Perspectives in Liposomes for Cutaneous Drug Delivery. *Current Medicinal Chemistry*, *25*(5), 606–635. https://doi.org/10.2174/0929867324666171009120154

Centers for Disease Control and Prevention. (2006). *Prevention and Control of Tuberculosis in Correctional and Detention Facilities: Recommendations from CDC Endorsed by the Advisory Council for the Elimination of Tuberculosis, the National Commission on Correctional Health Care, and the American Correctional Association*.

Christopoulos, A. I., Diamantopoulos, A. A., Dimopoulos, P. A., Goumenos, D. S., & Barbalias, G. A. (2009). Risk factors for tuberculosis in dialysis patients: A prospective multi-center clinical trial. *BMC Nephrology*, *10*(1). https://doi.org/10.1186/1471-2369-10-36

Clark, S., Hall, Y., & Williams, A. (2015). Animal models of tuberculosis: Guinea pigs. *Cold Spring Harbor Perspectives in Medicine*, *5*(5). https://doi.org/10.1101/cshperspect.a018572

Daffé, M., & Draper, P. (1997). The Envelope Layers of Mycobacteria with Reference to their Pathogenicity. *Advances in Microbial Physiology*, *39*, 131–203. https://doi.org/10.1016/S0065-2911(08)60016-8

Danaei, M., Dehghankhold, M., Ataei, S., Hasanzadeh Davarani, F., Javanmard, R., Dokhani, A., Khorasani, S., & Mozafari, M. R. (2018). Impact of Particle Size and Polydispersity Index on the Clinical Applications of Lipidic Nanocarrier Systems. *Pharmaceutics*, *10*(2), 57. https://doi.org/10.3390/pharmaceutics10020057

Danhier, F., Ansorena, E., Silva, J. M., Coco, R., Le Breton, A., & Préat, V. (2012a). PLGA-based nanoparticles: An overview of biomedical applications. In *Journal of Controlled Release* (Vol. 161, Issue 2, pp. 505–522). https://doi.org/10.1016/j.jconrel.2012.01.043

Danhier, F., Ansorena, E., Silva, J. M., Coco, R., Le Breton, A., & Préat, V. (2012b). PLGA-based nanoparticles: An overview of biomedical applications. *Journal of Controlled Release*, *161*(2), 505–522. https://doi.org/10.1016/j.jconrel.2012.01.043

Datta, D., Jamwal, S., Jyoti, N., Patnaik, S., & Kumar, D. (2024). Actionable mechanisms of drug tolerance and resistance in *Mycobacterium tuberculosis*. *The FEBS Journal*, *291*(20), 4433–4452. https://doi.org/10.1111/febs.17142

Dheda, K., Gumbo, T., Gandhi, N. R., Murray, M., Theron, G., Udwadia, Z., Migliori, G. B., & Warren, R. (2014). Global control of tuberculosis: From extensively drug-resistant to untreatable tuberculosis. In *The Lancet Respiratory Medicine* (Vol. 2, Issue 4, pp. 321–338). Lancet Publishing Group. https://doi.org/10.1016/S2213-2600(14)70031-1

Dheda, K., Gumbo, T., Maartens, G., Dooley, K. E., McNerney, R., Murray, M., Furin, J., Nardell, E. A., London, L., Lessem, E., Theron, G., van Helden, P., Niemann, S., Merker, M., Dowdy, D., Van Rie, A., Siu, G. K. H., Pasipanodya, J. G., Rodrigues, C., … Warren, R. M. (2017). The epidemiology, pathogenesis, transmission, diagnosis, and management of multidrug-resistant, extensively drug-resistant, and incurable tuberculosis. In *The Lancet Respiratory Medicine* (Vol. 5, Issue 4, pp. 291–360). Lancet Publishing Group. https://doi.org/10.1016/S2213-2600(17)30079-6

Diacon, A. H., Pym, A., Grobusch, M., Patientia, R., Rustomjee, R., Page-Shipp, L., Pistorius, C., Krause, R., Bogoshi, M., Churchyard, G., Venter, A., Allen, J., Carlos Palomino, J., De Marez, T., van Heeswijk, R. P., Lounis, N., Meyvisch, P., Verbeeck,

J., Parys, W., … Research Council, M. (2009). The Diarylquinoline TMC207 for Multidrug-Resistant Tuberculosis A bs tr ac t. In *n engl j med* (Vol. 360).

Dodd, P. J., Gardiner, E., Coghlan, R., & Seddon, J. A. (2014). Burden of childhood tuberculosis in 22 high-burden countries: A mathematical modelling study. *The Lancet Global Health*, *2*(8). https://doi.org/10.1016/S2214-109X(14)70245-1

Dookie, N., Rambaran, S., Padayatchi, N., Mahomed, S., & Naidoo, K. (2018). Evolution of drug resistance in *Mycobacterium tuberculosis*: a review on the molecular determinants of resistance and implications for personalized care. *Journal of Antimicrobial Chemotherapy*, *73*(5), 1138–1151. https://doi.org/10.1093/jac/dkx506

Drain, P. K., Bajema, K. L., Dowdy, D., Dheda, K., Naidoo, K., Schumacher, S. G., Ma, S., Meermeier, E., Lewinsohn, D. M., & Sherman, D. R. (2018). Incipient and Subclinical Tuberculosis: a Clinical Review of Early Stages and Progression of Infection. *Clinical Microbiology Reviews*, *31*(4). https://doi.org/10.1128/CMR.00021-18

Esim, O., & Hascicek, C. (2020). Lipid-Coated Nanosized Drug Delivery Systems for an Effective Cancer Therapy. *Current Drug Delivery*, *18*(2), 147–161. https://doi.org/10.2174/1567201817666200512104441

Falzon, D., Schünemann, H. J., Harausz, E., González-Angulo, L., Lienhardt, C., Jaramillo, E., & Weyer, K. (2017). World Health Organization treatment guidelines for drug-resistant tuberculosis, 2016 update. *European Respiratory Journal*, *49*(3). https://doi.org/10.1183/13993003.02308-2016

Farokhzad, O. C., & Langer, R. (2009). Impact of nanotechnology on drug delivery. *ACS Nano*, *3*(1), 16–20. https://doi.org/10.1021/nn900002m

Flynn, J. L., & Chan, J. (2001). Immunology of Tuberculosis. *Annual Review of Immunology*, *19*(1), 93–129. https://doi.org/10.1146/annurev.immunol.19.1.93

Frieden, T. R., Harold Jaffe, D. W., Rasmussen, S. A., Leahy, M. A., Martinroe, J. C., Spriggs, S. R., Starr, T. M., Doan, Q. M., King, P. H., Roper, W. L., Hill, C., Matthew Boulton, C. L., Arbor, A., Virginia Caine, M. A., Jonathan Fielding, I. E., Remington, P. L., & William Schaffner, W. (2015). Silicosis Mortality Trends and New Exposures to Respirable Crystalline Silica — United States, 2001–2010. In *Rep* (Vol. 64, Issue 5). http://www.bls.gov/opub/ee/2014/ces/

Gagneux, S. (2018). Ecology and evolution of Mycobacterium tuberculosis. *Nature Reviews Microbiology*, *16*(4), 202–213. https://doi.org/10.1038/nrmicro.2018.8

Gerberding, J. L., Snider, D. E., Popovic, T., Solomon, S. L., Bernhardt, J. M., Parker, M. S., Hewitt, S. M., Mcgee, P., Holland, B. J., Cupell, L. G., Lapete, M. A., Doan, Q. M., & Shaver, E. R. (2005). *Guidelines for Preventing the Transmission of Mycobacterium tuberculosis in Health-Care Settings, 2005*.

Gideon, H. P., & Flynn, J. L. (2011). Latent tuberculosis: What the host "sees"? *Immunologic Research*, *50*(2–3), 202–212. https://doi.org/10.1007/s12026-011-8229-7

Global tuberculosis report 2023. (2023). https://iris.who.int/.

Hiromatsu, K., Christopher, {, Dascher, C., Sugita, M., Gingrich-Baker, C., Behar, S. M., Leclair, K. P., Brenner, M. B., & Porcelli, S. A. (n.d.). *Characterization of guinea-pig group 1 CD1 proteins*.

Hoa, L. T. M., Chi, N. T., Nguyen, L. H., & Chien, D. M. (2012). Preparation and characterisation of nanoparticles containing ketoprofen and acrylic polymers prepared by emulsion solvent evaporation method. *Journal of Experimental Nanoscience*, *7*(2), 189–197. https://doi.org/10.1080/17458080.2010.515247

Honary, S., & Zahir, F. (2013). Effect of Zeta Potential on the Properties of Nano-Drug Delivery Systems - A Review (Part 1). *Tropical Journal of Pharmaceutical Research*, *12*(2). https://doi.org/10.4314/tjpr.v12i2.19

Jain, R. A. (2000). The manufacturing techniques of various drug loaded biodegradable poly(lactide-co-glycolide) (PLGA) devices. In *Biomaterials* (Vol. 21).

Jamous, Y. F., Altwaijry, N. A., Saleem, M. T. S., Alrayes, A. F., Albishi, S. M., & Almeshari, M. A. (2023). Formulation and Characterization of Solid Lipid Nanoparticles Loaded with Troxerutin. *Processes*, *11*(10). https://doi.org/10.3390/pr11103039

Jia, J., Zhang, Y., Xin, Y., Jiang, C., Yan, B., & Zhai, S. (2018). Interactions Between Nanoparticles and Dendritic Cells: From the Perspective of Cancer Immunotherapy. In *Frontiers in Oncology* (Vol. 8). Frontiers Media S.A. https://doi.org/10.3389/fonc.2018.00404

Khan, A. H., Sulaiman, S. A. S., Hassali, M. A., Khan, K. U., Ming, L. C., Mateen, O., & Ullah, M. O. (2020). Effect of smoking on treatment outcome among tuberculosis patients in Malaysia; A multicenter study. *BMC Public Health*, *20*(1). https://doi.org/10.1186/s12889-020-08856-6

Korf, J., Stoltz, A., Verschoor, J., De Baetselier, P., & Grooten, J. (2005). The Mycobacterium tuberculosis cell wall component mycolic acid elicits pathogen-associated host innate immune responses. *European Journal of Immunology*, *35*(3), 890–900. https://doi.org/10.1002/eji.200425332

Kumar, M., Virmani, T., Kumar, G., Deshmukh, R., Sharma, A., Duarte, S., Brandão, P., & Fonte, P. (2023). Nanocarriers in Tuberculosis Treatment: Challenges and Delivery Strategies. In *Pharmaceuticals* (Vol. 16, Issue 10). Multidisciplinary Digital Publishing Institute (MDPI). https://doi.org/10.3390/ph16101360

Lamprecht, A., Ubrich, N., Hombreiro Pérez, M., Lehr, C.-M., Hoffman, M., & Maincent, P. (1999). Biodegradable monodispersed nanoparticles prepared by pressure homogenization-emulsification. In *International Journal of Pharmaceutics* (Vol. 184).

Lemmer, Y., Kalombo, L., Pietersen, R. D., Jones, A. T., Semete-Makokotlela, B., Van Wyngaardt, S., Ramalapa, B., Stoltz, A. C., Baker, B., Verschoor, J. A., Swai, H. S., & De Chastellier, C. (2015). Mycolic acids, a promising mycobacterial ligand for targeting of nanoencapsulated drugs in tuberculosis. *Journal of Controlled Release*, *211*, 94–104. https://doi.org/10.1016/j.jconrel.2015.06.005

Libero, G. De, & Mori, L. (2014). The T-cell response to lipid antigens of Mycobacterium tuberculosis. In *Frontiers in Immunology* (Vol. 5, Issue MAY, pp. 1–1). Frontiers Research Foundation. https://doi.org/10.3389/fimmu.2014.00219

Lienhardt, C., Vernon, A., & Raviglione, M. C. (2010). New drugs and new regimens for the treatment of tuberculosis: review of the drug development pipeline and implications for national programmes. *Current Opinion in Pulmonary Medicine*, 1. https://doi.org/10.1097/MCP.0b013e328337580c

Lönnroth, K., Jaramillo, E., Williams, B. G., Dye, C., & Raviglione, M. (2009). Drivers of tuberculosis epidemics: The role of risk factors and social determinants. *Social Science and Medicine*, *68*(12), 2240–2246. https://doi.org/10.1016/j.socscimed.2009.03.041

Lonnroth, K., Williams, B. G., Cegielski, P., & Dye, C. (2010). A consistent log-linear relationship between tuberculosis incidence and body mass index. *International Journal of Epidemiology*, *39*(1), 149–155. https://doi.org/10.1093/ije/dyp308

Mai Hoa, L. T., Chi, N. T., Triet, N. M., Thanh Nhan, L. N., & Chien, D. M. (2009). Preparation of drug nanoparticles by emulsion evaporation method. *Journal of Physics: Conference Series*, *187*. https://doi.org/10.1088/1742-6596/187/1/012047

Makadia, H. K., & Siegel, S. J. (2011). Poly Lactic-co-Glycolic Acid (PLGA) as biodegradable controlled drug delivery carrier. *Polymers*, *3*(3), 1377–1397. https://doi.org/10.3390/polym3031377

Menzies, D., Adjobimey, M., Ruslami, R., Trajman, A., Sow, O., Kim, H., Obeng Baah, J., Marks, G. B., Long, R., Hoeppner, V., Elwood, K., Al-Jahdali, H., Gninafon, M., Apriani, L., Koesoemadinata, R. C., Kritski, A., Rolla, V., Bah, B., Camara, A., … Benedetti, A. (2018). Four Months of Rifampin or Nine Months of Isoniazid for Latent Tuberculosis in Adults. *New England Journal of Medicine*, *379*(5), 440–453. https://doi.org/10.1056/NEJMoa1714283

Mirzayev, F., Viney, K., Linh, N. N., Gonzalez-Angulo, L., Gegia, M., Jaramillo, E., Zignol, M., & Kasaeva, T. (2021). World health organization recommendations on the treatment of drug-resistant tuberculosis, 2020 update. In *European Respiratory Journal* (Vol. 57, Issue 6). European Respiratory Society. https://doi.org/10.1183/13993003.03300-2020

Mitchison, D. A. (2000). *Role of individual drugs in the chemotherapy of tuberculosis*.

Mitnick, C. D., Rodriguez, C. A., Hatton, M. L., Brigden, G., Cobelens, F., Grobusch, M. P., Horsburgh, R., Lange, C., Lienhardt, C., Oren, E., Podewils, L. J., Seaworth, B., Van Hof, S. Den, Daley, C. L., Gebhard, A. C., & Wares, F. (2016). Programmatic Management of Drug-Resistant Tuberculosis: An Updated Research Agenda. *PLoS ONE*, *11*(5). https://doi.org/10.1371/journal.pone.0155968

Munita, J. M., & Arias, C. A. (2016). Mechanisms of Antibiotic Resistance. *Microbiology Spectrum*, *4*(2). https://doi.org/10.1128/microbiolspec.VMBF-0016-2015

Mura, S., Nicolas, J., & Couvreur, P. (2013). Stimuli-responsive nanocarriers for drug delivery. *Nature Materials*, *12*(11), 991–1003. https://doi.org/10.1038/nmat3776

Nabi, B., Rehman, S., Aggarwal, S., Baboota, S., & Ali, J. (2020). Nano-based anti-tubercular drug delivery: an emerging paradigm for improved therapeutic intervention. *Drug Delivery and Translational Research*, *10*(4), 1111–1121. https://doi.org/10.1007/s13346-020-00786-5

Nahid, P., Dorman, S. E., Alipanah, N., Barry, P. M., Brozek, J. L., Cattamanchi, A., Chaisson, L. H., Chaisson, R. E., Daley, C. L., Grzemska, M., Higashi, J. M., Ho, C. S., Hopewell, P. C., Keshavjee, S. A., Lienhardt, C., Menzies, R., Merrifield, C., Narita, M., O'Brien, R., … Vernon, A. (2016). Official American Thoracic Society/Centers for Disease Control and Prevention/Infectious Diseases Society of America Clinical Practice Guidelines: Treatment of Drug-Susceptible Tuberculosis. In *Clinical Infectious Diseases* (Vol. 63, Issue 7, pp. e147–e195). Oxford University Press. https://doi.org/10.1093/cid/ciw376

Nair, A., Greeny, A., Nandan, A., Sah, R. K., Jose, A., Dyawanapelly, S., Junnuthula, V., Athira, K. V., & Sadanandan, P. (2023). Advanced drug delivery and therapeutic strategies for tuberculosis treatment. In *Journal of Nanobiotechnology* (Vol. 21, Issue 1). BioMed Central Ltd. https://doi.org/10.1186/s12951-023-02156-y

Ndlandla, F. L., Ejoh, V., Stoltz, A. C., Naicker, B., Cromarty, A. D., van Wyngaardt, S., Khati, M., Rotherham, L. S., Lemmer, Y., Niebuhr, J., Baumeister, C. R., Al Dulayymi, J. R., Swai, H., Baird, M. S., & Verschoor, J. A. (2016). Standardization of natural mycolic acid antigen composition and production for use in biomarker antibody detection to diagnose active tuberculosis. *Journal of Immunological Methods*, *435*, 50–59. https://doi.org/10.1016/j.jim.2016.05.010

Negin, J., Abimbola, S., & Marais, B. J. (2015). Tuberculosis among older adults - time to take notice. *International Journal of Infectious Diseases*, *32*, 135–137. https://doi.org/10.1016/j.ijid.2014.11.018

Orme, I. M. (2005). Mouse and guinea pig models for testing new tuberculosis vaccines. *Tuberculosis*, *85*(1–2), 13–17. https://doi.org/10.1016/j.tube.2004.08.001

Orme, I. M., & Roberts, A. D. (1999). Animal Models of Mycobacteria Infection. *Current Protocols in Immunology*, *30*(1). https://doi.org/10.1002/0471142735.im1905s30

Pandey, R., Ahmad, Z., Sharma, S., & Khuller, G. K. (2005). Nano-encapsulation of azole antifungals: Potential applications to improve oral drug delivery. *International Journal of Pharmaceutics*, *301*(1–2), 268–276. https://doi.org/10.1016/j.ijpharm.2005.05.027

Patil, K., Bagade, S., Bonde, S., Sharma, S., & Saraogi, G. (2018). Recent therapeutic approaches for the management of tuberculosis: Challenges and opportunities. In *Biomedicine and Pharmacotherapy* (Vol. 99, pp. 735–745). Elsevier Masson SAS. https://doi.org/10.1016/j.biopha.2018.01.115

Patra, J. K., Das, G., Fraceto, L. F., Campos, E. V. R., Rodriguez-Torres, M. D. P., Acosta-Torres, L. S., Diaz-Torres, L. A., Grillo, R., Swamy, M. K., Sharma, S., Habtemariam, S., & Shin, H. S. (2018). Nano based drug delivery systems: Recent developments and future prospects. In *Journal of Nanobiotechnology* (Vol. 16, Issue 1). BioMed Central Ltd. https://doi.org/10.1186/s12951-018-0392-8

Peer, D., Karp, J. M., Hong, S., Farokhzad, O. C., Margalit, R., & Langer, R. (2007). Nanocarriers as an emerging platform for cancer therapy. *Nature Nanotechnology*, *2*(12), 751–760. https://doi.org/10.1038/nnano.2007.387

Pérez-Herrero, E., & Fernández-Medarde, A. (2015). Advanced targeted therapies in cancer: Drug nanocarriers, the future of chemotherapy. In *European Journal of Pharmaceutics and Biopharmaceutics* (Vol. 93, pp. 52–79). Elsevier B.V. https://doi.org/10.1016/j.ejpb.2015.03.018

Pinto Reis, C., Neufeld, R. J., Ribeiro, A. J., & Veiga, F. (2006). Nanoencapsulation I. Methods for preparation of drug-loaded polymeric nanoparticles. In *Nanomedicine: Nanotechnology, Biology, and Medicine* (Vol. 2, Issue 1, pp. 8–21). Elsevier Inc. https://doi.org/10.1016/j.nano.2005.12.003

Prabhu, R. H., Patravale, V. B., & Joshi, M. D. (2015). Polymeric nanoparticles for targeted treatment in oncology: Current insights. In *International Journal of Nanomedicine* (Vol. 10, pp. 1001–1018). Dove Medical Press Ltd. https://doi.org/10.2147/IJN.S56932

Rabaan, A. A., Mutair, A. Al, Albayat, H., Alotaibi, J., Sulaiman, T., Aljeldah, M., Shammari, B. R. Al, Alfaraj, A. H., Al Fares, M. A., Alwarthan, S., Binjomah, A. Z., Alzahrani, M. S., Alhani, H. M., Almogbel, M. S., Abuzaid, A. A., Alqurainees, G., Al Ibrahim, F., Alhaddad, A. H., Alfaresi, M., … Alhumaid, S. (2022). Tools to Alleviate the Drug Resistance in Mycobacterium tuberculosis. *Molecules*, *27*(20), 6985. https://doi.org/10.3390/molecules27206985

Rehm, J., Samokhvalov, A. V, Neuman, M. G., Room, R., Parry, C., Lönnroth, K., Patra, J., Poznyak, V., & Popova, S. (2009). The association between alcohol use, alcohol

use disorders and tuberculosis (TB). A systematic review. *BMC Public Health*, *9*(1), 450. https://doi.org/10.1186/1471-2458-9-450

Sachan, R. S. K., Mistry, V., Dholaria, M., Rana, A., Devgon, I., Ali, I., Iqbal, J., Eldin, S. M., Mohammad Said Al-Tawaha, A. R., Bawazeer, S., Dutta, J., & Karnwal, A. (2023). Overcoming *Mycobacterium tuberculosis* Drug Resistance: Novel Medications and Repositioning Strategies. *ACS Omega*, *8*(36), 32244–32257. https://doi.org/10.1021/acsomega.3c02563

Seifert, M., Catanzaro, D., Catanzaro, A., & Rodwell, T. C. (2015). Genetic mutations associated with isoniazid resistance in Mycobacterium tuberculosis: A systematic review. *PLoS ONE*, *10*(3). https://doi.org/10.1371/journal.pone.0119628

Singh, A. K., & Gupta, U. D. (2018). Animal models of tuberculosis: Lesson learnt. In *Indian Journal of Medical Research* (Vol. 147, Issue May, pp. 456–463). Indian Council of Medical Research. https://doi.org/10.4103/ijmr.IJMR_554_18

Sotgiu, G., Centis, R., D'Ambrosio, L., & Battista Migliori, G. (2015). Tuberculosis treatment and drug regimens. *Cold Spring Harbor Perspectives in Medicine*, *5*(5). https://doi.org/10.1101/cshperspect.a017822

Steingart, K. R., Henry, M., Ng, V., Hopewell, P. C., Ramsay, A., Cunningham, J., Urbanczik, R., Perkins, M., Aziz, M. A., & Pai, M. (2006). Fluorescence versus conventional sputum smear microscopy for tuberculosis: a systematic review. In *Lancet Infectious Diseases* (Vol. 6, Issue 9, pp. 570–581). Lancet Publishing Group. https://doi.org/10.1016/S1473-3099(06)70578-3

Sterling, T. R., Elsa Villarino, M., Borisov, A. S., Shang, N., Gordin, F., Bliven-Sizemore, E., Hackman, J., Dukes Hamilton, C., Menzies, D., Kerrigan, A., Weis, S. E., Weiner, M., Wing, D., Conde, M. B., Bozeman, L., Robert Horsburgh, C., & Chaisson, R. E. (2011). Three Months of Rifapentine and Isoniazid for Latent Tuberculosis Infection. In *n engl j med* (Vol. 23, Issue 8).

Sun, H., Saeedi, P., Karuranga, S., Pinkepank, M., Ogurtsova, K., Duncan, B. B., Stein, C., Basit, A., Chan, J. C. N., Mbanya, J. C., Pavkov, M. E., Ramachandaran, A., Wild, S. H., James, S., Herman, W. H., Zhang, P., Bommer, C., Kuo, S., Boyko, E. J., & Magliano, D. J. (2022). IDF Diabetes Atlas: Global, regional and country-level diabetes prevalence estimates for 2021 and projections for 2045. *Diabetes Research and Clinical Practice*, *183*, 109119. https://doi.org/10.1016/J.DIABRES.2021.109119

Tedla, K., Medhin, G., Berhe, G., Mulugeta, A., & Berhe, N. (2020). Delay in treatment initiation and its association with clinical severity and infectiousness among new adult pulmonary tuberculosis patients in Tigray, northern Ethiopia. *BMC Infectious Diseases*, *20*(1). https://doi.org/10.1186/s12879-020-05191-4

Telenti, A., Philipp, W. J., Sreevatsan, S., Bernasconi, C., Stockbauer, K. E., Wieles, B., Musser, J. M., & Jacobs, W. R. (1997). The emb operon, a gene cluster of Mycobacterium tuberculosis involved in resistance to ethambutol. *Nature Medicine*, *3*(5), 567–570. https://doi.org/10.1038/nm0597-567

Tiberi, S., du Plessis, N., Walzl, G., Vjecha, M. J., Rao, M., Ntoumi, F., Mfinanga, S., Kapata, N., Mwaba, P., McHugh, T. D., Ippolito, G., Migliori, G. B., Maeurer, M. J., & Zumla, A. (2018). Tuberculosis: progress and advances in development of new drugs, treatment regimens, and host-directed therapies. In *The Lancet Infectious Diseases* (Vol. 18, Issue 7, pp. e183–e198). Lancet Publishing Group. https://doi.org/10.1016/S1473-3099(18)30110-5

Tiemersma, E. W., van der Werf, M. J., Borgdorff, M. W., Williams, B. G., & Nagelkerke, N. J. D. (2011). Natural history of tuberculosis: Duration and fatality of untreated pulmonary tuberculosis in HIV negative patients: A systematic review. In *PLoS ONE* (Vol. 6, Issue 4). https://doi.org/10.1371/journal.pone.0017601

Tsai, M. C., Chakravarty, S., Zhu, G., Xu, J., Tanaka, K., Koch, C., Tufariello, J. A., Flynn, J. A., & Chan, J. (2006). Characterization of the tuberculous granuloma in murine and human lungs: Cellular composition and relative tissue oxygen tension. *Cellular Microbiology*, *8*(2), 218–232. https://doi.org/10.1111/j.1462-5822.2005.00612.x

Turner, O. C., Basaraba, R. J., Frank, A. A., & Orme, I. M. (2014). Granuloma Formation in Mouse and Guinea Pig Models of Experimental Tuberculosis. In *Granulomatous Infections and Inflammations* (pp. 65–84). ASM Press. https://doi.org/10.1128/9781555817879.ch3

Udwadia, Z. F., Amale, R. A., Ajbani, K. K., & Rodrigues, C. (2012). Totally drug-resistant tuberculosis in India. In *Clinical Infectious Diseases* (Vol. 54, Issue 4, pp. 579–581). https://doi.org/10.1093/cid/cir889

Ulrichs, T., Moody, D. B., Grant, E., Kaufmann, S. H. E., & Porcelli, S. A. (2003). T-cell responses to CD1-presented lipid antigens in humans with Mycobacterium

tuberculosis infection. *Infection and Immunity*, *71*(6), 3076–3087. https://doi.org/10.1128/IAI.71.6.3076-3087.2003

Velayati, A. A., Masjedi, M. R., Farnia, P., Tabarsi, P., Ghanavi, J., ZiaZarifi, A. H., & Hoffner, S. E. (2009). Emergence of new forms of totally drug-resistant tuberculosis bacilli: Super extensively drug-resistant tuberculosis or totally drug-resistant strains in Iran. *Chest*, *136*(2), 420–425. https://doi.org/10.1378/chest.08-2427

Wang, E. Y., Arrazola, R. A., Mathema, B., Ahluwalia, I. B., & Mase, S. R. (2020). The impact of smoking on tuberculosis treatment outcomes: A meta-analysis. *International Journal of Tuberculosis and Lung Disease*, *24*(2), 170–175. https://doi.org/10.5588/ijtld.19.0002

Wang, H., Liu, D., & Zhou, X. (2024). Effect of Mycolic Acids on Host Immunity and Lipid Metabolism. In *International Journal of Molecular Sciences* (Vol. 25, Issue 1). Multidisciplinary Digital Publishing Institute (MDPI). https://doi.org/10.3390/ijms25010396

WHO consolidated guidelines on tuberculosis Module 4: Treatment Drug-resistant tuberculosis treatment 2022 update. (n.d.).

Woldesemayat, E. M. (2021). Tuberculosis in migrants is among the challenges of tuberculosis control in high-income countries. In *Risk Management and Healthcare Policy* (Vol. 14, pp. 2965–2970). Dove Medical Press Ltd. https://doi.org/10.2147/RMHP.S314777

World Health Organization. (2020). *Global tuberculosis report 2020.* World Health Organization.

Xu, X., Ho, W., Zhang, X., Bertrand, N., & Farokhzad, O. (2015). Cancer nanomedicine: From targeted delivery to combination therapy. In *Trends in Molecular Medicine* (Vol. 21, Issue 4, pp. 223–232). Elsevier Ltd. https://doi.org/10.1016/j.molmed.2015.01.001

Zhang, Y., & Yew, W. W. (2015a). Mechanisms of drug resistance in Mycobacterium tuberculosis: Update 2015. In *International Journal of Tuberculosis and Lung Disease* (Vol. 19, Issue 11, pp. 1276–1289). International Union Against Tuberculosis and Lung Disease. https://doi.org/10.5588/ijtld.15.0389

Zhang, Y., & Yew, W. W. (2015b). Mechanisms of drug resistance in Mycobacterium tuberculosis: Update 2015. In *International Journal of Tuberculosis and Lung Disease* (Vol. 19, Issue 11, pp. 1276–1289). International Union Against Tuberculosis and Lung Disease. https://doi.org/10.5588/ijtld.15.0389

Zong, K., Luo, C., Zhou, H., Jiang, Y., & Li, S. (2019). Xpert MTB/RIF assay for the diagnosis of rifampicin resistance in different regions: A meta-analysis. *BMC Microbiology*, *19*(1). https://doi.org/10.1186/s12866-019-1516-5

Appendix A:

Table 16: Detailed histopathological findings in lung, lymph node, and spleen tissues from guinea pigs in various treatment groups. The severity of different pathological changes such as granulomatous pneumonia, lymphoplasmacytic cuffing, and macrophage activity in the lungs, as well as lymphoid hyperplasia and granulomatous inflammation in lymph nodes and spleen, are graded on a scale (+ to 3+) across individual animals. "NS" denotes not sampled, "SFA" indicates Severe Freeze Artifacts.

Group	1			2					3					4					5					6				
Animal number	4	16	23	1	5	6	7	8	9	10	11	12	13	2	14	15	17	18	3	19	20	21	22	24	25	26	27	28
Lung:							SFA																					
Multifocal interstitial granulomatous pneumonia	-	-	-	3+	-	-	-	-	3+	-	-	-	-	1+	-	3+	3+	3+	3+	-	-	-	-	-	-	-	-	-
Diffuse interstitial granulomatous pneumonia	3+	3+	3+	-	3+	3+	-	3+	-	2+	2+	3+	3+	-	3+	-	-	-	-	3+	3+	3+	3+	3+	3+	3+	3+	3+
Peribronchial / perivascular lymphoplasmacytic cuffing	2+	2+	2+	1+	1+	-	-	1+	-	1+	1+	1+	1+	2+	2+	2+	2+	1+	1+	1+	1+	1+	1+	1+	1+	1+	1+	1+
Vacuolar hypertrophic alveolar macrophages	3+	3+	3+	3+	3+	3+	-	3+	-	3+	3+	3+	3+	2+	3+	2+	2+	2+	2+	3+	3+	3+	3+	3+	3+	3+	2+	3+

Group	1			2					3					4					5					6				
Lymph node:		NS	NS	NS	NS	NS	NS	NS	NS	NS	NS				NS	NS	NS	NS	NS	NS	NS	NS	NS		NS	NS	NS	NS
Lymphoid hyperplasia	3+											-	2+	-										1+				
Granulomatous lymphadenitis	3+											-	3+	-										1+				
Spleen:							NS															NS			NS			
Multinodular lymphoid hyperplasia	3+	3+	2+	3+	3+	3+		3+	2+	3+	2+	3+	3+	3+	3+	3+	NS	3+	3+	3+		3+	3+	1+		3+	3+	3+
Granulomatous multifocal splenitis	2+	3+	3+	1+	2+	1+		3+	1+	-	-	1+	2+	-	-	2+		-	-	-		1+	-	-		1+	1+	-
Liver:	NS	NS	NS	NS	NS		SFA	NS	NS		NS		NS		NS	NS	NS	NS	NS	NS	NS	NS	NS	NS				
Vacuolar centrilobular hepatopathy						-				-		-		-											3+	-	-	1+
Granulomatous multifocal hepatitis						3+				-		-		-											-	-	1+	-